2017

Database Plan Quality Impact on Knowledge-based Radiation Therapy Treatment Planning of Prostate Cancer

Phillip Douglas Hardenbergh Wall
Louisiana State University and Agricultural and Mechanical College, phillipdhwall@gmail.com

DATABASE PLAN QUALITY IMPACT ON KNOWLEDGE-BASED RADIATION THERAPY TREATMENT PLANNING OF PROSTATE CANCER

A Thesis

Submitted to the Graduate Faculty of the
Louisiana State University and
Agricultural and Mechanical College
in partial fulfillment of the
requirements for the degree of
Master of Science

in

The Department of Physics and Astronomy

by
Phillip Douglas Hardenbergh Wall
B.S., Davidson College, 2014
August 2017

ACKNOWLEDGEMENTS

My deepest gratitude goes to my major advisor, Dr. Jonas Fontenot, for the opportunity to work with him on this project. I have learned so much from him and I thank him for his helpful guidance and support over the course of this research. I also thank Dr. Robert Carver for his valuable contributions and insight, especially in our discussions of the more technical aspects of the project. I also thank committee members, Drs. Rui Zhang and Juhan Frank, for investing their time and expertise in supervising and monitoring this project.

I want to acknowledge all faculty and staff involved with the medical physics program at Louisiana State University (LSU) and Mary Bird Perkins Cancer Center. I appreciate the professors and thank them for helping me through my studies, particularly Dr. Kenneth Matthews for his incredible commitment to helping all program students. I want to especially thank David Perrin and Connel Chu for helping me with compiling the patient database for this project. I also express my sincerest thanks and appreciation for administrators Susan Hammond, Megan Jarrell, Katherine Pevey, and LaShawn Burns for helping with logistics and paperwork throughout my LSU career.

Additional thanks go to Jie Chen and Dr. David Blouin of the LSU Department of Experimental Statistics for their assistance in forming the statistical design and methods used in this project. Also, I thank Cameron Ditty, Senior Physics Specialist for RaySearch Laboratories, for assisting me with the nuances of scripting in RayStation, which allowed me to develop the scripts needed for this project.

I also want to thank all my student colleagues I have known in my time at LSU for their camaraderie. I specifically acknowledge my fellow classmates John Doiron, Krystal Kirby, and Xiaodong Zhao for helping me navigate through graduate studies.

Finally, I thank my mother, brother, and grandfather for their unwavering love and support, which have always been and will always be my biggest motivator and inspiration.

TABLE OF CONTENTS

LIST OF TABLES

LIST OF FIGURES

ABSTRACT

Purpose: Knowledge-based planning (KBP) leverages plan data from a database of previously treated patients to inform the plan design of a new patient. This work investigated bladder and rectum dose-volume prediction improvements in a common KBP method using a Pareto plan database in VMAT planning for prostate cancer.

Methods: We formed an anonymized retrospective patient database of 124 VMAT plans for prostate cancer treated at our institution. From these patient data, two plan databases were compiled. The clinical plan database (CPD) contained planning data from each patient's clinical plan, which were manually optimized by various planners. The multi-criteria optimization database (MCOD) contained Pareto plan data from plans created using a standardized MCO protocol. Overlap volume histograms, incorporating fractional OAR volumes only within the treatment fields, were computed for each patient and used to match new patient anatomy to similar database patients. For each database patient, CPD and MCOD KBP predictions were generated for D_{10}, D_{30}, D_{50}, D_{65}, and D_{80} of the bladder and rectum in a leave-one-out manner. Prediction achievability was verified through a re-planning study on a subset of 31 randomly selected database patients using the lowest KBP predictions, regardless of plan database origin, as planning goals.

Results: MCOD model predictions were significantly lower ($p < 0.001$) than CPD model predictions for all five bladder dose-volumes and rectum D_{50} ($p = 0.004$) and D_{65} ($p < 0.001$), while CPD model predictions for rectum D_{10} ($p = 0.005$) and D_{30} ($p < 0.001$) were significantly less than MCOD model predictions. KBP model predictions were statistically equivalent to re-planned values for all predicted dose-volumes, excluding D_{10} of bladder ($p = 0.03$) and rectum ($p = 0.04$). Compared to clinical plans, re-plans showed significant average reductions in D_{mean} for bladder (7.8 Gy; $p < 0.001$) and rectum (9.4 Gy; $p < 0.001$), while maintaining statistically similar PTV, femoral head, and penile bulb dose.

Conclusion: KBP dose-volume predictions derived from Pareto plans were lower overall than those resulting from manually optimized clinical plans. A re-planning study showed the KBP dose-volume predictions were achievable and led to significant reductions in bladder and rectum dose.

CHAPTER 1. INTRODUCTION

1.1 BACKGROUND

1.1.1 RADIATION THERAPY TREATMENT DELIVERY AND PLANNING

Radiation therapy (or radiotherapy) is the use of high-energy radiation, such as x-rays, gamma rays, electrons, or protons, to kill or damage cancer cells. Over half of all cancer patients will receive some form of radiotherapy during the course of their treatment.[1] Currently, there are two main approaches to delivering the prescribed radiation dose: external beam radiotherapy (EBRT), which involves large source-to-surface distances, or SSDs; and brachytherapy, which utilizes radioisotopes to treat internally or with small SSDs. In EBRT, linear accelerators are used to generate and direct megavoltage electrons or photons toward the cancer located within the patient.

Most modern linear accelerators support different options for delivering the prescribed radiation dose to the target for a given patient and disease. 3D conformal radiotherapy (3DCRT) collimates radiation fields of uniform intensity around lesions to simultaneously dose the target and spare surrounding healthy tissues using multi-leaf collimators (MLCs), which are motorized sets of thin, tungsten slabs that move in and out of the field to form different shapes.[2] 3DCRT was the first delivery technique based on 3D anatomical information provided by computed tomography (CT) scans. Access to 3D information allows more accurate delineations of targets and healthy organs and conformal dose distributions compared to previous delivery methods based on 2D radiographic projections.

Alternatively, fixed-field intensity modulated radiotherapy (IMRT) is a delivery technique typically combining five to seven fixed radiation fields of spatially varying fluence patterns. Each beam's modulated intensity profiles are achieved by combining complex sequences of MLC leaf travel, which are set to optimize the composite dose distribution. IMRT combines the non-uniform fluence maps from each beam (aimed from different directions) to create highly conformal dose

distributions that improve target coverage and in sparing of normal tissues compared to 3DCRT.[3,4] However, longer treatment delivery times and increased monitor units (MUs) are limitations for IMRT treatments. The latter can increase radiation exposure to parts of the body distant from the treatment field, whereas the former can impair patient comfort and reproducibility.[5] In order to overcome these deficiencies, arc-based or rotational treatment techniques were developed, where radiation is delivered while rotating the linear accelerator about the target.

Volumetric modulated arc therapy (VMAT), one such rotational IMRT technique, delivers intensity modulated fields by continuously varying three main parameters: rotation speed of the linear accelerator gantry, MLC positions, and dose rate (Figure 1).[6] VMAT dose is computed by approximating a continuous arc with a large number of discrete segments. The non-uniform fluence profiles and ensuing MLC sequences are optimized at each control point (each segment lies between two control points) to create highly conformal intensity modulated dose distributions. Compared to fixed-field IMRT, VMAT requires fewer MUs and provides a significantly shorter treatment time.[7] Due to the relatively recent clinical implementation of VMAT, its overall dosimetric advantages over fixed-field IMRT are uncertain. Some studies have reported potential benefits of VMAT for specific treatment sites like the prostate, while others have found inconsistent dosimetric results between IMRT and VMAT for head-and-neck treatments.[7-12] Primarily owing to efficiency, VMAT has quickly become a ubiquitous treatment technique for cases requiring intensity modulation.

Radiotherapy treatment planning is the process of defining how the prescribed dose is to be delivered during treatment. More specifically, a treatment plan specifies the machine parameters to produce the desired dose distribution for the given patient. These parameters can include the number of beams, beam energy, beam shape, beam weight, gantry angle, intensity modulators (e.g. wedges, tissue compensators, MLCs), and couch angle. Computerized treatment planning systems (TPSs) are used to help determine these parameters to arrive at a customized treatment plan for each

patient. Even with the assistance of computers, treatment plan design is time-consuming and highly complex given the large number of parameters the must be specified.

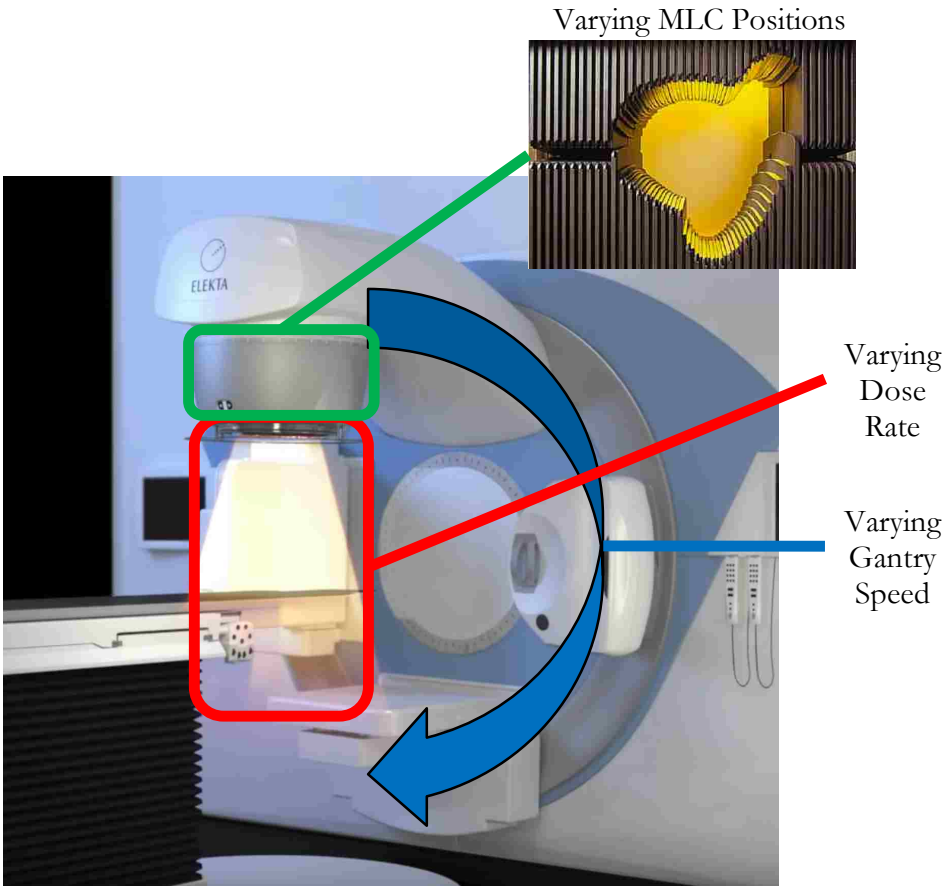

Figure 1: Diagram of a modern linear accelerator, highlighting the three varying parameters that differentiate VMAT from other EBRT delivery techniques.[13,14]

There are two main approaches to treatment planning used today, each of which facilitate specific delivery techniques. "Forward planning" is employed to design treatment plans for conventional, uniform intensity techniques (e.g. 3DCRT). Forward planning is the process of manually adjusting treatment parameters to obtain the desired dose distribution. If a patient is to be treated with 3DCRT, for instance, the planners must manually find the appropriate machine and treatment parameters to obtain an acceptable plan. This forward planning approach forces planners to determine these parameters effectively by trial-and-error, where the dose must be computed and evaluated each time a set of parameters is selected. Moreover, if the resulting dose distribution is not

acceptable, the parameters are manually adjusted and the dose is recomputed for evaluation. These iterations continue until the desired dose distribution is achieved.

Alternatively, "inverse planning" is used for planning more complex treatment delivery techniques such as IMRT and VMAT. These techniques require many intricate MLC sequences for each field or arc segment to generate the necessary modulated fluence patterns. Manually optimizing these varying fluence maps and corresponding MLC sequences for each beam via forward planning would prove prohibitively difficult and laborious.[15] Therefore, inverse planning optimization algorithms were developed and implemented into TPSs to plan these intensity modulated delivery techniques. Inverse planning requires the planner to specify the clinical treatment criteria, after which an optimization algorithm automatically determines modulated fluence maps for each beam or arc segment that achieve the treatment goals. More specifically, the user defines clinical dose-volume constraints (i.e. the dose a fractional volume of a planning structure receives) for the target and normal tissues, which are represented as cost objective functions for the optimization algorithm to minimize. Once the optimizer generates a set of modulated fluence segments and beam parameters for the given treatment objectives, the dose is computed and the dose distribution is evaluated. If improvement is needed or the planner wants to assess a clinical trade-off, the planner must adjust the initial dose-volume objectives and run another optimization. Additionally, clinical inverse planning algorithms utilize a gradient-based search for optimal intensity profiles, which usually requires multiple optimization rounds to ensure the solution reaches a global, and not a local, minimum. This trial-and-error nature of inverse planning resembles that of forward planning, but the two protocols differ in the parameters that planners modify after each iteration. Regardless, inverse planning can become increasingly time-consuming for complicated cases, like head-and-neck patients, that require the assessment of a large number of clinical trade-offs. Paired with the time limitations of a clinical environment, this can limit the quality of inverse plans.

While it drives the planning of IMRT techniques, inverse optimization reduces a three-dimensional dose distribution into a set of dose objectives based on one-dimensional dose volume histograms (DVHs). This dimensionality reduction in describing dose distributions underscores the importance of selecting and adjusting optimal inverse planning objectives. Planners do not currently know *a priori* what the fully optimal treatment plan is for a given patient, let alone the set of planning objectives needed to arrive at that plan. Further, clinical dose-volume goals for normal tissues are usually derived from population-based clinical studies (e.g. Emami *et al.*[16], Quantitative Analysis of Normal Tissue Effects in the Clinic[17], Radiation Therapy Oncology Group studies, etc.), which have recommended dose tolerances for clinical acceptability but do not provide any patient-specific information. This, in addition to unique patient anatomies and the heuristic nature of inverse planning, cause the quality of inversely optimized plans to be susceptible to planner bias and subjectivity. These limitations of inverse planning have led studies to observe a plan quality dependence on planner experience and "skill."[18] Batumalai *et al.* found within one institution that more experienced planners were able to produce superior IMRT plans for a head-and-neck case compared with less experienced planners, whose plans were also generally more difficult to deliver accurately.[19] Planner bias results in plan quality variations between planners and institutions, which lead to sub-optimal plans that are clinically-acceptable but more sparing of organs at risk (OARs) is possible.[20,21] Nelms *et al.* observed a wide inter-planner variation in plan quality of one prostate patient, which they quantified using a "Plan Quality Metric" (PQM) scoring mechanism. The PQM algorithm combines 14 target and OAR dose metrics, each assigned a unique value function, to serve as treatment goals from a hypothetical physician. With minimum and maximum possible PQM values of -10 and 150 respectively, they saw a large range of 58.2-142.5 in PQM (mean of 116.9; standard deviation of 16.4) over their 125 plan sample size. This variance in plan quality was independent of TPS, delivery modality (IMRT versus rotational), beam angles, total MUs, and

planner experience.[22] Moore *et al.* performed a secondary study on the quality of plan data accrued for the Radiation Therapy Oncology Group (RTOG) 0126 protocol comparing high dose to standard dose 3DCRT/IMRT in patients with localized prostate cancer. They observed 42.9% of 219 patients with ≥5% excess risk, 9.1% with ≥10% excess risk, and 0.9% with ≥15% excess risk of grade ≥2 rectal toxicities. This revealed how sub-optimal inverse planning can leave prostate patients vulnerable to excess risk of rectal complications.[23]

Inverse planning has been shown to efficiently produce clinically-acceptable plans for sophisticated delivery modalities such as VMAT. However, achieving a fully optimal plan via inverse optimization requires substantial time and effort to iteratively explore the relevant clinical trade-offs. Planners must often sacrifice plan quality for efficiency due to clinical time constraints. The trial-and-error and heuristic nature of inverse planning can also introduce planner subjectivity and bias, further affecting plan quality. Given these inverse planning deficiencies, novel planning methods and optimization algorithms aiming to improve patient-specific plan quality and consistency have become a focus in medical physics research.

1.1.2 MULTI-CRITERIA OPTIMIZATION

One such advanced optimization algorithm aiming to minimize the iterative and subjective nature of inverse planning is called multi-criteria optimization (MCO). MCO planning allows for the real-time assessment of clinical trade-offs by generating a database of Pareto optimal plans, which are plans that are computationally feasible with respect to all constraints and no objective can be improved without compromising another. While theoretically there are an infinite number of fluence-based Pareto plans, the clinical implementation of MCO used in this study approximates this Pareto solution surface through a discrete set of plans that emphasize user-specified planning objectives (Figure 2). The first N discrete Pareto plans, where N is the number of specified trade-off objectives, are called anchor plans and separately optimize each objective. The $N+1th$ plan, called

the "balance plan," is a Pareto plan that optimizes each trade-off objective with equal weighting. Additional auxiliary plans can be generated to better approximate the Pareto surface representation if desired.

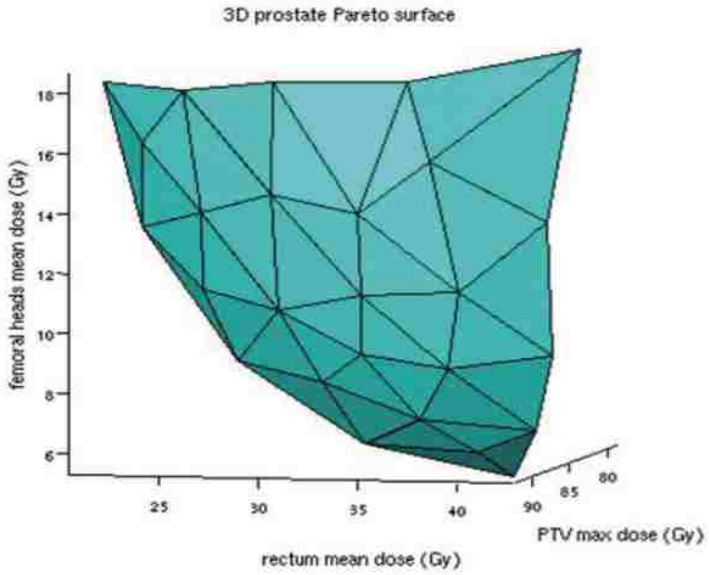

Figure 2: An example from RaySearch Laboratories of a three-dimensional Pareto surface for a prostate plan with three MCO trade-off objectives. The planner can search over this surface in real-time to consider different clinical trade-offs.[24]

After a patient-specific database of fluence-based Pareto plans is constructed, the planner can dynamically navigate over the computed solution space by adjusting weights assigned to each trade-off objective. Then the selected fluence-based Pareto plan is segmented into a deliverable plan through direct machine parameter optimization, which minimizes DVH differences between the navigated plan and the deliverable plan to optimize MLC segments.[25] Then finally, the clinical dose is computed.

Early investigations into the clinical viability of MCO suggest it improves IMRT plan quality and efficiency. Craft *et al.* reported an average IMRT planning time of five glioblastoma and five pancreatic cancer patients of 12 minutes using MCO, compared to 135 minutes using traditional inverse planning methods. The same study also found physicians blindly identified MCO IMRT plans as superior compared to the clinical plan designed through standard inverse optimization.[26]

Kierkels *et al.* showed novice planners using MCO could create high-quality IMRT head-and-neck plans with increased target dose homogeneity and reduced parotid dose compared with conventional clinical plans created by experienced planners.[27] Similar improvements in planning efficiency and quality have been found for MCO VMAT planning.[28,29] An example of the potential differences in dose distributions between inverse planning and MCO planning is shown in Figure 3.

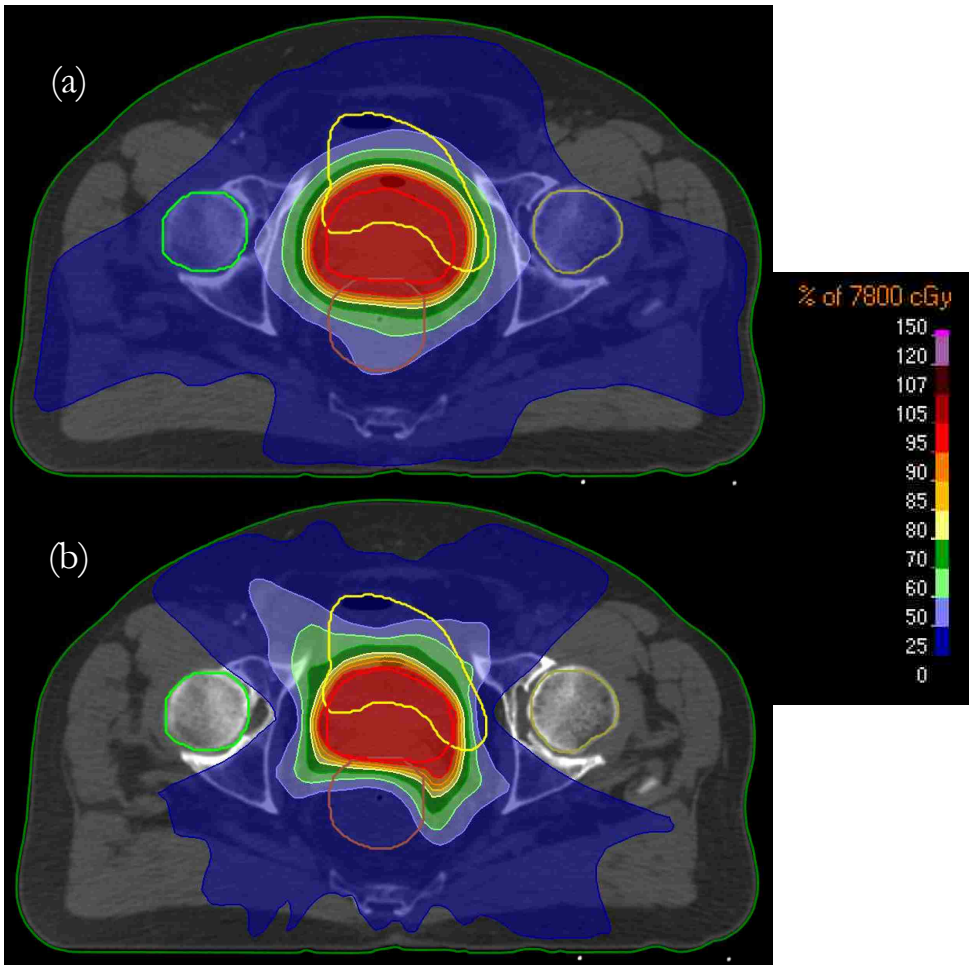

Figure 3: Example of dose distribution differences between inverse and MCO planning. The same axial CT slice of the same prostate patient is shown with the inversely optimized clinical VMAT plan on top (a) and a deliverable balance MCO VMAT plan on bottom (b). A noticeable reduction in OAR dose is shown in the MCO plan, particularly for both femoral heads.

While MCO is emerging as a viable clinical planning option for reducing inter-planner variations in plan quality, its overall dosimetric advantages versus traditional inverse planning remain inconclusive. The conversion of a navigated fluence-based dose distribution into a deliverable plan

can also degrade plan quality.[30] However, this effect is correlated with plan complexity and investigators have been working on multi-criteria direct-aperture optimization and other methods to maximally reduce this conversion error.[31-33] MCO's other limitations are its limited commercial availability and substantial computational cost, especially for cases requiring a large amount of trade-off objectives (e.g. head-and-neck cancer).[34,35]

1.1.3 KNOWLEDGE-BASED PLANNING

An alternative method proposed to reduce inter-planner variations in inversely optimized plan quality is knowledge-based planning (KBP). KBP methods have recently been introduced as a means of improving plan quality and consistency by leveraging anatomical and dosimetric data from previously treated patients to guide the planner in designing a plan for a new patient.

Knowledge-based concepts have been researched in many aspects of radiation oncology such as imaging informatics and segmentation.[36-39] However, KBP has become a main area of interest due to its potential applications in many aspects of the treatment planning process. For instance, KBP models have been used to predict patient-specific dose-volume objectives (based on the available previous knowledge) before inverse optimization. Chanyavanich *et al.* used such an approach with an algorithm based on mutual information to retrospectively predict prostate IMRT plans that were dosimetrically similar to the original clinical plans.[40] KBP models can also serve as post-planning quality control tools by flagging patient plans where lower OAR dose is predicted based on previous patient data. Wu *et al.* developed a quality control model to flag parotids planned with too high a dose in IMRT head-and-neck cases.[41] Also, KBP methods have been used in exploring the feasibility of automated planning systems that require no human intervention. Tol *et al.* recently assessed the ability of RapidPlan, Varian's commercial knowledge-based planning module, to automate plan quality assurance for clinical trials.[42] The possibility of achieving fully automated clinical treatment planning within the next ten years was recently debated.[43] If this goal is to be

realized at any point in the future, let alone in ten years, KBP research may be important in its development and implementation.

In a general KBP dose prediction model, a database of previously treated patients with high-quality treatment plans is established. Then for a new patient (to be planned), the database is searched for a subset of prior patients with similar anatomy to the new patient. The dose data from those anatomically similar database patients are then used to predict dose-volume objectives for the new patient's plan. This KBP method provides empirical dose predictions based on the patient's unique anatomy. This kind of patient-specific *a priori* information is not present in the current clinical planning paradigm, where population-based dose tolerances for OARs are typically applied as planning constraints. Moreover, a KBP model can explicitly predict personalized DVH objectives or dose-volumes for new patients using previous patient data.

Several approaches to KBP have been described in the literature. Appenzoller *et al.* proposed a KBP method using mathematical models to predict achievable OAR DVHs based on patient anatomy to reduce IMRT planning variability and improve treatment plan quality.[44] They separated each OAR into sub-volumes based on the distance a collective group of voxels was away from the planning target volume (PTV) surface. Then all sub-DVHs (DVHs of the individual sub-volumes) were fitted to skew-normal distributions, which were used to predict DVHs. This predictive DVH model has been successfully used in quality control studies for IMRT planning.[23,45] Shiraishi *et al.* further adapted this methodology to predict DVHs and identify sub-optimal plans for stereotactic radiosurgery (SRS) cases.[46] Good *et al.* developed a KBP model to predict dose for 7-field IMRT prostate plans based on the mutual information between the beam's-eye-view projections of a new patient and database patients. They found the KBP plans to have superior (i.e. lower) bladder and rectum DVHs compared to original clinical plan in 40% of cases.[47] Moore *et al.* observed increased normal tissue sparing and reduced inter-planner variability in IMRT prostate and head-and-neck

cases after implementing a KBP model that correlated OAR volume overlapping the PTV with mean OAR dose.[48] Principal component analysis (PCA) based KBP models have also been used to investigate how anatomical and dosimetric features affect OAR dose in prostate and head-and-neck patients for DVH prediction purposes.[49-52] Varian's commercial KBP optimization engine RapidPlan (Varian Medical Systems, Palo Alto, CA, USA) uses a combination of PCA and regression models to estimate DVH predictions.[53] Nwankwo *et al.* developed an algorithm that predicted dose to each OAR voxel in VMAT plans of prostate patients by learning OAR sparing patterns from a database of previous clinical plans.[54] Similarly, Shiraishi *et al.* used previously treated VMAT prostate and SRS head-and-neck plans to train an artificial neural network to predict patient-specific dose matrices for new cases.[55] Each of these studies aims to simultaneously improve plan quality and reduce plan variability regardless of changing patient and planning variables.

1.1.4 THE OVERLAP VOLUME HISTOGRAM IN KBP

The quality of a treatment plan depends primarily on patient anatomy, particularly the geometrical relationship between PTVs and OARs. Using mathematical phantoms, Hunt *et al.* showed that PTV uniformity and maximum OAR dose depend strongly on PTV-OAR geometry, specifically the distances between them.[56] They also performed a separate study that showed a correlation between the OAR volume overlapping the PTV and OAR sparing in head-and-neck cases.[57] Similarly, studies on examining prostate cancer have shown an increase in rectum and bladder dose as prostate and seminal vesicle volumes increase.[58]

The investigations on anatomical influence on dosimetric outcomes have led to several novel metrics relating patient anatomy to dose prediction. One common metric used in KBP DVH prediction models to correlate patient geometry to OAR dose is called the overlap volume histogram (OVH). Introduced by Kazhdan *et al.*, the OVH is a shape relationship descriptor that quantifies a patient's anatomy by defining the distance a fractional OAR volume lies from the PTV surface.

More specifically, it is defined for a target *T* and organ *O*, where the value of the OVH of *O* with respect to *T* at distance *r* is defined as the fractional organ volume a distance of *r* or less from the target:

$$OVH_{O,T}(r) = \frac{|\{p \in O | d(p,T) \leq r\}|}{|O|}, \quad (1.1)$$

where *d(p,T)* is the signed distance of a point *p* from the target's boundary and $|O|$ is the volume of the OAR.[59]

The clinical viability of OVH-driven quality control tools and KBP methods have been investigated due to the metric's robustness and ease of clinical implementation. Wu *et al.* used the OVH within a KBP method as an anatomical similarity metric for matching a new patient to previous IMRT head-and-neck patients in a database. Their OVH-driven KBP model predicted DVH objectives for the new patients, which led to significant decreases in planning time and dose to the spinal cord, brainstem, and contralateral parotid.[60] They have also shown the effectiveness of KBP methods utilizing the OVH in improving the quality, efficiency, and consistency of simultaneous integrated boosted-IMRT and VMAT planning for head-and-neck cancer.[61,62] Further, they have adapted their OVH-driven KBP methodology for robotic stereotactic body radiotherapy (SBRT) and were able to improve bladder and rectum sparing in prostate cases.[63] Likewise, Zhu *et al.* introduced the distance-to-target histogram (DTH) as a metric to estimate OAR DVHs to improve IMRT plan quality.[49] The DTH is virtually identical to the OVH, but Zhu *et al.* differentiate their DTH by incorporating non-Euclidean distance metrics.[64]

All OVH-driven KBP methods assume that the dose received by a fractional OAR volume depends on its proximity to the PTV, which is described quantitatively by the OVH. Therefore, each point on an OAR's OVH can be mapped to one point on the corresponding DVH, establishing a one-to-one relationship for each OAR of each database patient. This one-to-one distance-to-dose mapping can be formed by relating a distance r_v of an OVH for a fractional OAR volume *v* to a

dose-volume D_v of a DVH (Figure 4). This serves as the foundation of using the OVH as an anatomical similarity metric in a KBP model for predicting DVH dose-volumes. Further, the simple yet powerful nature of the OVH makes it a desirable metric to relate patient anatomical features to optimally achievable dose distributions in KBP methods.

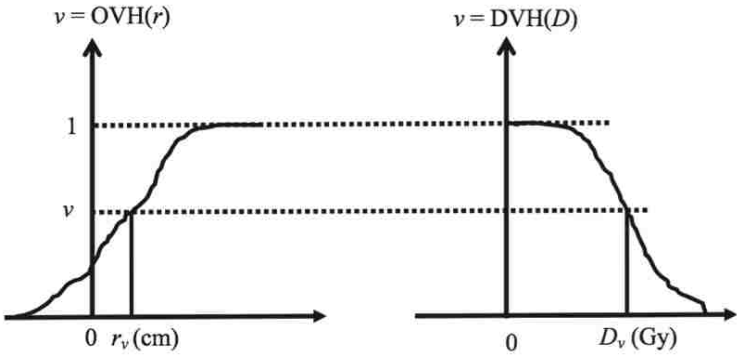

Figure 4: Illustration from Wu *et al.* relating the distance a fractional OAR volume (v) lies from the PTV surface (r_v) on the OVH (left) to the dose the fractional volume receives (D_v) on the DVH (right).[63]

1.2 MOTIVATION FOR RESEARCH

Many of the previous studies have concluded that the performance or accuracy of a particular KBP model depends directly on the quality of the plans in the patient database.[60,65-69] These original database plans in a majority of KBP studies were created via inverse planning, which means the KBP models are still subject to the same deficiencies of inverse planning. Recognizing this, Schmidt *et al.* utilized dose warping and scaling reduce the impact of sub-optimal inverse plans on the performance on their mutual information-based KBP model.[66] Sub-optimal clinical plans are difficult to detect due to the substantial time and labor involved in fully assessing clinical trade-offs through the trial-and-error process of inverse optimization. Plan quality fluctuations can also result from varying planning priorities from patient-to-patient and planner-to-planner (or physician-to-physician). In fact, Wang *et al.* recently used an in-house TPS to evaluate the performance of an OVH-driven KBP method based on Pareto optimal treatment plans for prostate cases, independent of these non-uniform treatment planning priorities.[69] They found the OVH model was highly

accurate in predicting rectum and anus dose, but systematically underestimated achievable bladder dose likely due to the bladder's lower planning priority relative to the rectum. However, the potential improvements in OVH-driven KBP performance utilizing a plan database with uniform planning priorities and void of sub-optimal inverse plans have not been examined to our knowledge.

KBP's susceptibility to planner bias and plan variations can be avoided through the use of MCO at the cost of computational burden. Therefore, the purpose of this study was to investigate the performance of a MCO-driven KBP planning approach as an efficient solution. Specifically, this work examined OVH-driven KBP dose-volume prediction dependence on database plan quality for VMAT treatment planning of the prostate. The study compared the use of a database containing manual, inversely optimized clinical plans (referred to as the CPD – clinical plan database) against a database of plans generated with MCO (referred to as the MCOD). Two sets of OVH-driven KBP dose-volume predictions for the bladder and rectum were generated: one set derived from the original clinical plan data (CPD) and the other set derived from the Pareto optimal plan data (MCOD). The optimality of the two sets of predictions were compared and their achievability was verified through a re-planning study.

1.3 HYPOTHESIS AND SPECIFIC AIMS

The hypothesis of this work was that OVH-driven KBP predictions using a MCO plan database (MCOD) will lead to plans with statistically significant improvements ($p < 0.017$) in bladder and rectum dose while maintaining statistically equivalent or superior target and secondary OAR (femoral heads and penile bulb) dose, compared with using a clinical plan database (CPD). In order to test this hypothesis, three specific aims were developed for this study:

Aim 1: Establish a retrospective anonymous patient database; compile the OVH, CPD, and MCOD knowledge databases; investigate second-order factors influencing the distance-to-dose correlation strength while accounting for inter-planner variability.

Aim 2: Develop and apply OVH-driven KBP model for predicting bladder and rectum dose-volumes using each plan database; statistically analyze any dosimetric differences between CPD and MCOD KBP model predictions.

Aim 3: Perform a re-planning study by applying KBP dose-volume predictions as planning goals; statistically analyze differences between re-planned and predicted KBP model values to verify the achievability of KBP model predictions.

1.4 OVERVIEW OF THESIS

This document follows a manuscript-style thesis format. The introductory Chapter 1 contains background information for the entire study and establishes the motivation and central themes of this research. Chapter 2 and Chapter 3 mirror two separate manuscripts respectively prepared for submission to peer-reviewed scientific journals, of which the former has been submitted for peer-review at the time of writing this thesis. These two chapters contain their own materials and methods, results, discussion, and conclusions sections. Background and introductory information for both manuscript chapters were consolidated into Chapter 1 to avoid redundancies. Chapter 4 summarizes the overall findings of the study and discusses limitations and directions for future work. This thesis contains only one References section (again to avoid redundancies) and each cited work is listed in the order in which they appear in the document. Lastly, the Appendix contains extraneous methods and supplementary data either not mentioned or implicitly mentioned in the materials and methods sections of the thesis.

Generally, the specific aims laid out in Chapter 1.3 are addressed chronologically in this thesis. In other words, if aligning the specific aims to specific chapters, Aim 1 is contained in Chapter 2 while Aims 2 and 3 are contained in Chapter 3. However, certain aspects of the specific aims are inherently present in both manuscript chapters.

CHAPTER 2. AN IMPROVED DISTANCE-TO-DOSE CORRELATION FOR PREDICTING BLADDER AND RECTUM DOSE-VOLUMES IN KNOWLEDGE-BASED VMAT PLANNING FOR PROSTATE CANCER

2.1 MATERIALS AND METHODS

2.1.1 PATIENT DATABASE

We developed a database, compliant with the Health Insurance Portability and Accountability Act (HIPAA), of 124 prostate cancer patients previously treated at Mary Bird Perkins Cancer Center. Selected patients were prescribed dose to a single PTV and treated using two coplanar, 6 MV VMAT beam arcs. Patients with artificial hip prostheses, where beams are prohibited from entering through the implant, and patients with sequential boosts were excluded. Selected patients included those having post-operative prostate fossa, seminal vesicle involvement, and pelvic lymph node involvement where only a single PTV was irradiated. A statistical summary of the resulting patient database is shown in Table 1.

All patients in the database had an existing treatment plan that had been manually optimized by different planners using the commercial TPS currently used clinically at our institution (Pinnacle3, v9.8, Philips Medical Systems, Hanover, WI, USA). For the purpose of the present study, it was desirable to reduce planner-to-planner variability. Accordingly, all database patients were re-planned with a different commercial TPS with available tools for minimizing inter-planner variability (RayStation, v4.5.1.14, RaySearch Laboratories, Stockholm, Sweden).

Specifically, re-plans were objectively generated for each database patient using MCO. As mentioned previously, MCO is a novel optimization algorithm based on a combination of Pareto optimal plans generated from user-specified trade-off objectives and constraints. Pareto optimal plans are those where the constraints are computationally feasible and no objective can be improved without worsening another. In the TPS, a "balanced plan" is the Pareto plan giving equal weight to all objectives.[24] Previous studies have indicated MCO can provide superior plan quality and planning

Table 1: Distribution of patient characteristics in the database. The selected patients cover a wide range of prescription doses, treatment areas, and target volumes. SV stands for seminal vesicle involvement and LN stands for lymph node involvement.

Prescription Dose Range (cGy)	Number of Patients
4500 - 7000	38
7000 - 7600	43
7600 - 8100	33
8100	10
Treatment Area	
Prostate Only	66
Prostate Fossa	23
Prostate + SV Or Prostate + SV + LN	35
PTV Volume Range (cm^3)	
69 - 150	22
150 - 225	56
225 - 300	19
300 - 729	27

efficiency compared to traditional inverse planning.[26,29] Therefore, the MCO balance plan for each patient was used to maximize both plan consistency and quality. Each MCO plan was created to match the previous prescription dose using a standard set of trade-off objectives and constraints, which produced consistent Pareto optimal dose distributions (Table 2). In order to account for patients with different prescription doses, the dose for each patient was normalized such that 95% of the PTV received 7600 cGy. It is important to note the effects of this scaling were examined and found to have no measurable impact on the dose distributions, allowing for inter-plan comparisons.

The scripting feature in RayStation was leveraged to automate the computation of bladder and rectum OVHs for each database patient by uniformly contracting or expanding the PTV in 1 mm step sizes. This OVH data was used to describe the PTV-OAR geometrical information of the database patients.

To determine the strength of the distance-to-dose relationship for 30, 50, 65, and 80% bladder and rectum dose-volumes of database patients, the correlations between database OVHs

and DVHs for those specific bladder or rectum dose-volumes were calculated using the Pearson product-moment correlation coefficient (R).

Table 2: MCO planning objectives and constraints used in generating balance plans for each database patient. The Dose Fall-off objective for the External structure reduces dose outside of the target. Rx refers to the prescription dose.

Structure	Trade-off Objectives (cGy)	Constraints (cGy)
PTV	Uniform Dose = Rx	Min Dose = Rx Max Dose = Rx + 100
Bladder	Max EUD = 0, (a=2)	
Rectum	Max EUD = 0, (a=2)	
Left and Right Femoral Heads	Max EUD = 0, (a=2)	
Penile Bulb	Max EUD = 0, (a=2)	
External	Dose Fall-off = [H] 3000 [L] 0, Low Dose Distance = 5 cm	

2.1.2 SECOND-ORDER FACTORS

An array of dosimetric and anatomical second-order factors were chosen to examine for correlation with OAR dose. These factors included the derivative of the OVH (dOVH), prescription dose, PTV volume, bladder volume, rectum volume, and in-field OAR volume. The dOVH quantifies the specific orientation of the OAR relative to the PTV, where a higher dOVH value describes an OAR likely more difficult to spare than one with a lower dOVH. For example, it is possible for equal fractional OAR volumes in two different patients to have similar OVH distances, but have differing dOVH values that could lead to a difference in the dose each volume receives. In-field OAR volume was defined as the amount of OAR volume that lies within transverse planes located 6 mm (approximating the beam penumbra at depth) superior and inferior to the most superior and inferior aspects of the PTV respectively.

The ability of each second-order term to strengthen distance-to-dose correlations was quantified by computing the Pearson product-moment correlation coefficient (R). This coefficient was calculated for each factor and OAR dose-volume pair over each of the four fractional bladder

and rectum volumes previously listed in Chapter 2.1.1. The resulting correlation coefficients were averaged over the four fractional volumes for each OAR. The second-order factor with the strongest mean correlation with OAR dose was determined to be the strongest contributor to the DVH-OVH correlation variation for the given OAR.

2.1.3 IMPROVED DISTANCE-TO-DOSE CORRELATION

After the factor with the strongest effect on the distance-to-dose correlation variation was determined for the bladder and rectum, the DVH-OVH correlations were recomputed while including the second-order factor. These improved (OVH plus second-order term) correlations were compared to the nominal (OVH only) correlations to quantify any improvements in the database distance-to-dose correlations.

As will be shown in the Results section, the in-field OAR volume was found to be the strongest contributor to variations in correlation between distance and dose for both the bladder and the rectum. As such, the OVH was also recomputed by disregarding out-of-field volume. Described by Petit *et al.*, the in-field OVH is calculated similarly to the total OVH except only the in-field OAR volume is considered when determining the overlapping OAR volume with the contracted or expanded target volume.[65] This introduces a slight modification to Equation (1.1):

$$OVH_{O,T}(r) = \frac{|\{p \in O' | d(p,T) \leq r\}|}{|O|} \tag{2.1}$$

where *O'* is the portion of the organ *O* within the treatment fields (defined previously). The computational endpoint for the in-field OVH of a given OAR is when the PTV is expanded to overlap the entire in-field portion of the OAR's volume. Further, the in-field OVH distance for 100% overlap volume exists only when the entire OAR is within the defined treatment fields. Therefore, those patients in the database with fractional in-field OAR volumes less than the selected dose-volume value will not contribute to forming the dose-to-distance correlation. For example, if

only 67% of the bladder is within the treatment fields for a particular database patient, then that patient will not be included when calculating the correlation between the 80% dose-volume and the in-field OVH.

2.2 RESULTS

2.2.1 NOMINAL DVH-OVH CORRELATION

Using the nominal OVH to quantify anatomy, the DVH-OVH correlation showed a negatively linear relationship in both OARs for each fractional volume observed. Bladder dose showed a strong anticorrelation with distance, having a mean R = -0.79 over the four fractional volumes analyzed. Rectum dose also showed a strong anticorrelation with distance, having a mean R = -0.82 (Table 3). Figure 5 shows each nominal DVH-OVH scatter plot associated with each Pearson correlation coefficient listed in Table 3.

Table 3: Pearson correlation coefficients between nominal OVH distances and DVH dose-volumes of the bladder and rectum. An absolute value greater than 0.7 indicates a strong linear correlation with a maximum value of 1.

Dose-Volume	DVH-OVH R
Bladder	
D_{30}	-0.92
D_{50}	-0.83
D_{65}	-0.74
D_{80}	-0.66
Mean	-0.79
Rectum	
D_{30}	-0.94
D_{50}	-0.86
D_{65}	-0.78
D_{80}	-0.70
Mean	-0.82

The variation in distance-to-dose correlation across patients can be seen in Figure 5. For example, the reader is directed to the DVH-OVH plot for 65% of the rectum (Figure 5 (f)), where the range of D_{65} for an OVH distance of 2 cm was 643 to 3011 cGy. This spread in dose of greater

than 2300 cGy for a given OVH distance is consistent with previous studies and illustrates the motivation of the present study.[52,63,70]

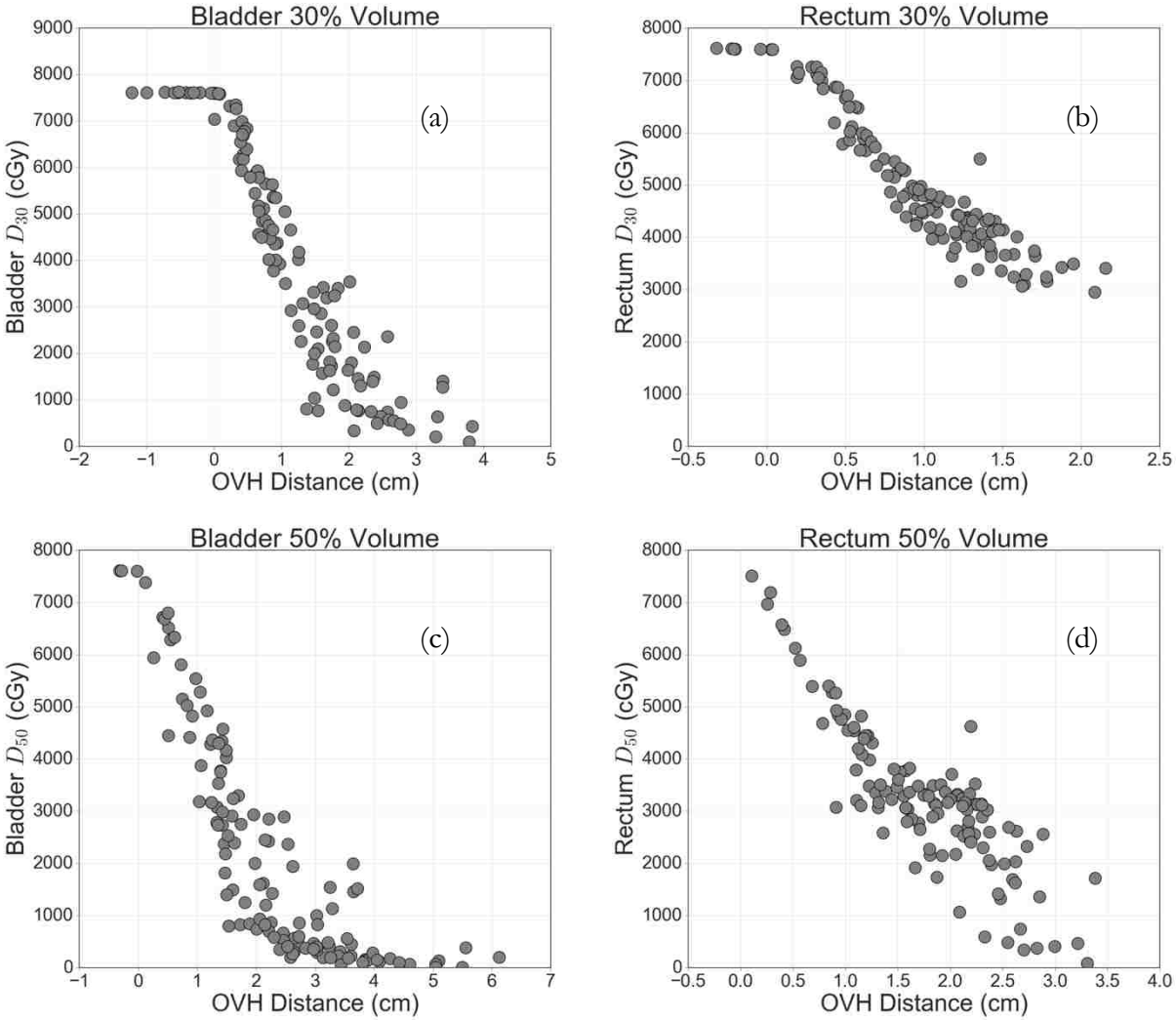

Figure 5: Nominal DVH-OVH correlations for 30, 50, 65, and 80% dose-volumes of the bladder (a, c, e, g) and rectum (b, d, f, h).

(Figure 5 continued)

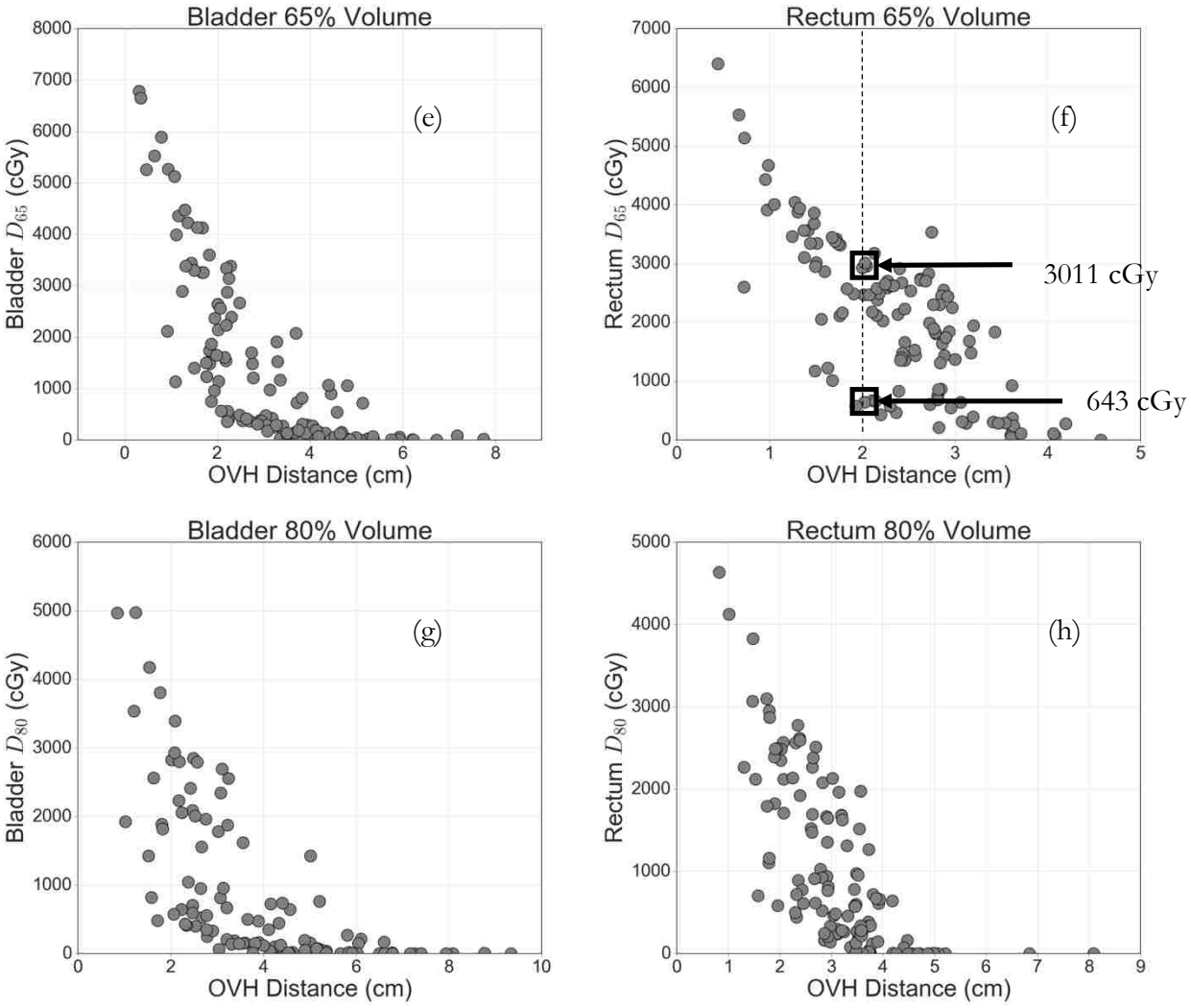

2.2.2 SECOND-ORDER FACTORS

Each previously investigated second-order factor was introduced as a variable into the nominal DVH-OVH correlation for each fractional volume of the bladder and rectum via a color bar. The variables were visually inspected via these color bar scatter plots to assess relational dependence between the second-order factors and dose for the fractional OAR volumes. Of all the factors studied, only the in-field OAR volume showed any noticeable influence on OAR dose, as seen in Figure 6 (c) and (d). The data indicated that, as the in-field OAR volume increases, the dose-volume value for the associated OAR also increases. This trend was observed in all scatter plots for

every fractional volume DVH-OVH of the bladder and the rectum. For the other factors investigated, no such trends were noted (see Figure 6 (a) and (b)).

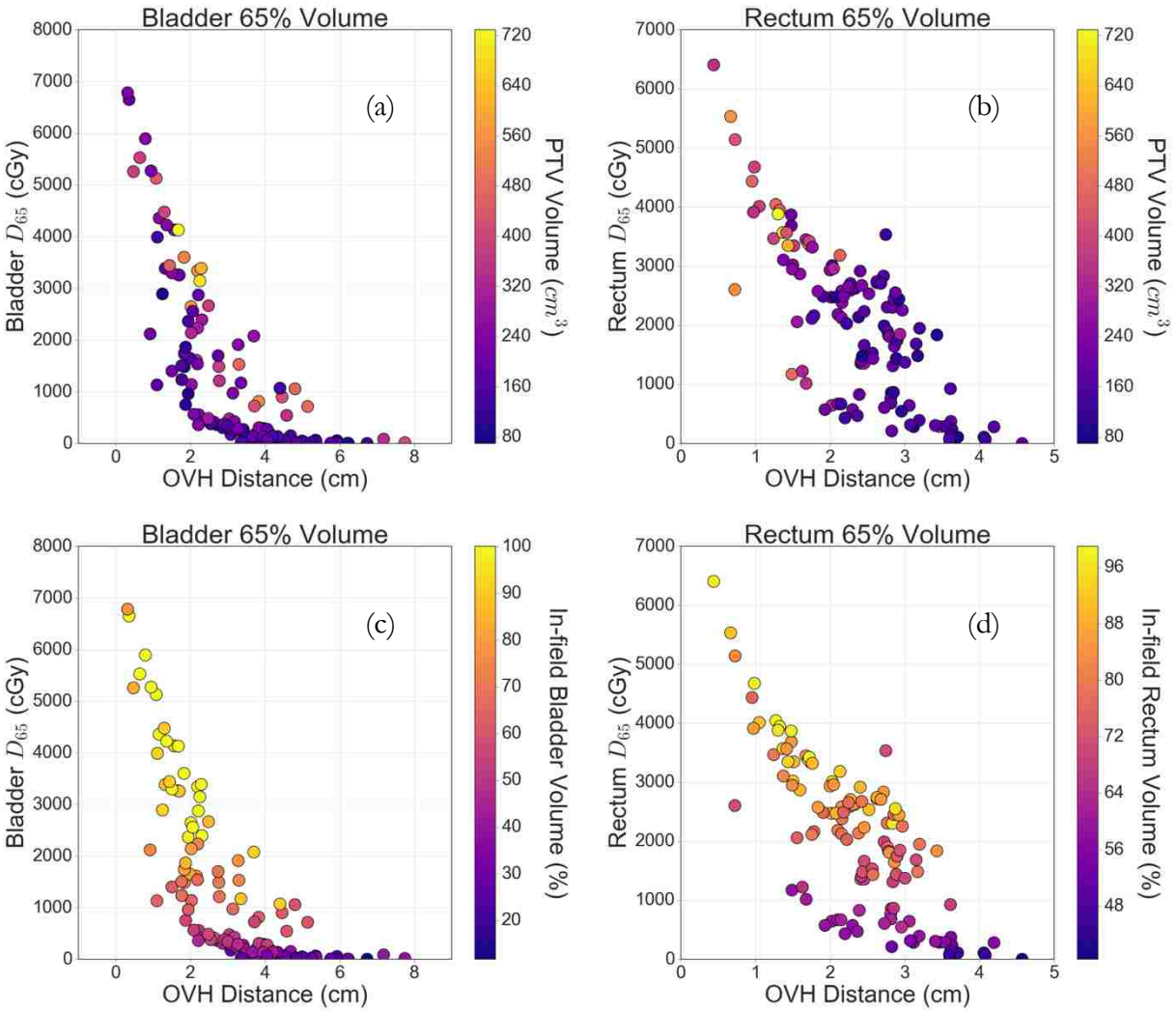

Figure 6: Sample color scatter plots for qualitative review of dependence on the examined second-order factors. There is no visible relationship between dose and PTV volume for neither 65% of the bladder (a) nor the rectum (b). When analyzing in-field OAR volume however, a clear relationship with D_{65} for the bladder (c) and rectum (d) can be seen.

Pearson correlation coefficients between second-order factors and bladder and rectum dose-volumes are listed in Table 4. Of the six variables inspected, only in-field OAR volume showed a strong correlation with OAR dose for both the bladder (mean R = 0.86) and the rectum (mean R = 0.76). The in-field OAR volume had a correlation coefficient of greater than 0.7 for each bladder and rectum dose-volume, except for D_{30} of the rectum. While the dOVH was strongly correlated

with D_{30} (R = 0.75) and D_{50} (R = 0.74) of the rectum, the in-field OAR volume resulted in a stronger correlation with rectum dose overall. This indicates in-field OAR volume had the strongest correlation with OAR dose out of the evaluated factors, confirming the qualitative indications.

Table 4: Pearson correlation coefficients between each second-order factor and DVH dose-volumes for the bladder and rectum. The mean Pearson coefficient over the four fractional volumes is also listed. Only the in-field OAR volume was strongly correlated (mean greater than 0.7) for both the bladder and rectum.

Dose-Volume	dOVH	Rx Dose	PTV Volume	Bladder Volume	Rectum Volume	In-field OAR Volume
Bladder						
D_{30}	0.62	-0.44	0.50	-0.53	0.20	0.90
D_{50}	0.56	-0.41	0.41	-0.55	0.19	0.88
D_{65}	0.52	-0.41	0.39	-0.52	0.17	0.85
D_{80}	0.48	-0.43	0.38	-0.53	0.18	0.83
Mean	0.54	-0.42	0.42	-0.53	0.19	0.86
Rectum						
D_{30}	0.75	-0.60	0.77	0.16	-0.11	0.56
D_{50}	0.74	-0.49	0.67	0.05	-0.07	0.74
D_{65}	0.67	-0.43	0.56	-0.07	-0.02	0.87
D_{80}	0.55	-0.53	0.60	-0.11	-0.09	0.85
Mean	0.68	-0.51	0.65	< 0.01	-0.05	0.76

2.2.3 IMPROVED DVH-OVH CORRELATION

The distance-to-dose correlation showed improvement when the in-field OAR volume was accounted for in the computation of the OVH (Table 5). For the bladder, the in-field OVH strengthened the mean correlation coefficient from -0.79 to -0.85 over the four fractional volumes. While for the rectum, the mean correlation strengthened from -0.82 to -0.86. This increase in correlation strength was especially noticeable at the 80% fractional volume level for both the bladder and rectum, where the 80% bladder DVH-OVH R strengthened from -0.66 to -0.77 and the value for 80% rectum improved from -0.70 to -0.86.

An illustrative example of the differences between the DVH-OVH correlations using the nominal OVH versus the in-field OVH can be seen in Figure 7. Accounting for the in-field OAR volume in the OVH computation resulted in an improvement in the distance-to-dose correlation for

65% and 80% of the bladder (Figure 7 (a) and (c) respectively) and rectum (Figure 7 (b) and (d) respectively). It is important to reiterate that the decrease in data points for the higher fractional in-field OAR volumes is due to certain database patients not meeting the given in-field OAR volume threshold.

Table 5: Pearson correlation coefficients between in-field OVH distances and DVH dose-volumes of the bladder and rectum. The correlation coefficients between the nominal OVH distances and DVH dose-volumes from Table 3 are also listed for comparison. Note that n refers to the number of database patients with in-field OAR volumes greater than or equal to the given dose-volume.

	DVH-OVH R	
Dose-Volume	Nominal OVH	In-field OVH
Bladder		
D_{30}	-0.92	-0.91 (n = 108)
D_{50}	-0.83	-0.88 (n = 76)
D_{65}	-0.74	-0.85 (n = 52)
D_{80}	-0.66	-0.77 (n = 35)
Mean	-0.79	-0.85
Rectum		
D_{30}	-0.94	-0.93 (n = 124)
D_{50}	-0.86	-0.84 (n = 117)
D_{65}	-0.78	-0.82 (n = 90)
D_{80}	-0.70	-0.86 (n = 49)
Mean	-0.82	-0.86

With regards to the representative example of the distance-to-dose correlation variation at 65% of the rectum introduced earlier (referencing Figure 5 (f)), Figure 7 (b) shows the reduction in the dose spread at an OVH distance of 2 cm from using the in-field OVH method. The group of patients with rectum D_{65} less than 10 Gy have very low doses to the rectum, most likely due to having less than 65% of the rectum inside the treatment fields. The removal of these patients using the in-field OVH term reduces the dose spread at the OVH distance of 2 cm from over 20 Gy with the nominal OVH method to less than 10 Gy.

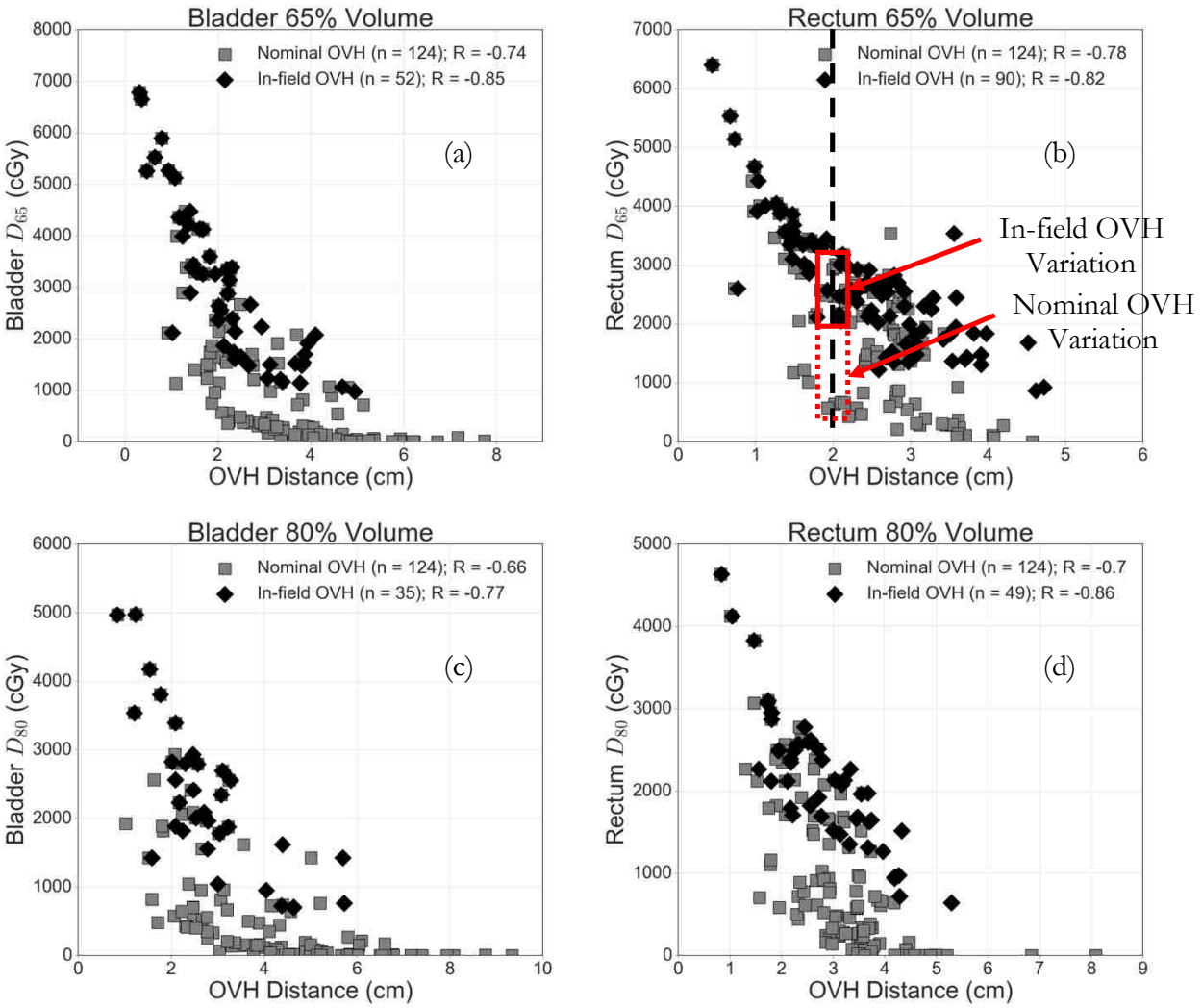

Figure 7: Representative examples of improved distance-to-dose correlations using the in-field OVH compared with the nominal OVH. The figure legends contain the number of patients (n) and the Pearson correlation coefficients (R) for each OVH method. The square nominal OVH data points are equivalent to the scatter plots shown in Figure 5.

2.3 DISCUSSION

In-field OAR volume was observed to be the largest contributor to variations in the distance-to-dose relationship for fractional overlap volumes of bladder and rectum in prostate patients treated with VMAT, independent of inter-planner bias. Specifically accounting for OAR volume within the treatment fields when computing the OVH strengthened the OVH's correlation with the bladder and rectum dose in these patients. This proposed OVH refinement eliminates data points that would likely produce unachievable dose predictions in an OVH-guided KBP tool. This

was evidenced by the consistent removal of a large portion of low-dose data points, which facilitated the strengthening of the distance-to-dose correlations. This was seen most clearly for the lower dose-volumes of both OARs e.g. D_{65} and D_{80} shown in Figure 7. Therefore, determining in-field OAR volume as an influencing factor in the DVH-OVH correlation, and accounting for this through the in-field OVH, will allow for more achievable and accurate dose predictions for OVH-guided KBP models.

Previous studies have refined OVH-guided KBP methods for different treatment sites to generate more precise planning predictions without fully quantifying the resulting effects on the distance-to-dose correlation used to estimate the DVH objectives. Reddy *et al.* found prostate volume was directly proportional to bladder and rectum dose in 3D-CRT and IMRT plans.[58] Similarly, Wu *et al.* implemented an empirical PTV volume filter, querying a patient database for a subset of patients with specific OVH values and similar PTV volumes for their KBP method for localized prostate patients treated with robotic SBRT.[63] This work shows PTV volume to be moderately correlated with bladder dose (mean R = 0.42) and rectum dose (mean R = 0.65), which validates PTV volume as a simple, yet viable second-order factor when predicting bladder and rectum dose-volumes for OVH-guided KBP methods for prostate patients. However, our work also shows that filtering patients based on in-field bladder and rectum volume and even dOVH would provide an even stronger distance-to-dose model compared to using PTV volume, resulting in more robust dose-volume predictions. While in-field OAR volume may not be as easily defined for robotic SBRT as with VMAT treatments given the multitude of non-coplanar and non-isocentric beams, the relationship between OAR dose and in-field volume should hold across different treatment techniques.

This work also confirms and builds upon the findings by Petit *et al.*, who demonstrated that utilizing the in-field OVH will result in more accurate and fewer unachievable dose predictions for

cases with sizable portions of nearby OARs lying outside the treatment fields.[65] While their group analyzed the in-field OVH's effects with pancreatic adenocarcinoma patients treated with IMRT, our similar findings with VMAT prostate cases support the in-field OVH's efficacy in OVH-guided KBP methods in any treatment site. A novel component of our study is the reduction of inter-planner variability through the generation and implementation of a Pareto optimal plan database. Even with this decrease in inter-planner subjectivity, the in-field OAR volume was still found to be the strongest second-order factor correlating with OAR dose in these standardized plans. Another noted difference between these two studies is the definition of in-field volumes. Petit *et al.* defined a 1 cm margin around the beams-eye-view of the PTV as the field edges, where we defined our in-field transverse plans to be 0.6 cm superior and inferior of the most superior and inferior aspects of the PTV. Differences in results depending on in-field volume definitions would require further analysis. Regardless, our results support the claim that accounting for in-field OAR volume will lead to more precise and accurate OVH-driven KBP dose predictions.

Additionally, this study supplements the results reported by Yuan *et al.*, who analyzed factors impacting interpatient OAR dose sparing. While they used a stepwise multiple regression model on prostate and head-and-neck IMRT treatments, out-of-field OAR volume (converse to in-field volume) was found to be a significant factor in determining OAR dose sparing.[52] It should also be noted this group utilized a non-Euclidean form of the OVH to account for voxels outside treatment fields to form their distance-to-dose correlation, resulting in a reduction in the correlation variation. Our work shows a similar reduction in distance-to-dose correlation spread using the in-field OVH.

This study presents a comprehensive analysis and review of second-order factors potentially influencing the distance-to-dose relationship, which serves as the foundation for OVH-driven KBP dose prediction methods. As opposed to previous studies using patient cohorts with uniform beam configurations, dose prescriptions, and disease types, this work analyzes distance-to-dose correlation

behavior in a large patient database with a wide range of treatment parameters and structure volume sizes. Another feature unique to this work, that must be reiterated, was the implementation of an objective and standardized MCO planning protocol applied to each of the 124 database patients. This served to maximally reduce plan quality variations from patient to patient due to the inherent subjectivity and inconsistencies from inverse treatment planning and inter-planner variations. The composite impact of these factors was inspected over the low-, medium-, and high-dose levels of the OAR DVHs, capturing the overall influence each factor has on the distance-to-dose correlation.

These results indicate an improvement in the distance-to-dose correlation, which can be implemented in existing OVH-guided KBP dose prediction tools by recalculating the OVH based on in-field OAR volume. While this reduction in the DVH-OVH correlation variation should lead directly to more accurate and less unachievable predictions in a prostate KBP protocol, a comprehensive retrospective study needs to be performed to confirm this conclusion. However, this study was primarily focused on how second-order factors impacted the distance-to-dose relationship in prostate patients treated with VMAT. Although knowledge from this and previous studies indicate in-field OVH strengthening the DVH-OVH correlation should generalize to other treatment sites, site-specific investigations are needed to support implementation of the in-field OVH.

Although the in-field OVH demonstrated a reduction in distance-to-dose correlation spread, further study is needed to investigate how accounting for moderately influencing factors (such as the dOVH) would affect this spread. Further, these models could be applied in an existing OVH-guided KBP dose prediction tool and a study could be performed to quantify and compare the accuracy and achievability of the predictions generated from the unadjusted and adjusted distance-to-dose correlations.

2.4 CONCLUSIONS

This work shows the use of the OVH in KBP methods can be improved by accounting for in-field OAR volume. Planner bias was minimized by objectively generating Pareto optimal VMAT plans for each prostate patient in a large, retrospective database. This facilitated the examination of non-systematic contributors or second-order factors affecting inter-plan variability. Out of the various treatment and patient parameters investigated, in-field OAR volume was found to correlate strongest with OAR dose for both the bladder and rectum. Also, the dOVH was found to be the next strongest correlating factor with both bladder and rectum doses, while rectum volume correlated least with bladder dose and bladder volume correlated least with rectum volume. Differences in prescription dose and PTV volume were found to be moderately correlated with bladder and rectum doses. The incorporation of the in-field volume into the OVH showed a reduction in distance-to-dose correlation variation, which can lead to more precise and achievable dose predictions in KBP methods.

CHAPTER 3. USING THE BEST KNOWLEDGE: IMPROVED KNOWLEDGE-BASED DOSE PREDICTIONS IN VMAT PLANNING FOR PROSTATE CANCER BY USING A PARETO PLAN DATABASE

3.1 MATERIALS AND METHODS

3.1.1 PATIENT DATABASE

A HIPAA-compliant database of 124 prostate cancer patients previously treated at our institution was created for this study. Selected patients had only one PTV and were treated with two coplanar 6 MV VMAT arcs. Patients with artificial hip implants were excluded due to the reduction in degrees of freedom of the treatment arc. Additionally, patients with a sequential boost to a sub-volume of the initial PTV were excluded. However, post-operative prostate fossa patients were included, as were patients with seminal vesicle and lymph node involvement so long as only one PTV was defined (Table 1). In order to compare patient plans with differing prescription doses, each patient's dose was normalized so that 95% of the PTV received 76 Gy.

3.1.2 KNOWLEDGE DATABASES

The DICOM image set, structure, plan and dose files of all 124 selected database patients were imported into a research database of a commercial TPS (RayStation v4.5.1.14, RaySearch Laboratories, Stockholm, Sweden). Anatomical and dosimetric knowledge databases were then compiled.

The clinical viability of the OVH as a feature metric in KBP methods has been tested due to the metric's robustness and simple clinical implementation.[60-63] Early research into the effectiveness of the OVH for sites with large OARs extending outside the treatment fields has demonstrated the potential advantages of accounting for the out-of-field OAR volumes through the OVH.[52,65] This can be done through the in-field OVH, which modifies the standard OVH to include the OAR volume only within the treatment fields. Compared to the standard OVH, we have observed the in-field OVH to improve the distance-to-dose correlation for bladder and rectum dose-volumes in

VMAT prostate cases independent of planner-bias. Therefore, the in-field OVH metric was used to quantify the anatomical information of each database patient.

A custom script supported by the TPS (IronPython, Apache) was written to calculate the in-field OVH for each patient's bladder and rectum. The in-field OVH was computed by expanding and contracting the PTV in 1 mm increments until there was either complete overlap or no overlap with the in-field portion of the given OAR. In this study, "in-field" was defined as the volume extending laterally to the external patient surface and longitudinally between planes located 6 mm superior and 6 mm inferior to the edges of the PTV. The value of 6 mm was chosen to approximate the penumbra of the treatment fields.

To establish the clinical plan database (CPD), a separate script was developed to extract the dose volume histogram (DVH) data from each patient clinical treatment plan. The DVHs of the PTV, bladder, rectum, femoral heads, and penile bulb (if segmented) for each patient were extracted from the TPS and placed in a repository which, along with the anatomic information, formed the CPD. Here, the bladder and rectum will be referred to as the primary OARs and the femoral heads and penile bulb as secondary OARs.

For the creation of the MCO database (MCOD), each database patient was re-planned using MCO functionality available within the TPS and using the original DICOM image and structure sets of the patient. In the TPS, a Pareto plan is generated for each of the user-defined objectives, with each plan fully optimized for that specific objective. An additional Pareto plan, called the "balance plan," is created with each of the trade-off objectives weighted equally. The user is then able to dynamically navigate over a linear combination of these plans (i.e. the Pareto surface) to assess different clinical trade-offs in search of a desired solution for the specific patient. In this study, each MCO plan was optimized with a standard set of prescription-specific trade-off objectives and constraints (Table 2). After the generation of the Pareto plan databases were completed for each

patient, a script was written to extract DVHs from each patient's balance plan. These dose data were placed into a different repository which, along with the same anatomic information used with the CPD, formed the MCOD.

3.1.3 KBP PREDICTIONS AND ANALYSIS

A KBP method of predicting dose-volumes for the rectum and bladder using the in-field OVH was developed for this study. The process generally follows the methodology described by Wu *et al.* and is briefly described here.[60]

The fundamental assumption of the approach is that the dose received by a fractional OAR volume depends on its proximity to the PTV, which is described quantitatively by the in-field OVH. Therefore, each point on an OAR's in-field OVH can be mapped to one point on the corresponding DVH, establishing a one-to-one relationship for each OAR of each database patient. This in-field OVH to DVH mapping, in turn, allows the DVH of a new patient to be predicted from database patients queried to have similar OAR-PTV anatomy (i.e. in-field OVH values).

Mathematically, given a new patient *n* with an in-field OVH distance of $r_{v,n}$ for a specified fractional OAR volume of *v*, the dose that fractional volume receives ($D_{v,n}$) can be estimated from a knowledge database of *i* patients by:

$$D_{v,n} = \min\{D_{v,i} | r_{v,i} \leq r_{v,n}\} \tag{3.1}$$

The subset of database patients where $r_{v,i} \leq r_{v,n}$ represents cases where the in-field OVH values imply the fractional OAR volumes are at least as difficult to spare as the new patient's geometry.

Dose-volumes were predicted for D_{10}, $D_{30,}$ D_{50}, D_{65}, and D_{80} fractional volumes of bladder and rectum. The dose-volume predictions were generated using a leave-one-out method, whereby each patient was removed from the database and assumed to be the "new" patient for whom dose-volumes would be predicted with the 123 database patients that remained.[71] This process was repeated until predictions were made for each database patient. Two sets of dose-volume predictions

were made for each database patient: one set using the CPD model and the other set using the MCOD model. For the case where $r_{v,n}$ was less than $r_{v,i}$ for all i database patients, no dose prediction was made. In this case, the newly introduced patient would have a fractional OAR volume closer to the PTV than any patient in the database. So an achievable dose-volume prediction cannot be accurately generated with the given knowledge. Also, given the nature of the in-field OVH, predictions were not possible for patients with fractional in-field OAR volumes less than the desired dose-volume prediction. For example, a prediction for a patient's bladder D_{50} would not be possible if less than 50% of that patient's bladder was within the treatment fields.

For each of the five dose-volumes of both OARs, three distributions of dose-volumes were compared: the set of original clinical values, the set of CPD KBP model predictions, and the set of MCOD KBP model predictions. Differences between the three data sets were tested for statistical significance using two-sided Wilcoxon signed-rank tests for each dose-volume. Statistical significance was set at $p = 0.017$, which results from applying a Bonferroni correction of three to the traditional significance level of 0.05.

3.1.4 PREDICTION PERFORMANCE AND ACHIEVABILITY

In order to confirm the achievability of KBP-predicted dose-volumes, 31 patients were randomly selected from the original database and re-planned using inverse optimization with the bladder and rectum KBP predictions as planning objectives. Because each patient had two sets of KBP dose-volume predictions, the lowest dose-volume prediction between the CPD and MCOD KBP models was used as the planning goal for each "new" patient. Again, bladder and rectum D_{10}, D_{30}, D_{50}, D_{65}, and D_{80} dose-volumes were used for these re-planning goals.

Re-plans attempted to maintain similar PTV and secondary OAR dose compared the original clinical plans while simultaneously aiming to attain the bladder and rectum KBP dose-volume predictions. This was done in order to make an assessment of the clinical achievability of the

predicted bladder and rectum KBP dose-volumes. Two-sided Wilcoxon signed-rank tests between the bladder and rectum KBP dose-volume predictions and the re-planned values were used to quantify prediction achievability. Two-sided Wilcoxon signed-rank tests were also used to verify the re-plans maintained clinical PTV and secondary OAR dose. The significance level for these statistical tests was set at $p = 0.05$. Various dose metrics were analyzed to compare PTV and secondary OAR dose shown in Table 6. In this study, the homogeneity index (HI) and conformity index (CI) were calculated according to their ICRU definitions:[72,73]

$$\mathrm{HI} = \frac{\mathrm{D_2} - \mathrm{D_{98}}}{\mathrm{D_{50}}} \tag{3.2}$$

$$\mathrm{CI} = \frac{\text{treated volume}}{\text{target volume}} \tag{3.3}$$

where the treated volume is defined in this study as the tissue volume that receives at least 95% of the prescription dose.

Table 6: Dose metrics used to statistically verify clinical PTV and secondary OAR dose was maintained in the re-plans. V_x represents the percent volume receiving x% of the prescription dose.

Planning Structure	Evaluated Dose Metrics
PTV	D_2, D_{50}, D_{98}, D_{max}, D_{mean}, D_{min}, V_{95}, V_{98}, V_{100}, V_{107}, HI, CI
Femoral Heads	D_2, D_{max}, D_{mean}
Penile Bulb	D_{mean}

3.2 RESULTS

3.2.1 DATABASE AND PREDICTION ANALYSIS

When comparing the DVHs from the two KBP plan databases, the MCOD showed better PTV coverage, primary OAR sparing and secondary OAR sparing (Figure 8). On average over the 124 database patients, the MCOD plans improved PTV HI ($p < 0.001$) and CI ($p < 0.001$) compared to the CPD plans. The MCOD plans yielded average decreases in D_{mean} of 21.9 Gy over both femoral heads ($p < 0.001$) and 9.9 Gy for the penile bulb ($p < 0.001$) compared to the CPD plans.

The MCOD plans also decreased the average D_{mean} of the bladder and rectum by 5.8 ($p < 0.001$) and 4.3 Gy ($p < 0.001$) respectively from the original clinical plans.

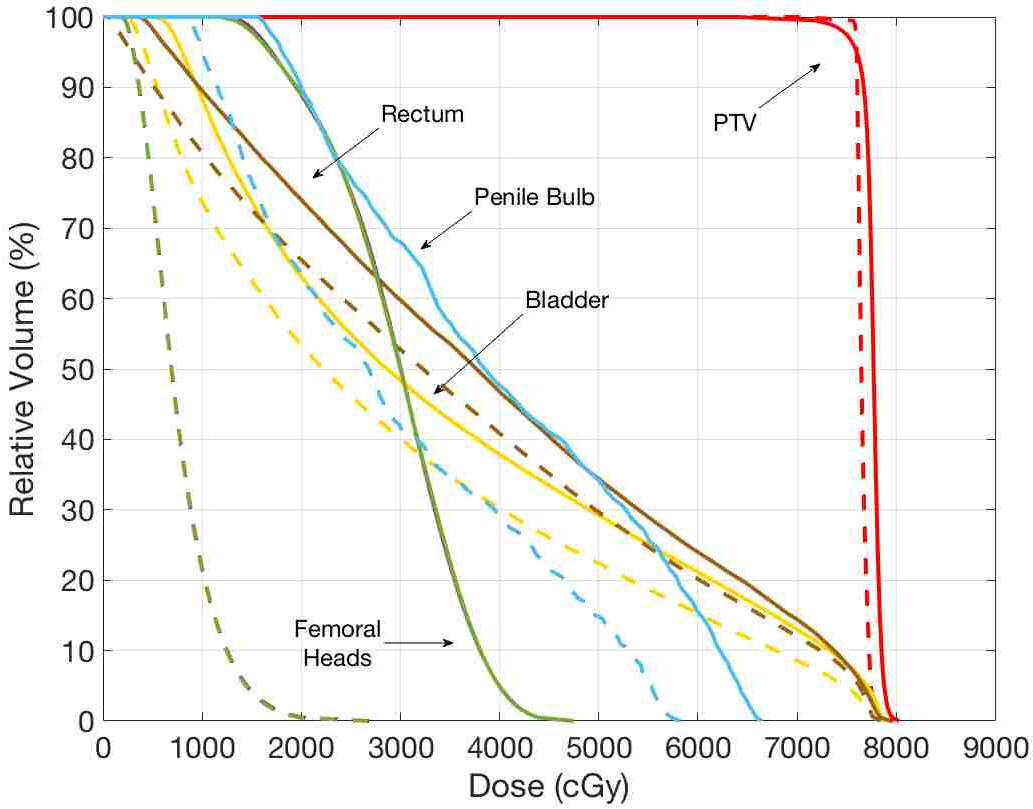

Figure 8: Comparison between the average DVHs of the labeled planning structures from plans in the CPD (solid lines) and MCOD (dashed lines). Note: the femoral heads are plotted separately (i.e. left and right femoral heads) but are difficult to resolve as they are nearly identical and their curves overlap each other.

Figure 9 shows boxplots of differences in bladder and rectum dose-volumes from the original clinical plans, the CPD KBP model predictions, and MCOD KBP model predictions. These boxplots show how both KBP models compare with the original clinical values including how the two KBP models compare with each other. When interpreting the plots in Figure 9, a positive value for either of the first two boxes indicates the KBP model prediction was lower than the corresponding clinical dose-volume. Additionally, positive values for the third box indicate the MCOD model prediction was lower than the corresponding CPD model prediction.

Both KBP models generated predictions with a lower median dose than the clinical plans for all five bladder and all five rectum dose-volumes. The medians of the MCOD KBP dose predictions were lower for all five bladder and three rectum dose-volume points compared to the corresponding CPD KBP medians.

The results from the statistical analysis comparing the patient database dose-volumes from the clinical plans, CPD KBP model, and MCOD KBP model are shown in Table 7. For each of the five bladder and five rectum dose-volumes analyzed, both the CPD and MCOD KBP model predicted statistically lower dose compared to the clinical plans ($p < 0.001$).

(a)

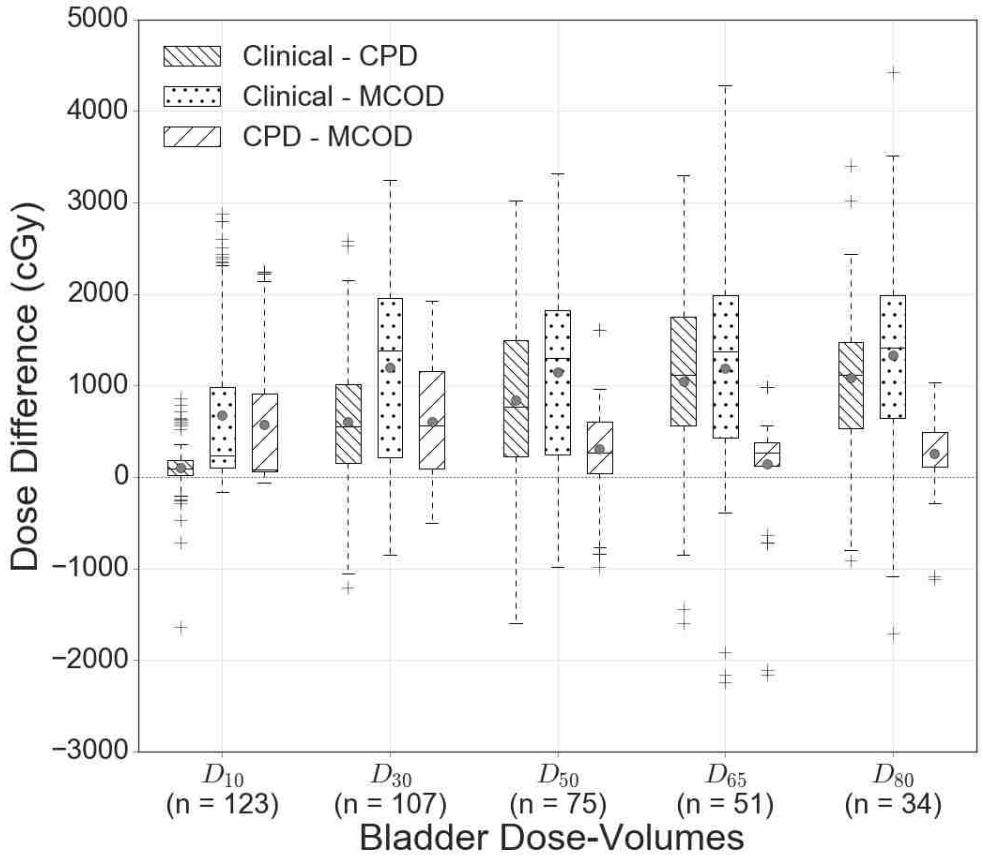

Figure 9: Set of boxplots showing differences in dose-volumes between the clinical plan values, the CPD KBP model predictions, and MCOD KBP model predictions for the bladder (a) and the rectum (b). Below each dose-volume lists the number of patients, n, where a KBP prediction was possible under the protocol detailed in Chapter 3.1.3. Note: data points outside boxplot whiskers are more than 1.5 times the interquartile range (first quartile to third quartile i.e. length of boxes) from the first or third quartiles, the grey circles represent the mean of each distribution, and the horizontal black lines within each box represent the median of each distribution.

(Figure 9 continued)

(b)

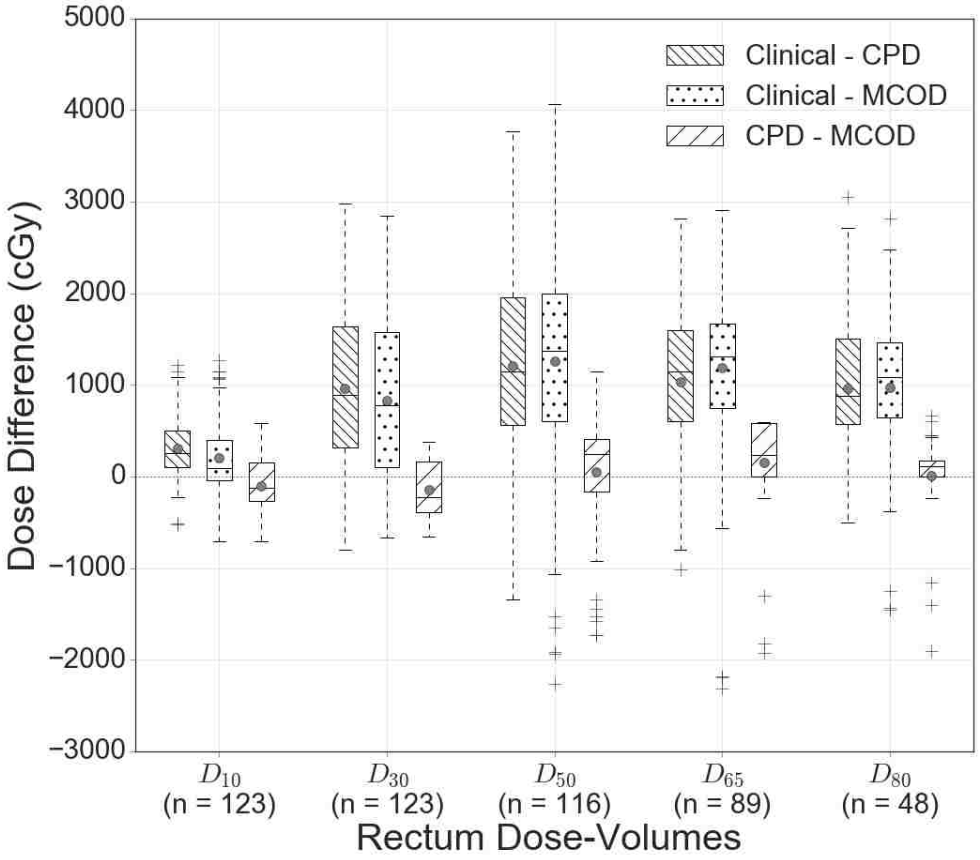

Bladder dose-volumes predicted from the CPD and MCOD models were on average 7.34 and 11.09 Gy lower than the clinical values respectively. As for the rectum, the predicted dose-volumes from the CPD and MCOD models were on average 8.96 and 8.91 Gy less than the clinical plans respectively.

When comparing the two KBP methods, the MCOD model predicted significantly lower dose than the CPD model for all five bladder ($p < 0.001$) and two of the five rectum dose-volumes (D_{50}; $p = 0.004$ and D_{65}; $p < 0.001$). The MCOD model bladder dose predictions were on average 3.75 Gy less than the CPD model predictions over the five dose-volumes. Whereas the MCOD model predictions were on average 1.04 Gy less than the CPD model values of D_{50} and D_{65} for the rectum. CPD model predictions of rectum D_{10} ($p = 0.005$) and D_{30} ($p < 0.001$) doses were

statistically lower than the MCOD model. These predicted dose-volumes were on average 1.19 Gy lower for the CPD model compared to the MCOD model.

Table 7: Statistical comparison of CPD and MCOD KBP model and clinical dose-volumes, with associated mean differences between combinations of the clinical, CPD model, and MCOD model dose values. These mean differences correspond to the grey circles in Figure 9.

		Mean Differences (cGy)			Two-sided Wilcoxon *p*-values		
Dose Metric	N†	Clinical – CPD	Clinical – MCOD	CPD – MCOD	Clinical vs. CPD	Clinical vs. MCOD	CPD vs. MCOD
Bladder							
D_{10}	123	105.4	677.2	571.8	< 0.001*	< 0.001*	< 0.001*
D_{30}	107	598.8	1199.8	600.9	< 0.001*	< 0.001*	< 0.001*
D_{50}	75	840.2	1143.4	303.2	< 0.001*	< 0.001*	< 0.001*
D_{65}	51	1043.8	1189.6	145.7	< 0.001*	< 0.001*	< 0.001*
D_{80}	34	1080.4	1335.7	255.3	< 0.001*	< 0.001*	< 0.001*
Rectum							
D_{10}	123	302.4	204.0	-98.4	< 0.001*	< 0.001*	0.005*
D_{30}	123	966.5	827.7	-138.8	< 0.001*	< 0.001*	< 0.001*
D_{50}	116	1211.5	1262.5	51.0	< 0.001*	< 0.001*	0.004*
D_{65}	89	1036.3	1192.3	156.0	< 0.001*	< 0.001*	< 0.001*
D_{80}	48	961.1	969.0	7.8	< 0.001*	< 0.001*	0.049

*Indicates a statistically significant result of $p < 0.017$, which was Bonferroni corrected from 0.05

†N represents the number of database patients where an in-field OVH-driven KBP prediction was possible i.e. predictions were not made for patients with fractional in-field OAR volumes less than the given dose-volume

3.2.2 KBP PREDICTION ACHIEVABILITY

Figure 10 shows the average PTV and secondary OAR DVHs from the 31 re-plans compared with the corresponding DVHs from the clinical plans. Re-planned PTV dose was statistically equivalent to clinical dose and showed a significant improvement in CI (Table 8). Re-plans also significantly decreased D_{mean} of both femoral heads by an average of 2.76 (left; $p < 0.001$) and 2.50 Gy (right; $p < 0.001$). A statistically significant increase ($p = 0.007$) in re-planned right femoral head D_{max} was observed. However, D_2 serves as a more stable surrogate for maximum dose since D_{max} represents a point dose that is susceptible to interpolation errors, especially in large dose gradients. Compared with the clinical plans, the re-planned D_2 values were 0.91($p = 0.02$) and 0.56

Gy ($p = 0.16$) lower for the left and right femoral heads respectively. Lastly, the mean dose to the penile bulb decreased by an average of 4.0 Gy ($p < 0.001$) in the re-plans.

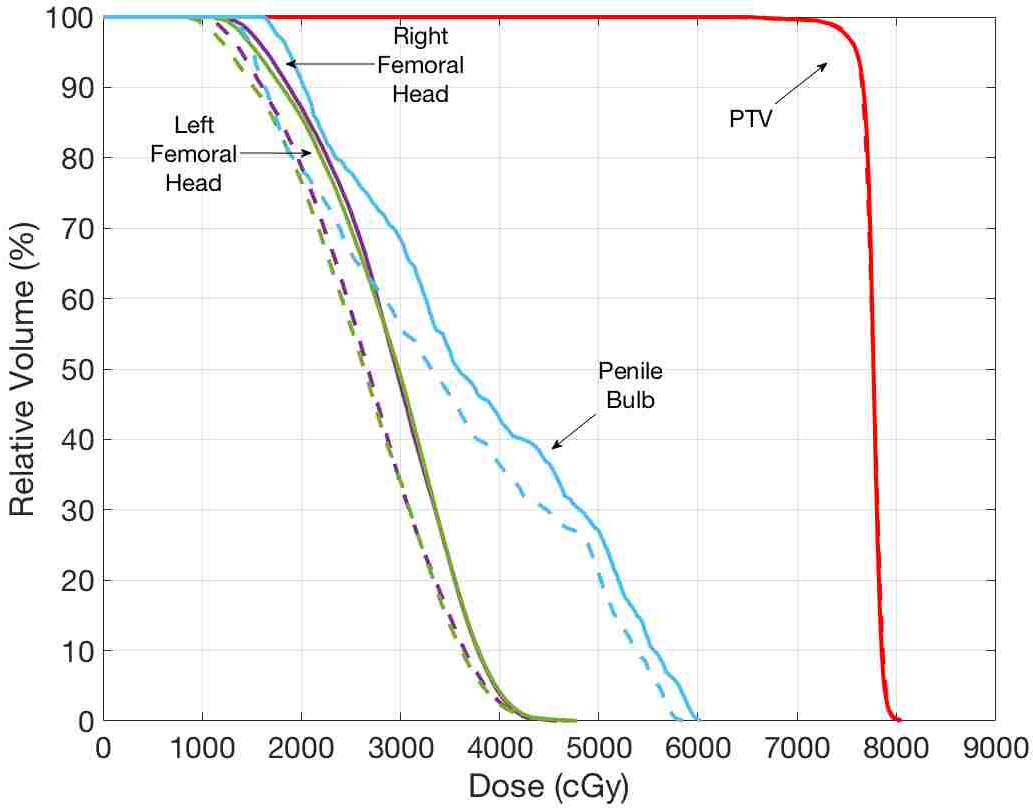

Figure 10: Average PTV and secondary OAR DVHs of the 31 re-planned patients comparing the clinical plans (solid lines) and re-plans (dashed lines). Note the penile bulb was not segmented in 3 of the 31 patients.

The average bladder and rectum DVHs from the re-plans and the clinical plans are shown in Figure 11. The re-planned bladder and rectum dose was statistically lower ($p < 0.001$) than the clinical plan dose for each dose-volume observed (Table 9). This resulted in an average decrease in mean dose of 7.81 ($p < 0.001$) and 9.41 Gy ($p < 0.001$) for the bladder and rectum respectively.

Statistical results from comparing KBP model and re-planned bladder and rectum dose are shown in Table 10. Overall, seven of the ten predicted bladder and rectum dose-volumes were statistically equivalent to the attained re-planned values. The re-planned D_{10} dose-volumes of the bladder and rectum were on average 1.06 ($p = 0.03$) and 0.82 Gy ($p = 0.04$) higher respectively than

the KBP model predicted values. Additionally, the KBP model predicted D_{65} of the rectum were on average 1.74 Gy lower ($p = 0.03$) than the re-planned values.

Table 8: Statistical results of the dose comparison between the clinical plans and re-plans for the PTV and secondary OARs. While the PTV and femoral head dose metrics were averaged over the 31 patients, the penile bulb was averaged over the 28 patients in which it was segmented.

Dose Metric	Mean Re-plan – Clinical	Wilcoxon p-value
PTV		
D_2 (cGy)	8.8	0.62
D_{50} (cGy)	-0.4	0.98
D_{98} (cGy)	21.9	0.37
D_{min} (cGy)	-160.1	0.08
D_{mean} (cGy)	0.6	0.95
D_{max} (cGy)	20.7	0.43
V_{95} (%)	0.06	0.89
V_{98} (%)	0.07	0.98
V_{100} (%)	-0.2	0.22
V_{107} (%)	-0.4	0.80
HI	-0.002	0.84
CI	-0.07	0.03*
Left Femoral Head		
D_2 (cGy)	-91.2	0.02*
D_{max} (cGy)	80.8	0.11
D_{mean} (cGy)	-275.7	< 0.001*
Right Femoral Head		
D_2 (cGy)	-55.6	0.16
D_{max} (cGy)	127.0	0.007*
D_{mean} (cGy)	-249.7	< 0.001*
Penile Bulb		
D_{mean} (cGy)	-404.9	< 0.001*

*Indicates a statistically significant result of $p < 0.05$

3.3 DISCUSSION

This study showed the KBP models utilizing either plan database predicted a significant improvement in both bladder and rectum dose compared with clinical plans. Concretely, the two KBP models predicted that more than 7 and 8 Gy dose decreases to the bladder and rectum respectively were possible. These observed improvements are consistent with previous results from similar KBP models for prostate cancer.[40,68,74] The large dose reductions again reveal the presence of

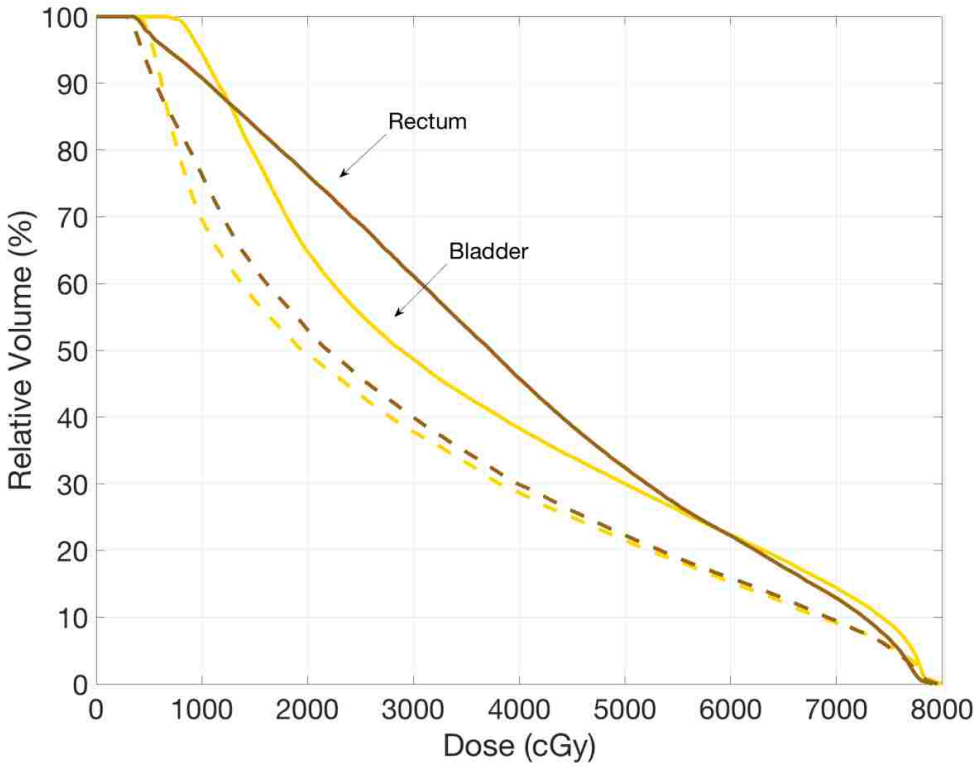

Figure 11: Average DVHs over the 31 patients of the bladder and rectum for the clinical plans (solid lines) and re-plans (dashed lines).

sub-optimal clinical plans, resulting from the inconsistent nature of current inverse planning processes. This emphasizes the need for planning quality control methods, such as KBP, in clinical workflows to consistently achieve the best treatment plans for each patient.

When comparing differences between the two individual KBP methods, the MCOD model predicted significantly lower bladder dose-volumes than the CPD model. Averaged over the five bladder dose-volumes, the MCOD KBP model predicted dose 3.75 Gy less than the corresponding CPD KBP model. While the MCOD KBP model did not predict statistically lower dose-volumes for every rectum dose-volume observed, it predicted an average of 1.04 Gy lower rectum dose than the CPD KBP model for D_{50} and D_{65}. Also, the results from the re-planning study affirm the achievability of these lower MCOD KBP dose-volume predictions. Therefore, this study shows how

a KBP model using a database of Pareto plans can lead to a higher degree of plan quality than a clinical plan database overall.

This study supplements and advances the implications from Wang *et al.*'s validation of the OVH KBP model using an in-house MCO protocol with consistent prostate planning priorities.[69] They realized the shortfalls of evaluating the accuracy of planning quality assurance methods by comparing predictions with the potentially sub-optimal clinical plans. However, their set of Pareto plans was generated based on a hierarchical wish-list that prioritized certain OAR sparing over others, which they suspect may have led to an underestimation of bladder dose. Our study used a uniformly weighted MCO planning protocol within a commercial TPS to generate consistent Pareto plans. This study also quantified the degree to which an OVH KBP method can be improved by using a Pareto plan database compared to using a clinical, inversely optimized plan database. Further, these more optimal dose-volume predictions obtained through the MCOD KBP model were shown to be achievable through traditional inverse optimization.

Table 9: Average differences in re-planned and clinical dose values over the 31 patients with Wilcoxon test results for the primary OARs.

		Wilcoxon *p*-value
Dose Metric	Mean Re-plan – Clinical (cGy)	Re-plan vs. Clinical
Bladder		
D_{10}	-584	< 0.001*
D_{30}	-1184	< 0.001*
D_{50}	-939	< 0.001*
D_{65}	-833	< 0.001*
D_{80}	-703	< 0.001*
D_{mean}	-781	< 0.001*
Rectum		
D_{10}	-345	< 0.001*
D_{30}	-1223	< 0.001*
D_{50}	-1543	< 0.001*
D_{65}	-1366	< 0.001*
D_{80}	-857	< 0.001*
D_{mean}	-941	< 0.001*

*Indicates a statistically significant result of $p < 0.05$

This suggests that institutions without MCO capabilities could leverage external Pareto plan data in an existing KBP model to achieve treatment plans more optimal than those predicted by historical clinical plans. In other words, a MCO-driven KBP model can be made portable and used to achieve MCO-type plans through traditional inverse optimization.

Table 10: Dosimetric and statistical results for evaluating prediction performance and achievability.

Dose Metric	Number Of Predictions	Mean Re-plan – Prediction (cGy)	Wilcoxon *p*-value Re-plan vs. Prediction
Bladder			
D_{10}	31	106	0.03*
D_{30}	27	-5	0.77
D_{50}	18	-12	0.65
D_{65}	13	-165	0.13
D_{80}	9	17	0.95
Rectum			
D_{10}	31	82	0.04*
D_{30}	31	-174	0.23
D_{50}	30	-13	0.52
D_{65}	23	-174	0.03*
D_{80}	13	-151	0.12

*Indicates a statistically significant result of $p < 0.05$

Our study shows that predictions from an OVH KBP model can be improved through the use of a consistently generated Pareto plan database without compromising prediction achievability or accuracy. However, we did not find the MCOD model to be more optimal in each analyzed dose-volume, namely the two high-dose rectum volumes. It is possible the CPD model predicted lower doses for rectum D_{10} and D_{30} due to varying clinical priorities placed on the rectum. Conversely, it may be a result of the fixed planning priorities imposed on the Pareto plans of the MCOD. The minimum dose constraint to the target used in the MCO planning protocol (Table 2) likely serves to increase the dose to rectum volumes close to the target. This could suggest a refinement of the Pareto plan generation, such as additional trade-off objectives emphasizing high-dose rectal volumes, could further improve these rectum dose-volume predictions.

Planning efficiency was not accounted for or analyzed in the present study as the main purpose was to investigate the effects of utilizing a dose database of improved quality and consistency on KBP performance. The present workflow was also not optimized for efficiency. However, given the previous findings of KBP methods improving planning efficiency, it would seem reasonable that incorporating another dose database into an existing KBP protocol would not compromise the method from an efficiency standpoint. However, an examination on treatment planning efficiency of a KBP method with a separately constructed plan database is needed to verify this claim.

In order to further improve KBP model performance, a logical progression of the OVH-driven KBP dose-volume prediction method would be the development of an OVH-based KBP prediction tool for equivalent uniform dose (EUD) planning objectives. The accurate prediction of an optimally achievable EUD objective could further improve patient-specific KBP plan quality. Additionally, as with all KBP planning methods, the plan databases may be continuously updated to include high-quality plans generated via the KBP method.

3.4 CONCLUSIONS

The results from this study showed the dosimetric advantages of an OVH-driven KBP model using either a clinical plan database or a Pareto plan database. This study also demonstrated that a Pareto plan database can produce lower dose-volume KBP predictions than a clinical plan database without jeopardizing achievability. Five out of five bladder and two out of five rectum dose-volume predictions were found to be more optimal using the MCOD compared with the conventional CPD. Overall, dose-volume predictions were shown to be achievable regardless of plan database origin, with average differences of no more than 1.74 Gy with the re-planned bladder and rectum dose-volumes. Further, these results indicate the possibility of achieving MCO-type plans through inverse planning optimization.

CHAPTER 4. CONCLUSIONS

4.1 SUMMARY OF FINDINGS

The main goal of this study was to evaluate the extent to which the performance of an OVH-driven KBP model for predicting dose-volumes is affected by plan quality deficiencies and variations in the plan database. Sub-optimal and inconsistent treatment plans in a large database of prostate patients due to inter-planner subjectivity were controlled for by applying a uniform MCO planning protocol to create a balanced Pareto optimal plan for each database patient. KBP model dose-volume predictions generated from the clinical, manually-optimized plan data (i.e. the CPD) were compared to those derived from the database of Pareto plans (i.e. the MCOD). Achievability of those dose-volume predictions were verified by re-planning a subset of randomly selected patients with the KBP model predictions as planning goals.

When establishing the distance-to-dose relationship for querying new patients against the database for patients with similar anatomies (see Chapter 2), we observed a sizable variation in dose a specific fractional OAR volume received (i.e. a DVH point) at a given distance away from the PTV surface (i.e. a OVH point). These large spreads in the DVH-OVH correlations for a fractional OAR volume could lead to less accurate and namely less achievable dose-volumes in an OVH-driven KBP model. Therefore, we investigated the influence of second-order factors on this distance-to-dose correlation variation while again accounting for sub-optimal planning due to inter-planner bias. We found the in-field OAR volume correlated strongest with MCOD dose for each observed dose-volume of both the bladder and rectum. Other second-order variables, such as prescription dose and bladder and rectum fill volumes, did not correlate with OAR dose. The derivative of the OVH and PTV volume moderately correlated with OAR dose. Recalculating the OVH to only consider OAR volume within the treatment fields resulted in an overall strengthening in the distance-to-dose correlation of the bladder and rectum. This in-field OVH removed data points that would likely

result in unachievably low dose-volume predictions and was selected to be the feature querying metric for the KBP model used in this study.

Chapter 3 detailed the results from comparing an OVH-based KBP model using a clinical plan database (CPD) with one using a Pareto plan database (MCOD). The MCOD KBP model predicted statistically lower dose than the CPD KBP model for all five bladder dose-volumes and two of five rectum dose-volumes observed. A re-planning study confirmed the achievability of these KBP predictions while maintaining statistically similar PTV and secondary OAR dose as the original clinical plans. Therefore, a database of uniform Pareto plans can produce more optimal dose-volume predictions that lead to improved plan quality compared with a conventional clinical plan database.

The hypothesis of this study was that OVH-driven KBP bladder and rectum dose-volume predictions derived from the MCOD database of Pareto plans versus those derived from the CPD database of inversely optimized clinical plans would result in plans with statistically improved ($p < 0.017$) sparing of the bladder and rectum, while also maintaining statistically equivalent PTV and secondary OAR dose. To this end, the results fully support this hypothesis for the bladder as the MCOD model produced achievable and statistically lower predictions than the CPD model for each dose-volume considered. As for rectum, however, MCOD model predictions were statistically lower than those from the CPD model for only D_{50} and D_{65} dose-volumes. Nonetheless, the MCOD KBP model led to improved and achievable overall bladder and rectum dose sparing, while still maintaining statistically similar PTV and secondary OAR dose.

4.2 LIMITATIONS

One limitation of this work is the size of the patient database. Naturally, the larger the patient database, the more robust a KBP method should be. Boutilier *et al.*'s study found that more than 200 samples gives the most consistent OVH-driven KBP model dose-volume predictions.[74] However, they also show a database size of 100 patients still results in a similarly consistent and

accurate KBP model compared with a 200 patient database. Specifically, a KBP model with a sample size of 100 patients produced a similar number of "over-predictions" (i.e. predictions where a dosimetric value was worse than the clinical value) for bladder and rectum dose-volumes compared to a model with 200 patients. Given time constraints, the working sample size of 124 was predetermined to yield adequate model performance and statistical power for the purposes of this project.

This study also restricts database patients to those with only one prescribed PTV. This aspect has been discussed by previous groups dealing distance-to-dose KBP methods similar to the one used in this study.[44,69] For cases that require more than one segmented PTV, such as simultaneous integrated boosts (SIB), an OAR will have separate OVHs for each defined PTV with likely differing prescription doses. However, the model in this study could theoretically be adapted to predict dose-volumes for SIB treatments by compiling a database of previous SIB patients. Wang *et al.* provides an example of such a formalism.[69] This logic extends to other, more complex treatment sites as well (e.g. head and neck), although model testing would still be needed to confirm the method's clinical viability.

There was also not a comprehensive analysis of how the in-field OVH KBP predictions compared to the nominal OVH KBP predictions in this study. Despite being out of the scope of this thesis, results from qualitative inspection comparing the two OVH methods in the re-planning study can be found in the supplemental material (see Appendix F). A preliminary statistical analysis between the achieved re-planned and the predicted nominal OVH dose-volumes can also be found in Appendix G. Additionally, Petit *et al.* performed a similar comparison study with IMRT pancreatic adenocarcinoma patients and they found the in-field OVH produced more accurate and achievable liver dose-volume predictions than the standard OVH. These findings suggest a similar discovery is likely with the VMAT prostate patients in this study.

Since in-field OVH-driven KBP dose-volume predictions were not made for patients with less than the given in-field OAR volume threshold, there were missing statistical data when evaluating the prediction achievability in the re-planning study. The signed-rank Wilcoxon statistical function used for these comparisons cautions the inability to perform a normal approximation with a sample size of less than 10. This warning only arises for D_{80} of the bladder, which had only 9 KBP predictions. Although these missing data do decrease the statistical power of the Wilcoxon test, 31 re-planned patients is a sufficient overall sample size to confidently interpret the results. Further, a pilot study determined that 30 or more patients was an adequate sample size in order to detect a significant difference of about 2 Gy with 80% power.

Another limitation of this study is the lack of biological plan quality metrics (e.g. target control probability, normal tissue complication probability, secondary cancer complication probability etc.) that could be used to evaluate potential outcome differences in two treatment plans. The purpose of this study was to assess dosimetric differences between plans only. Although outside the scope of this project, investigation into the differences in biology-based metrics between both sets of KBP predictions and results from the re-planning study could supplement the dosimetric findings in this study.

4.3 FUTURE WORK

The next logical and immediate step for this project would be to further identify outliers present in the patient database. This was addressed primarily through the in-field OVH in the present study. However, one could imagine taking other factors that were found to moderately influence the distance-to-dose relationship (e.g. dOVH and PTV volume) and incorporating them into the dose-volume prediction through multiple linear regression, for example.

Another direction that one could take is the investigation of a more optimal MCO planning protocol than the one used in this work. While the MCO balance plan yields a plan independent of

inter-planner variations, there likely exist Pareto plans that are more optimal for a specific OAR. The MCO planning protocol applied to each database patient in this study produced uniformly consistent Pareto plans, regardless of relative OAR priorities. This is in contrast to the manually optimized clinical plans, where physician preference can result in plans where one particular OAR was emphasized at the expense of the other. The independence of OAR sparing priorities in the MCO planning protocol may explain, at least partially, why the CPD model predicted statistically lower D_{10} and D_{30} rectum dose-volumes. Regardless, a custom optimization protocol could be developed to search each patient's Pareto surface based on certain planning priorities, which could result in even more optimal KBP dose-predictions, albeit at the expense of increased computational overhead.

As mentioned in Chapter 1.1.3, KBP methods can be applied at multiple levels of the treatment planning process. The KBP method developed in this study can be adapted for pre- or post-planning quality assurance. Therefore, clinically implementing this KBP method for either pre-planning dose-volume predictions or flagging sub-optimal plans post-planning is a natural progression from this work. Further, the extension of this KBP structure to other treatment sites should be investigated before considering clinical implementation.

As part of the clinical validation of this KBP model, a study would need to be done verifying the deliverability of the KBP-assisted plans (e.g. the re-plans in this study). While not studied in detail, a cursory inspection of the re-plans indicated a sizeable increase in the MUs required relative to the original clinical plans. The amount of required MUs is a general, although not exact, indicator of plan complexity as defined by the modulation complexity score.[75,76] The increased complexity of the re-plans trying to achieve the KBP model dose-volume predictions may affect the plans ability to pass quality assurance tests. As the re-plans were not planned under the exact same conditions (from a technical perspective e.g. different TPS, machine, etc.) as the clinical plans, a quality assurance

assessment of the re-plans is needed to confirm the clinical viability of the resulting plans. This, however, was outside the purpose and scope of the current project.

REFERENCES

1. Radiation Therapy Basics. 2017; https://www.cancer.org/treatment/treatments-and-side-effects/treatment-types/radiation/basics.html. Accessed June 12, 2017.

2. Fraass BA. The development of conformal radiation therapy. *Med Phys.* 1995;22(11 Pt 2):1911-1921.

3. Staffurth J, Radiotherapy Development B. A review of the clinical evidence for intensity-modulated radiotherapy. *Clin Oncol (R Coll Radiol).* 2010;22(8):643-657.

4. Veldeman L, Madani I, Hulstaert F, De Meerleer G, Mareel M, De Neve W. Evidence behind use of intensity-modulated radiotherapy: a systematic review of comparative clinical studies. *The Lancet Oncology.* 2008;9(4):367-375.

5. Teoh M, Clark CH, Wood K, Whitaker S, Nisbet A. Volumetric modulated arc therapy: a review of current literature and clinical use in practice. *Br J Radiol.* 2011;84(1007):967-996.

6. Otto K. Volumetric modulated arc therapy: IMRT in a single gantry arc. *Med Phys.* 2008;35(1):310-317.

7. Tsai CL, Wu JK, Chao HL, Tsai YC, Cheng JC. Treatment and dosimetric advantages between VMAT, IMRT, and helical tomotherapy in prostate cancer. *Med Dosim.* 2011;36(3):264-271.

8. Hardcastle N, Tome WA, Foo K, Miller A, Carolan M, Metcalfe P. Comparison of prostate IMRT and VMAT biologically optimised treatment plans. *Med Dosim.* 2011;36(3):292-298.

9. Kopp RW, Duff M, Catalfamo F, Shah D, Rajecki M, Ahmad K. VMAT vs. 7-field-IMRT: assessing the dosimetric parameters of prostate cancer treatment with a 292-patient sample. *Med Dosim.* 2011;36(4):365-372.

10. Deng Z, Shen L, Zheng X, et al. Dosimetric advantage of volumetric modulated arc therapy in the treatment of intraocular cancer. *Radiat Oncol.* 2017;12(1):83.

11. Vanetti E, Clivio A, Nicolini G, et al. Volumetric modulated arc radiotherapy for carcinomas of the oro-pharynx, hypo-pharynx and larynx: a treatment planning comparison with fixed field IMRT. *Radiother Oncol.* 2009;92(1):111-117.

12. Bertelsen A, Hansen CR, Johansen J, Brink C. Single Arc Volumetric Modulated Arc Therapy of head and neck cancer. *Radiother Oncol.* 2010;95(2):142-148.

13. Radiation Therapy Treatment Process. [Image]. https://www.elekta.com/patients/radiation-therapy-treatment-process/. Accessed May 10, 2017.

14. Millennium MLC. [Image]. http://newsroom.varian.com/imagegallery?mode=gallery&cat=2473. Accessed May 10, 2017.

15. Oldham M, Neal A, Webb S. A comparison of conventional 'forward planning' with inverse planning for 3D conformal radiotherapy of the prostate. *Radiother Oncol.* 1995;35(3):248-262.

16. Emami B, Lyman J, Brown A, et al. Tolerance of normal tissue to therapeutic irradiation. *Int J Radiat Oncol Biol Phys.* 1991;21(1):109-122.

17. Bentzen SM, Constine LS, Deasy JO, et al. Quantitative Analyses of Normal Tissue Effects in the Clinic (QUANTEC): an introduction to the scientific issues. *Int J Radiat Oncol Biol Phys.* 2010;76(3 Suppl):S3-9.

18. Matsuo Y, Takayama K, Nagata Y, et al. Interinstitutional variations in planning for stereotactic body radiation therapy for lung cancer. *Int J Radiat Oncol Biol Phys.* 2007;68(2):416-425.

19. Batumalai V, Jameson MG, Forstner DF, Vial P, Holloway LC. How important is dosimetrist experience for intensity modulated radiation therapy? A comparative analysis of a head and neck case. *Pract Radiat Oncol.* 2013;3(3):e99-e106.

20. Berry SL, Boczkowski A, Ma R, Mechalakos J, Hunt M. Interobserver variability in radiation therapy plan output: Results of a single-institution study. *Pract Radiat Oncol.* 2016;6(6):442-449.

21. Das IJ, Cheng CW, Chopra KL, Mitra RK, Srivastava SP, Glatstein E. Intensity-modulated radiation therapy dose prescription, recording, and delivery: patterns of variability among institutions and treatment planning systems. *J Natl Cancer Inst.* 2008;100(5):300-307.

22. Nelms BE, Robinson G, Markham J, et al. Variation in external beam treatment plan quality: An inter-institutional study of planners and planning systems. *Pract Radiat Oncol.* 2012;2(4):296-305.

23. Moore KL, Schmidt R, Moiseenko V, et al. Quantifying Unnecessary Normal Tissue Complication Risks due to Suboptimal Planning: A Secondary Study of RTOG 0126. *Int J Radiat Oncol Biol Phys.* 2015;92(2):228-235.

24. Multi-criteria optimization in RayStation. *RaySearchLabs White Paper.* RaySearch Laboratories 2015. <http://www.raysearchlabs.com/globalassets/about-overview/media-center/wp-re-ev-n-pdfs/white-papers/white-paper-1---mco-aug-2015.pdf>. Accessed October 1, 2016.

25. Hardemark B, Liander A, Rehbinder H, Lof J. Direct machine parameter optimization with RayMachine in Pinnacle3. RaySearch white paper. *RaySearch Laboratories.* 2003.

26. Craft DL, Hong TS, Shih HA, Bortfeld TR. Improved planning time and plan quality through multicriteria optimization for intensity-modulated radiotherapy. *Int J Radiat Oncol Biol Phys.* 2012;82(1):e83-90.

27. Kierkels RG, Visser R, Bijl HP, et al. Multicriteria optimization enables less experienced planners to efficiently produce high quality treatment plans in head and neck cancer radiotherapy. *Radiat Oncol.* 2015;10:87.

28. Chen H, Craft DL, Gierga DP. Multicriteria optimization informed VMAT planning. *Med Dosim.* 2014;39(1):64-73.

29. Ghandour S, Matzinger O, Pachoud M. Volumetric-modulated arc therapy planning using multicriteria optimization for localized prostate cancer. *J Appl Clin Med Phys.* 2015;16(3):5410.

30. McGarry CK, Bokrantz R, O'Sullivan JM, Hounsell AR. Advantages and limitations of navigation-based multicriteria optimization (MCO) for localized prostate cancer IMRT planning. *Med Dosim.* 2014;39(3):205-211.

31. Craft D, Richter C. Deliverable navigation for multicriteria step and shoot IMRT treatment planning. *Phys Med Biol.* 2013;58(1):87-103.

32. Fredriksson A, Bokrantz R. Deliverable navigation for multicriteria IMRT treatment planning by combining shared and individual apertures. *Phys Med Biol.* 2013;58(21):7683-7697.

33. Salari E, Unkelbach J. A column-generation-based method for multi-criteria direct aperture optimization. *Phys Med Biol.* 2013;58(3):621-639.

34. Craft D, Bortfeld T. How many plans are needed in an IMRT multi-objective plan database? *Phys Med Biol.* 2008;53(11):2785-2796.

35. Spalke T, Craft D, Bortfeld T. Analyzing the main trade-offs in multiobjective radiation therapy treatment planning databases. *Phys Med Biol.* 2009;54(12):3741-3754.

36. Liu BJ. A knowledge-based imaging informatics approach for managing proton beam therapy of cancer patients. *Technol Cancer Res Treat.* 2007;6(4 Suppl):77-84.

37. Lee KJ, Barber DC, Walton L. Automated gamma knife radiosurgery treatment planning with image registration, data-mining, and Nelder-Mead simplex optimization. *Med Phys.* 2006;33(7):2532-2540.

38. Chen HC, Wang YY, Lin CH, et al. A knowledge-based approach for carpal tunnel segmentation from magnetic resonance images. *J Digit Imaging.* 2013;26(3):510-520.

39. Foruzan AH, Zoroofi RA, Hori M, Sato Y. A knowledge-based technique for liver segmentation in CT data. *Comput Med Imaging Graph.* 2009;33(8):567-587.

40. Chanyavanich V, Das SK, Lee WR, Lo JY. Knowledge-based IMRT treatment planning for prostate cancer. *Med Phys.* 2011;38(5):2515.

41. Wu B, Ricchetti F, Sanguineti G, et al. Patient geometry-driven information retrieval for IMRT treatment plan quality control. *Med Phys.* 2009;36(12):5497.

42. Tol JP, Dahele M, Delaney AR, Slotman BJ, Verbakel WF. Can knowledge-based DVH predictions be used for automated, individualized quality assurance of radiotherapy treatment plans? *Radiat Oncol.* 2015;10:234.

43. Sharpe MB, Moore KL, Orton CG. Point/Counterpoint: Within the next ten years treatment planning will become fully automated without the need for human intervention. *Med Phys.* 2014;41(12):120601.

44. Appenzoller LM, Michalski JM, Thorstad WL, Mutic S, Moore KL. Predicting dose-volume histograms for organs-at-risk in IMRT planning. *Med Phys.* 2012;39(12):7446-7461.

45. Moore KL, Appenzoller LM, Tan J, Michalski JM, Thorstad WL, Mutic S. Clinical implementation of dose-volume histogram predictions for organs-at-risk in IMRT planning. *Journal of Physics: Conference Series.* 2014;489:012055.

46. Shiraishi S, Tan J, Olsen LA, Moore KL. Knowledge-based prediction of plan quality metrics in intracranial stereotactic radiosurgery. *Med Phys.* 2015;42(2):908.

47. Good D, Lo J, Lee WR, Wu QJ, Yin FF, Das SK. A knowledge-based approach to improving and homogenizing intensity modulated radiation therapy planning quality among treatment centers: an example application to prostate cancer planning. *Int J Radiat Oncol Biol Phys.* 2013;87(1):176-181.

48. Moore KL, Brame RS, Low DA, Mutic S. Experience-based quality control of clinical intensity-modulated radiotherapy planning. *Int J Radiat Oncol Biol Phys.* 2011;81(2):545-551.

49. Zhu X, Ge Y, Li T, Thongphiew D, Yin F-F, Wu QJ. A planning quality evaluation tool for prostate adaptive IMRT based on machine learning. *Med Phys.* 2011;38(2):719.

50. Sohn M, Alber M, Yan D. Principal component analysis-based pattern analysis of dose-volume histograms and influence on rectal toxicity. *Int J Radiat Oncol Biol Phys.* 2007;69(1):230-239.

51. Wang J, Jin X, Zhao K, et al. Patient feature based dosimetric Pareto front prediction in esophageal cancer radiotherapy. *Med Phys.* 2015;42(2):1005-1011.

52. Yuan L, Ge Y, Lee WR, Yin FF, Kirkpatrick JP, Wu QJ. Quantitative analysis of the factors which affect the interpatient organ-at-risk dose sparing variation in IMRT plans. *Med Phys.* 2012;39(11):6868-6878.

53. Fogliata A, Belosi F, Clivio A, et al. On the pre-clinical validation of a commercial model-based optimisation engine: application to volumetric modulated arc therapy for patients with lung or prostate cancer. *Radiother Oncol.* 2014;113(3):385-391.

54. Nwankwo O, Sihono DS, Schneider F, Wenz F. A global quality assurance system for personalized radiation therapy treatment planning for the prostate (or other sites). *Phys Med Biol.* 2014;59(18):5575-5591.

55. Shiraishi S, Moore KL. Knowledge-based prediction of three-dimensional dose distributions for external beam radiotherapy. *Med Phys.* 2016;43(1):378.

56. Hunt MA, Hsiung CY, Spirou SV, Chui CS, Amols HI, Ling CC. Evaluation of concave dose distributions created using an inverse planning system. *Int J Radiat Oncol Biol Phys.* 2002;54(3):953-962.

57. Hunt MA, Jackson A, Narayana A, Lee N. Geometric factors influencing dosimetric sparing of the parotid glands using IMRT. *Int J Radiat Oncol Biol Phys.* 2006;66(1):296-304.

58. Reddy NMS, Nori D, Chang H, Lange CS, Ravi A. Prostate and seminal vesicle volume based consideration of prostate cancer patients for treatment with 3D-conformal or intensity-modulated radiation therapy. *Med Phys.* 2010;37(7):3791.

59. Kazhdan M, Simari P, McNutt T, et al. A shape relationship descriptor for radiation therapy planning. *Med Image Comput Comput Assist Interv.* 2009;12(Pt 2):100-108.

60. Wu B, Ricchetti F, Sanguineti G, et al. Data-driven approach to generating achievable dose-volume histogram objectives in intensity-modulated radiotherapy planning. *Int J Radiat Oncol Biol Phys.* 2011;79(4):1241-1247.

61. Wu B, McNutt T, Zahurak M, et al. Fully automated simultaneous integrated boosted-intensity modulated radiation therapy treatment planning is feasible for head-and-neck cancer: a prospective clinical study. *Int J Radiat Oncol Biol Phys.* 2012;84(5):e647-653.

62. Wu B, Pang D, Simari P, Taylor R, Sanguineti G, McNutt T. Using overlap volume histogram and IMRT plan data to guide and automate VMAT planning: a head-and-neck case study. *Med Phys.* 2013;40(2):021714.

63. Wu B, Pang D, Lei S, et al. Improved robotic stereotactic body radiation therapy plan quality and planning efficacy for organ-confined prostate cancer utilizing overlap-volume histogram-driven planning methodology. *Radiother Oncol.* 2014;112(2):221-226.

64. Kazhdan M, McNutt T, Taylor R, Wu B, Simari P. Comment on "A planning quality evaluation tool for prostate adaptive IMRT based on machine learning" [Med. Phys. 38, 719 (2011)]. *Med Phys.* 2011;38(5):2820; author reply 2821.

65. Petit SF, Wu B, Kazhdan M, et al. Increased organ sparing using shape-based treatment plan optimization for intensity modulated radiation therapy of pancreatic adenocarcinoma. *Radiother Oncol.* 2012;102(1):38-44.

66. Schmidt M, Lo JY, Grzetic S, Lutzky C, Brizel DM, Das SK. Semiautomated head-and-neck IMRT planning using dose warping and scaling to robustly adapt plans in a knowledge database containing potentially suboptimal plans. *Med Phys.* 2015;42(8):4428-4434.

67. Song T, Staub D, Chen M, et al. Patient-specific dosimetric endpoints based treatment plan quality control in radiotherapy. *Phys Med Biol.* 2015;60(21):8213-8227.

68. Wang Y, Zolnay A, Incrocci L, et al. A quality control model that uses PTV-rectal distances to predict the lowest achievable rectum dose, improves IMRT planning for patients with prostate cancer. *Radiother Oncol.* 2013;107(3):352-357.

69. Wang Y, Breedveld S, Heijmen B, Petit SF. Evaluation of plan quality assurance models for prostate cancer patients based on fully automatically generated Pareto-optimal treatment plans. *Phys Med Biol.* 2016;61(11):4268-4282.

70. Zhang X, Li X, Quan EM, Pan X, Li Y. A methodology for automatic intensity-modulated radiation treatment planning for lung cancer. *Phys Med Biol.* 2011;56(13):3873-3893.

71. Boutilier JJ, Lee T, Craig T, Sharpe MB, Chan TC. Models for predicting objective function weights in prostate cancer IMRT. *Med Phys.* 2015;42(4):1586-1595.

72. ICRU report 83: Prescribing, Recording, and Reporting Photon-Beam Intensity-Modulated Radiation Therapy (IMRT). *Journal of the International Commission on Radiation Units and Measurements.* 2010;10(1).

73. Report 62: Prescribing, Recording and Reporting Photon Beam Therapy (Supplement to ICRU Report 50). *Journal of the International Commission on Radiation Units and Measurements.* 1999;os32(1).

74. Boutilier JJ, Craig T, Sharpe MB, Chan TCY. Sample size requirements for knowledge-based treatment planning. *Med Phys.* 2016;43(3):1212-1221.

75. Masi L, Doro R, Favuzza V, Cipressi S, Livi L. Impact of plan parameters on the dosimetric accuracy of volumetric modulated arc therapy. *Med Phys.* 2013;40(7):071718.

76. McNiven AL, Sharpe MB, Purdie TG. A new metric for assessing IMRT modulation complexity and plan deliverability. *Med Phys.* 2010;37(2):505-515.

77. Michalski JM, Yan Y, Watkins-Bruner D, et al. Preliminary toxicity analysis of 3-dimensional conformal radiation therapy versus intensity modulated radiation therapy on the high-dose arm of the Radiation Therapy Oncology Group 0126 prostate cancer trial. *Int J Radiat Oncol Biol Phys.* 2013;87(5):932-938.

78. Chaikh A, Giraud JY, Perrin E, Bresciani JP, Balosso J. The choice of statistical methods for comparisons of dosimetric data in radiotherapy. *Radiat Oncol.* 2014;9:205.

APPENDIX A. EXTRANEOUS MATERIALS AND METHODS

A.1 PATIENT ANONYMIZATION

The process of patient data anonymization is an important step in performing treatment planning research. This task was laborious in this study due to the various locations patient data can reside within Mary Bird Perkins Cancer Center (MBPCC) depending on the treatment status of a particular patient. In other words, a patient could be in the middle of his or her treatment or fully completed, meaning the DICOM data could be active or archived respectively. For the purposes of this project, active patient DICOM data within MBPCC can most easily be obtained from within Mobius3D (Mobius Medical Systems LP, Houston, TX), a software application for quality assurance and treatment plan verification that also features a DICOM anonymization tool. On the other hand, archived patient data housed in MBPCC's radiation oncology information system MOSAIQ (Elekta, Stockholm, Sweden) must be restored before anonymization.

At MBPCC, the DICOM data is transferred to Mobius3D for a plan check once a plan has been completed and physician-approved in Pinnacle. This patient data and the plan report remain in the plan check list for a given amount of time before the data is archived to MOSAIQ. From this list, a patient's anonymized DICOM data can be downloaded using the Mobius3D anonymization feature. Therefore, this plan check list was first searched for suitable database patients. If a patient met the previously defined selection criteria, the anonymized DICOM data was downloaded before being transferred to and imported into RayStation.

After the patient search through the Mobius3D plan check list was exhausted, archived database candidates were searched using MOSAIQ. A report categorized by primary diagnosis was run in MOSAIQ in order to selectively search the entire MOSAIQ database for a cohort of possible candidates. The report was configured to return a list of all patients treated within a specified time frame in the MBPCC system with a primary cancer diagnosis of "Prostate." Patients with statuses

other than "New" were reviewed for database selection (i.e. only patients with clinically-approved treatment plans). The plan summary of each potential database patient was examined to determine whether selection criteria were met. The DICOM data of patients meeting the selection criteria needed to be restored in the TPS.

Patient data can be backed up to electronic media in Pinnacle. Patients at MBPCC are archived to the MOSAIQ Data Director (MDD), an integrated image and data archiving software system. When patient data is ready to be archived, all image sets and DICOM-RT files associated with that patient are backed up to MDD. Specifically, all archived image sets are listed along with a Pinnacle-specific .tar file that contains header information needed to restore the patient DICOM data to Pinnacle. In order to restore an archived database patient to Pinnacle, the original primary image set and the corresponding .tar file need to be downloaded and pushed to the Pinnacle server.

Once the .tar file was transferred to the Pinnacle server, the patient was restored via the header file contained in the tarball. The primary CT set transferred from MOSAIQ was then imported into that patient. However, for the DICOM image set to be exported to Mobius3D with the same instance as the other DICOM-RT files (i.e. so that all DICOM files can be properly imported into RayStation), the restored DICOM image set must be assigned as the primary image set of the patient. This was done by copying the restored plan to the imported DICOM image set, which produced an identical plan to the restored plan except with no dose. The dose was recomputed for both VMAT beams and the patient data was ready to be exported to Mobius3D for anonymization.

All patient data was anonymized in Mobius3D and imported into RayStation in this fashion until the target number of database patients was achieved. In total, 124 database patients were imported into RayStation for this study.

A.2 DATABASE STANDARDIZATION AND PREPARATION

There are numerous benefits to standardizing nomenclature for body and organ structures, DVH metrics, toxicity, units etc. in radiation therapy. For example, standardizing RT nomenclature can enable easy pooling of data across institutions as well as minimize systematic communication errors within a single institution. With the growing prevalence of large data studies and clinical trials, the American Association of Physicists in Medicine recently approved the formation of Task Group No. 263 for Standardizing Nomenclature for Radiation Therapy. For this study, the nomenclature standardization of select patient data objects was necessary for scripting automation and analysis purposes.

Each anonymized patient imported into RayStation underwent a series of modifications in order to standardize each patient for future use, including OVH computations and DVH data extraction. First, the Tissue Name under the regions of interest (ROI) properties for each specified ROI was designated according to the list in Table 11, which were largely adapted from the RTOG 0126 protocol.[77] These labels would serve as object identifiers in future automation routines, as the names of the structures created by original planners were not uniform. Additionally, each External ROI was modified in RayStation to encompass the entire patient surface included in the CT set.

Each patient image set was required to have an assigned Imaging System. Therefore, each database patient's Imaging System was set to the Generic CT table used to commission the TPS. Then, each imported plan was copied and renamed "MCO_pw," which would serve as the plan file where the MCOD plan would be generated for each database patient. Plan properties were set to uniquely differentiate the MCO plan from the clinical plan and each MCOD plan was set to the same treatment machine. From there, MCO plan development commenced.

Table 11: List of structures used in this study and their assigned standardized Tissue Name labels. The in-field structures were created for computing the in-field OVH in this study as will be discussed in A.3.

Patient Structure	Standardized Tissue Name
PTV	PTV
Bladder	BLADDER
Rectum	RECTUM
Left Femoral Head	FEMUR_LT
Right Femoral Head	FEMUR_RT
Penile Bulb	PENILE_BULB
External	EXTERNAL
In-field Bladder	BLADDER_IN
In-field Rectum	RECTUM_IN

A.3 NOMINAL AND IN-FIELD OVH COMPUTATIONS

An IronPython script was written to automate the OVH computation process from within RayStation. The script was designed to loop through a list of patients in the RayStation database and compute the OVHs for the bladder and rectum of each patient. The script takes a list of unique patient IDs as input and outputs the bladder and rectum OVH data in a patient-specific text files.

The script algorithm takes advantage of the built-in ROI tools of RayStation by first selecting and copying the PTV ROI in the plan, which serves as the working copy of the original PTV contour. Then, ROI algebra is performed to find the intersections between the bladder and PTV ROIs and between the rectum and PTV ROIs, which represent the bladder and rectum volume overlapping with the PTV respectively. Then those overlap volumes are divided by the total volumes of the bladder and rectum ROIs respectively, yielding the bladder and rectum OVH values at a 0 cm expansion distance. Three data items are then written to a patient-specific text file: the current OVH expansion/contraction distance (cm), the bladder OVH value, and the rectum OVH value. The newly created ROIs required for this process are deleted before moving to the next OVH data point to prevent memory leaks. Then a new copy of the PTV is created with a surface uniformly expanded by 1 mm and the process continues as just described. This entire process continues until both the bladder and rectum OVH values are above 85% volume.

Once the OVH expansions are completed for both bladder and rectum ROIs, the same iterations described previously are executed, except the PTV ROI surface is uniformly contracted in 1 mm steps. This process continues until both the bladder and rectum OVH values are 0%. At this point, the text file contains both bladder and rectum OVHs from 0% to at least 85% volumes. This script prevented the computation from continuing until 100% volume overlap due to time efficiency and the specific needs of this project (i.e. largest value needed was 80% to predict the D_{80} dose-volume). The PTV ROI copying process becomes prohibitively time-consuming the larger the expansion value presumably due to the memory requirements from the large number of structure voxels.

This script would then loop to the next database patient in the input list and begin the OVH computation for that patient. The script would continue in this manner until each patient in the list was complete.

In order to compute the in-field OVHs for the bladder and rectum ROIs, in-field ROIs for each structure needed to be generated. A separate IronPython script was written to consistently automate this process like the OVH computation script. In-field volume was defined as ROI volume within the transverse planes located 6 mm (to approximate beam penumbra at depth) superior and inferior to the most superior and inferior aspects of the PTV, respectively. Therefore, to create these in-field ROIs, a copy of the PTV ROI was expanded by 6 mm in the superior and inferior directions and 15 cm in the left, right, anterior, and superior directions. Then the intersections between the bladder and new PTV ROI and between the rectum and new PTV ROI were created to represent the in-field bladder and rectum ROIs. An example of the ROIs generated from this script is shown in Figure 12. This process was repeated for each database patient.

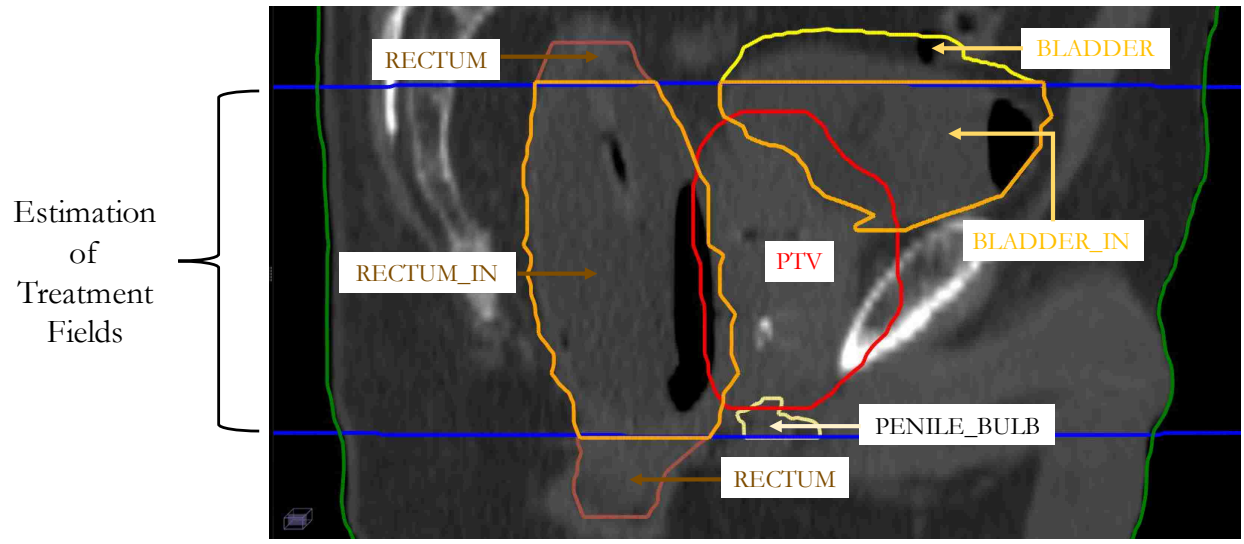

Figure 12: Sagittal CT slice of a database patient showing the estimation of the treatment fields. The horizontal lines are part of the ROI created from the original PTV contour to represent the treatment fields. Given Tissue Names are listed with their corresponding ROIs, with the in-field OAR portions indicated by "_IN." Note the femoral heads are not visible and are located to the left and right of the shown CT slice.

The OVH computation script was modified and adapted to compute the in-field OVHs for the bladder and rectum ROIs in each patient. The major adjustment was to select the "BLADDER_IN" and "RECTUM_IN" planning objects instead of the nominal objects at the beginning of the script. The in-field OVH computation process was identical to the standard OVH script, except the in-field OVH script continued expanding until 100% of the in-field bladder and rectum ROIs were overlapped by the expanded PTV. Again, patient-specific text files were written to contain the in-field OVH data for both the in-field bladder and rectum ROIs.

A.4 STATISTICAL ANALYSIS OF CLINICAL AND PREDICTED DOSE-VOLUMES

The Wilcoxon signed-rank test used in this study is a non-parametric test for testing the null hypothesis that two related paired samples come from the same distribution. It is the non-parametric version of the student t-test. Deciding to use this particular test was based on results from testing data distribution assumptions. The use of parametric statistical tests assumes the data are normally distributed and the variances of the compared samples are similar. Therefore, prior to the individual statistical comparisons performed on the dose-volume distributions of the clinical, CPD, and

MCOD data (detailed in Chapter 3.1), normality and omnibus statistical tests were performed on the three distributions of data. This statistical analysis process was adapted and based on the methods described by Chaikh *et al.*[78] Also, all statistical tests were performed using the statistical functions module in SciPy (scipy.stats), an open-source Python library for scientific computing.

Out of the numerous possible statistical tests designed to assess normality, the Shapiro-Wilk test was used in this work (scipy.stats.shapiro). The Shapiro-Wilk test tests the null hypothesis that the data was drawn from a normal distribution, where a *p*-value of less than 0.05 indicates a significant difference between the test data and a normal distribution (i.e. the data is likely non-normal). Normality tests are often complemented by measuring the skewness and the kurtosis of the data distributions. The skewness describes the symmetry of the data while kurtosis quantifies the spread or peak sharpness of the distribution. A statistical test based on D'Agostino and Pearson's test was used in this study to further evaluate normality of the distributions of data (scipy.stats.normaltest). This test combines skew and kurtosis tests to produce an omnibus test of normality where again, a *p*-value of less than 0.05 indicates a significant difference (i.e. the data is likely non-normal).

These normality statistical tests were performed on each of the three distributions of data: the original, clinical data, the CPD-derived KBP predictions, and the MCOD-derived KBP predictions. These tests yielded p-values for each of the five bladder and five rectum dose-volumes observed in this study and can be seen in Table 12. These results indicated that a large majority of the data sets tested were likely non-normal distributions. To further support this interpretation, each data set was visually inspected via histograms and compared with fitted normal distributions. Two representative examples can be seen in Figure 13. Boxplots of the data may also be used as a visual tool when determining normality. The data visualization confirmed the normality tests and the

decision was made to proceed with non-parametric statistical tests. Uniform variance was not tested in this study since a repeated measures design was used.

Table 12: Normality statistical test *p*-values for the three distributions of data. A statistically significant result may be interpreted as the given data likely representing a non-normal distribution.

Dose-Volume	N†	Clinical Data		CPD Model		MCOD Model	
		Shapiro	Normal	Shapiro	Normal	Shapiro	Normal
Bladder							
D_{10}	123	< 0.001*	< 0.001*	< 0.001*	< 0.001*	< 0.001*	< 0.001*
D_{30}	107	0.01*	0.046*	0.001*	0.002	< 0.001*	< 0.001*
D_{50}	75	0.03*	0.10	< 0.001*	<0.001*	< 0.001*	0.006*
D_{65}	51	0.03*	0.03*	< 0.001*	<0.001*	< 0.001*	< 0.001*
D_{80}	34	0.08	0.03*	< 0.001*	<0.001*	< 0.001*	< 0.001*
Rectum							
D_{10}	123	< 0.001*	< 0.001*	< 0.001*	0.43	< 0.001*	< 0.001*
D_{30}	123	0.25	0.72	< 0.001*	< 0.001*	< 0.001*	< 0.001*
D_{50}	116	0.86	0.77	< 0.001*	0.005*	< 0.001*	< 0.001*
D_{65}	89	0.63	0.76	< 0.001*	< 0.001*	< 0.001*	< 0.001*
D_{80}	48	0.31	0.28	< 0.001*	0.005*	< 0.001*	< 0.001*

*Indicates a statistically significant result of $p < 0.05$

†N represents the number of database patients where an in-field OVH-driven KBP prediction was possible i.e. predictions were not made for patients with fractional in-field OAR volumes less than the given dose-volume

After carrying out the normality statistical test, an omnibus test was performed. Conducting an omnibus test is typically the first step when performing more than one statistical comparison. A total of three comparisons were made in this part of the study: Clinical vs. CPD, Clinical vs. MCOD, and CPD vs. MCOD distributions. The omnibus test checks whether there exists a difference between any of the datasets. In other words, it tests whether all datasets are statistically equivalent. If no statistically significant result is achieved, there is no need to continue to one-on-one comparisons between the individual datasets.

This study used the Friedman test to conduct the omnibus test (scipy.stats.friedmanchisquare), which tests the null hypothesis that repeated samples of the same individuals have the same distribution. Therefore, a statistically significant result means it is likely a difference exists between the distributions tested. This test is the non-parametric equivalent of the repeated measures analysis of variance (ANOVA) test. The *p*-values resulting from the Friedman test

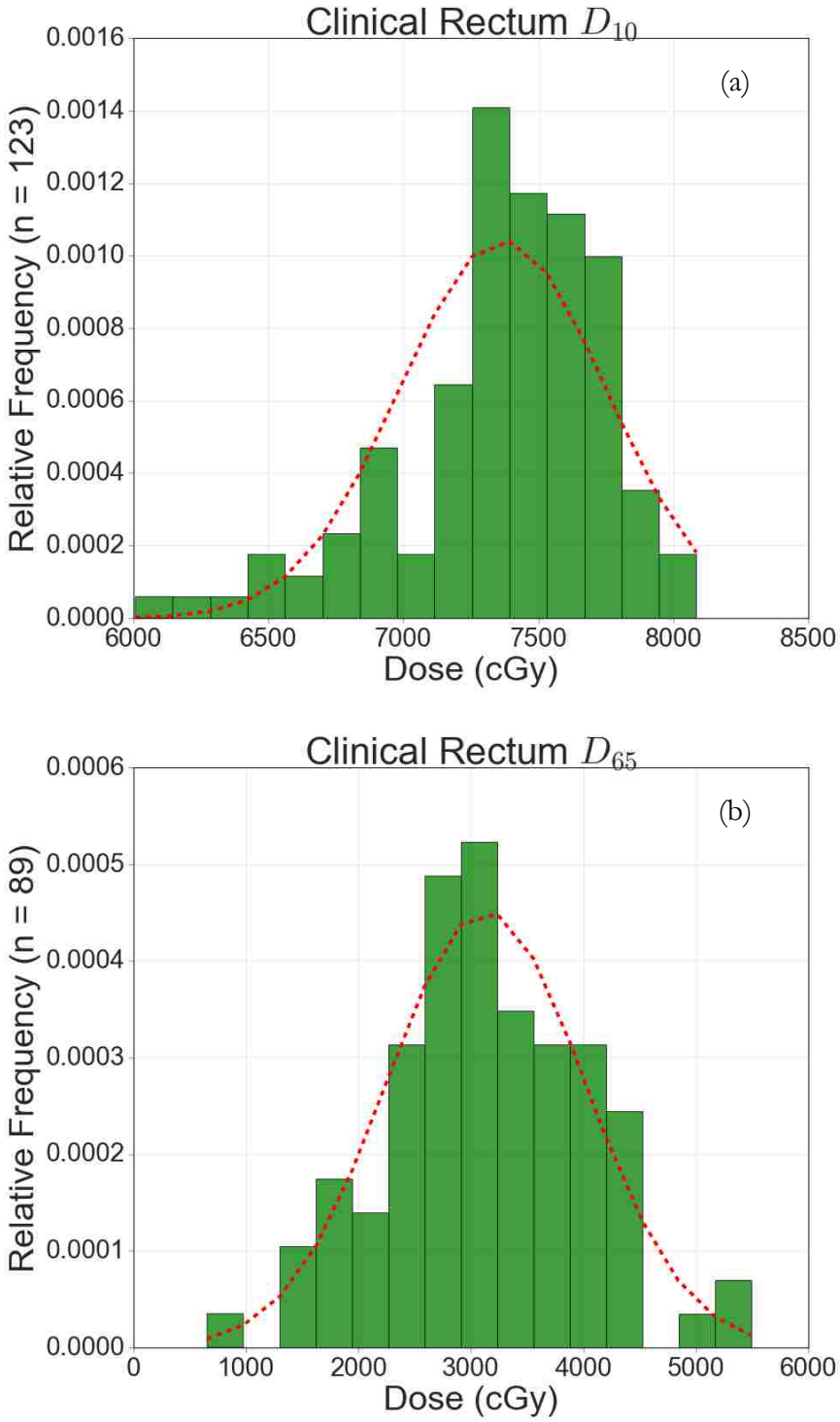

Figure 13: Representative examples of data visualization via density distribution histograms along with estimated normal curves, plotted using the mean and standard deviation of the data. (a) is an example of a distribution determined to likely be non-normal and (b) is an example of a distribution deemed to be normal.

are shown in Table 13. Each bladder and rectum dose-volume yielded a statistically significant result, indicating the need to perform one-on-one comparisons. This was accomplished via multiple Wilcoxon signed-rank tests, the results of which are detailed in Chapter 3.1.3.

Table 13: Results from the omnibus test. Each dose-volume yielded statistically significant results, indicating a difference likely exists between the three distributions of data.

Dose-Volume	N†	Friedman Test *p*-value
Bladder		
D_{10}	123	<0.001*
D_{30}	107	<0.001*
D_{50}	75	<0.001*
D_{65}	51	<0.001*
D_{80}	34	<0.001*
Rectum		
D_{10}	123	<0.001*
D_{30}	123	<0.001*
D_{50}	116	<0.001*
D_{65}	89	<0.001*
D_{80}	48	<0.001*

*Indicates a statistically significant result of $p < 0.05$

†N represents the number of database patients where an in-field OVH-driven KBP prediction was possible i.e. predictions were not made for patients with fractional in-field OAR volumes less than the given dose-volume

APPENDIX B. CPD VERSUS MCOD NOMINAL DVH-OVH CORRELATIONS

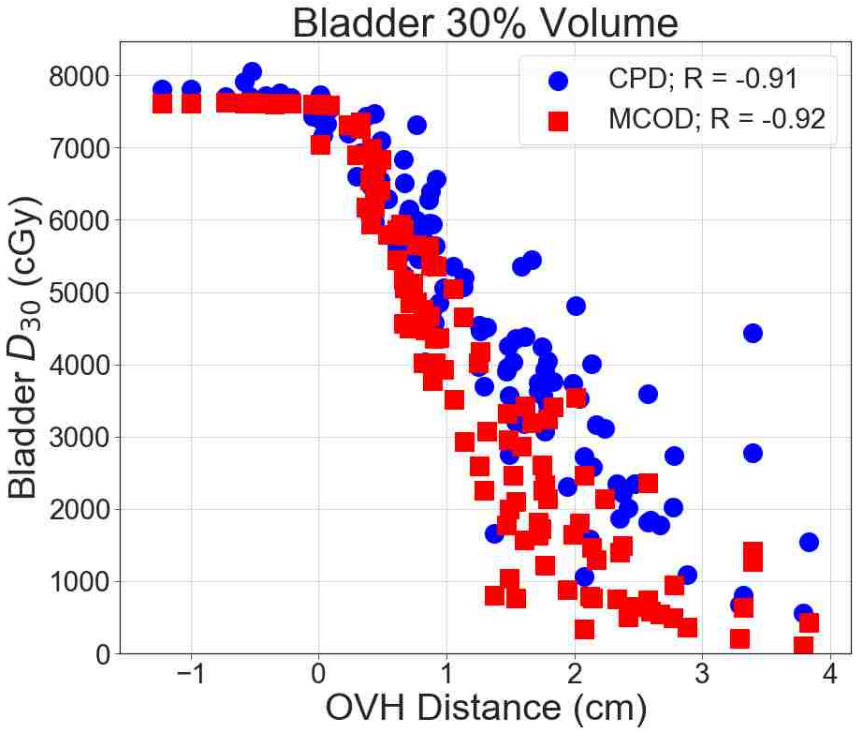

Figure 14: Nominal DVH-OVH correlation (R) using the CPD DVH data (circles) and the MCOD DVH data (squares) for the 30% dose-volume of the bladder.

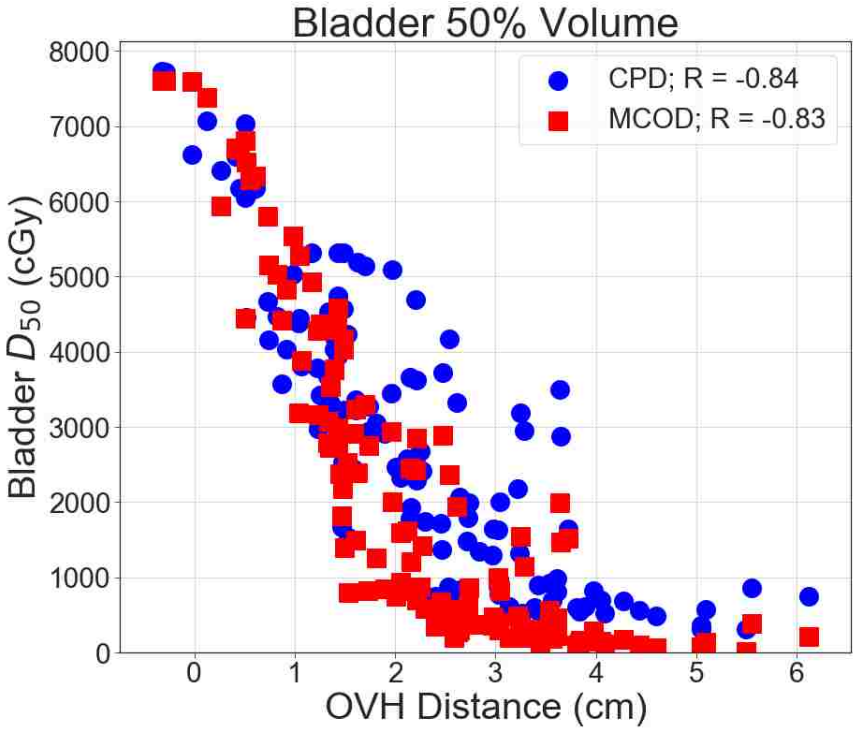

Figure 15: Nominal DVH-OVH correlation (R) using the CPD DVH data (circles) and the MCOD DVH data (squares) for the 50% dose-volume of the bladder.

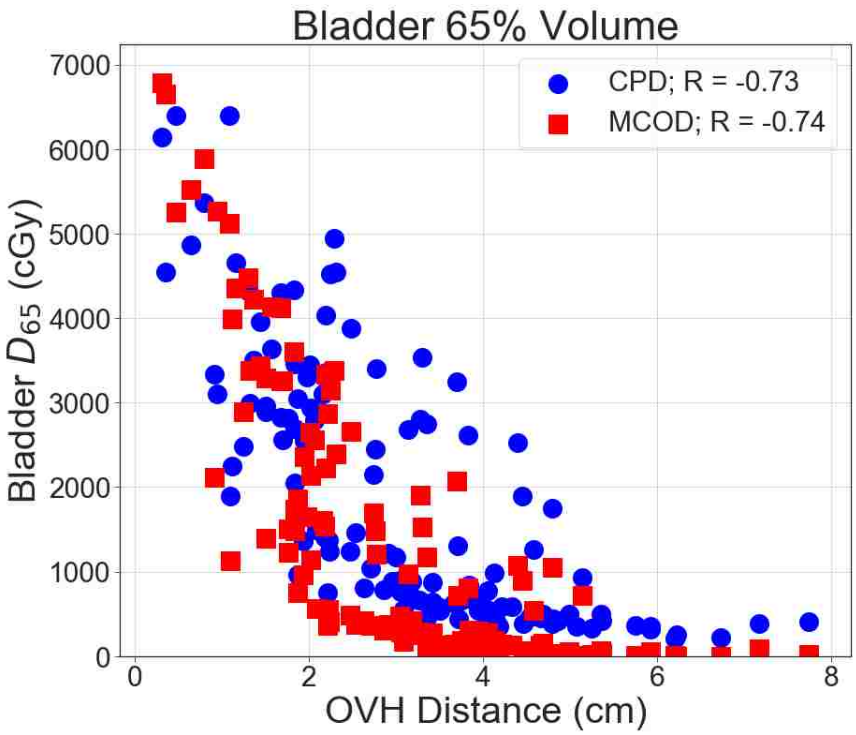

Figure 16: Nominal DVH-OVH correlation (R) using the CPD DVH data (circles) and the MCOD DVH data (squares) for the 65% dose-volume of the bladder.

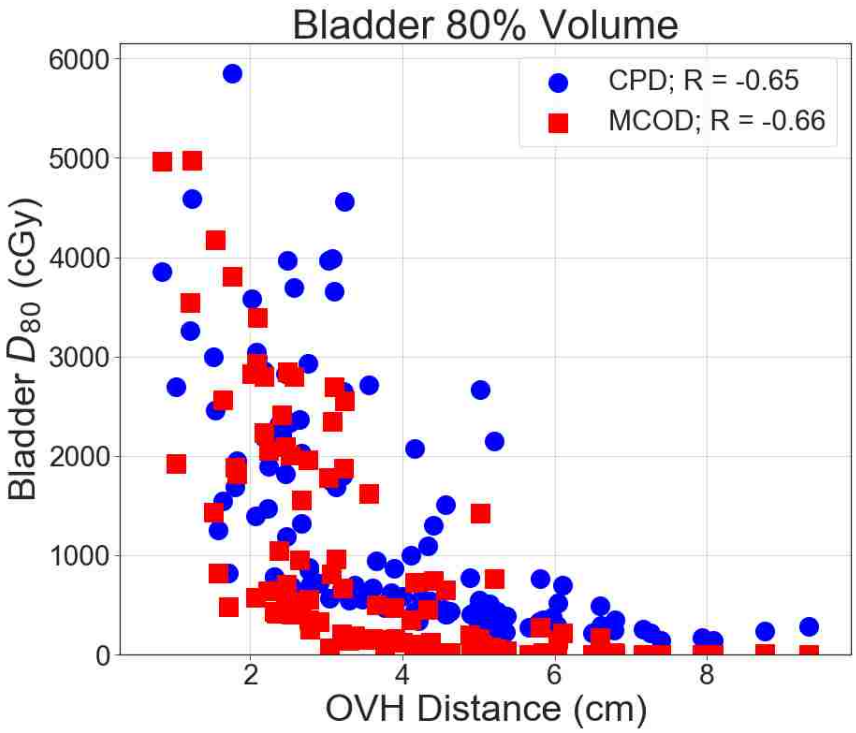

Figure 17: Nominal DVH-OVH correlation (R) using the CPD DVH data (circles) and the MCOD DVH data (squares) for the 80% dose-volume of the bladder.

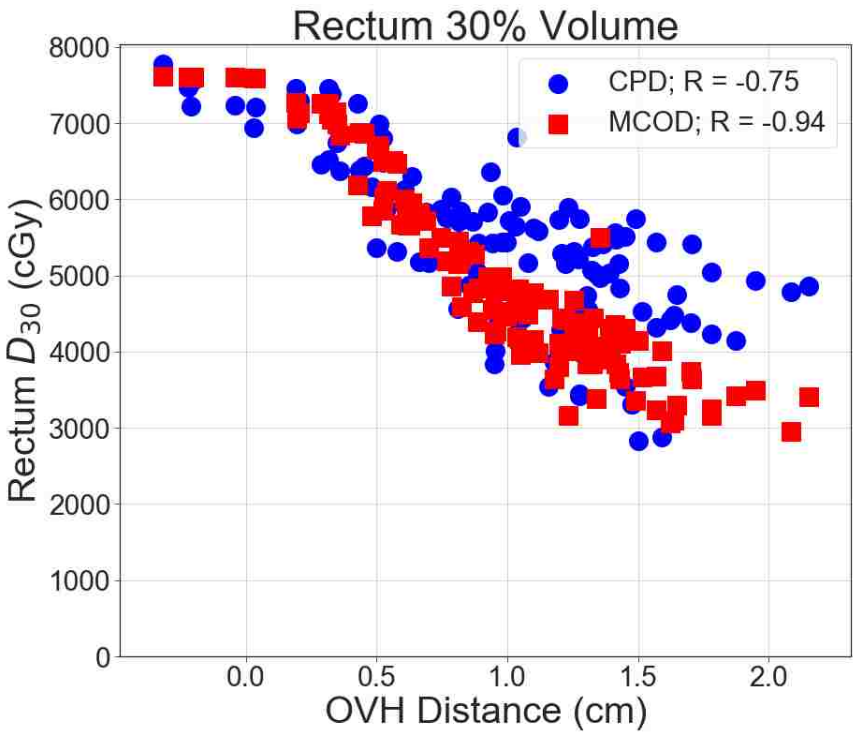

Figure 18: Nominal DVH-OVH correlation (R) using the CPD DVH data (circles) and the MCOD DVH data (squares) for the 30% dose-volume of the rectum.

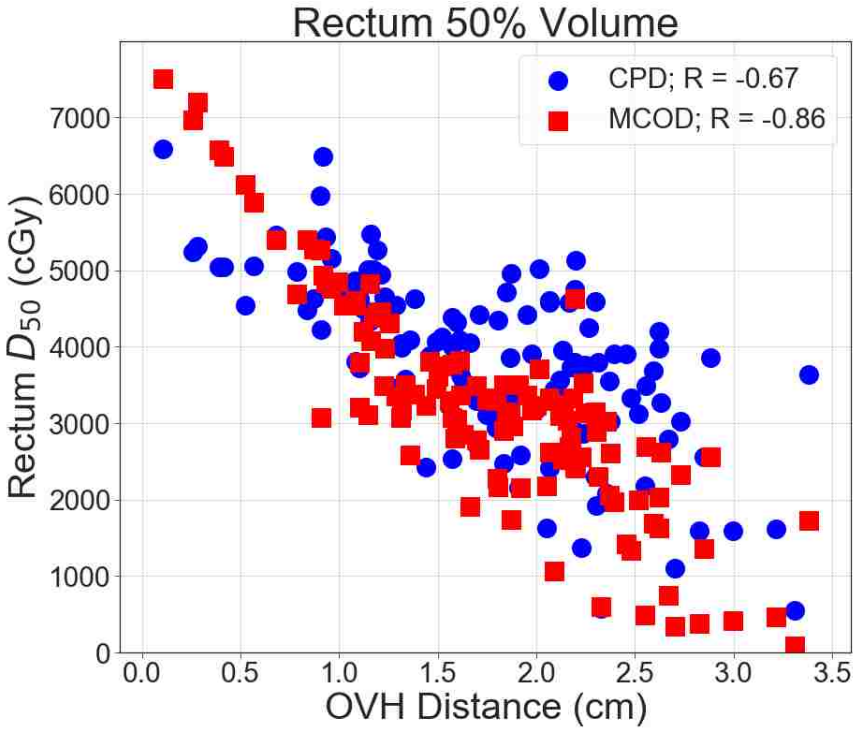

Figure 19: Nominal DVH-OVH correlation (R) using the CPD DVH data (circles) and the MCOD DVH data (squares) for the 50% dose-volume of the rectum.

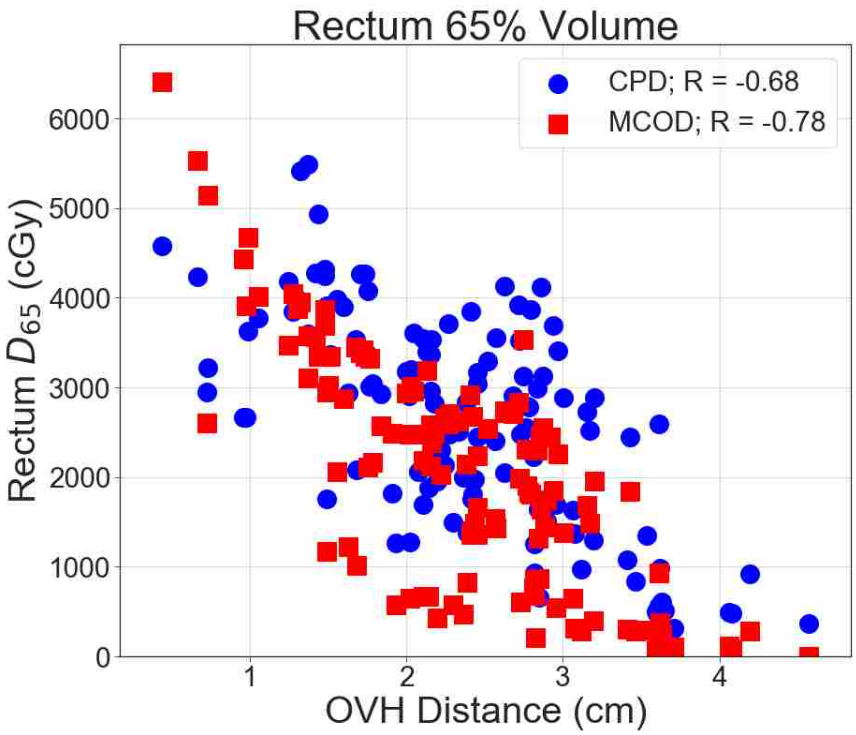

Figure 20: Nominal DVH-OVH correlation (R) using the CPD DVH data (circles) and the MCOD DVH data (squares) for the 65% dose-volume of the rectum.

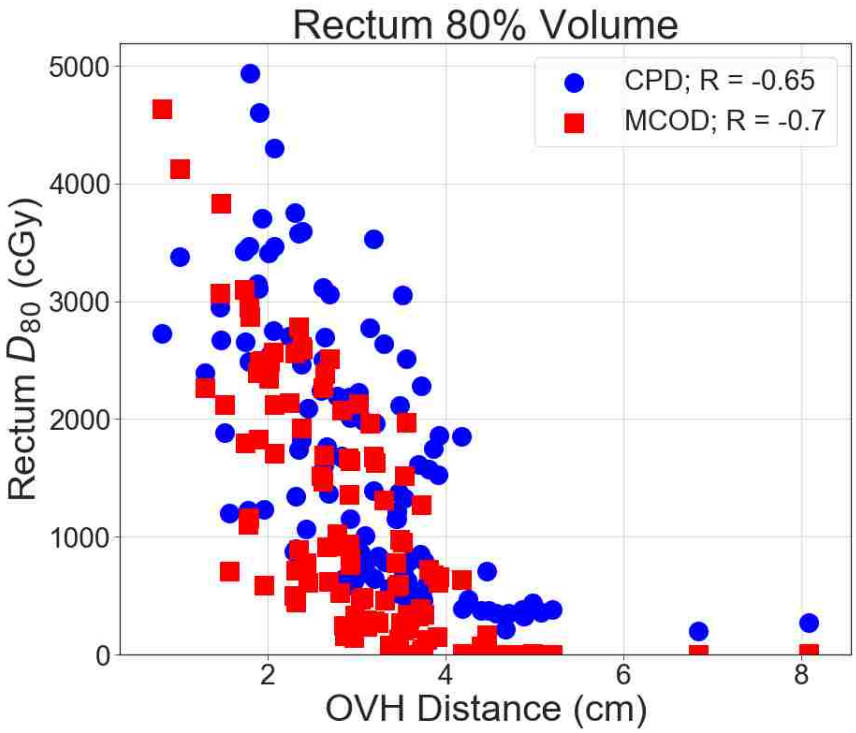

Figure 21: Nominal DVH-OVH correlation (R) using the CPD DVH data (circles) and the MCOD DVH data (squares) for the 80% dose-volume of the rectum.

Table 14: Summary of the Pearson correlation coefficients for the distance-to-dose relationships formed with the CPD and MCOD dose data. The nominal OVH data was used for these correlations. The MCOD dose produced a stronger correlation with distance overall, most noticeably in the rectum. This is most likely due to the removal of the inter-planner subjectivity present in the CPD dose data.

Dose-Volume	DVH-OVH R	
	CPD	MCOD
Bladder		
D_{30}	-0.91	-0.92
D_{50}	-0.84	-0.83
D_{65}	-0.73	-0.74
D_{80}	-0.65	-0.66
Mean	-0.78	-0.79
Rectum		
D_{30}	-0.75	-0.94
D_{50}	-0.67	-0.86
D_{65}	-0.68	-0.78
D_{80}	-0.65	-0.70
Mean	-0.69	-0.82

APPENDIX C. COLOR BAR CORRELATION PLOTS OF SECOND-ORDER FACTORS

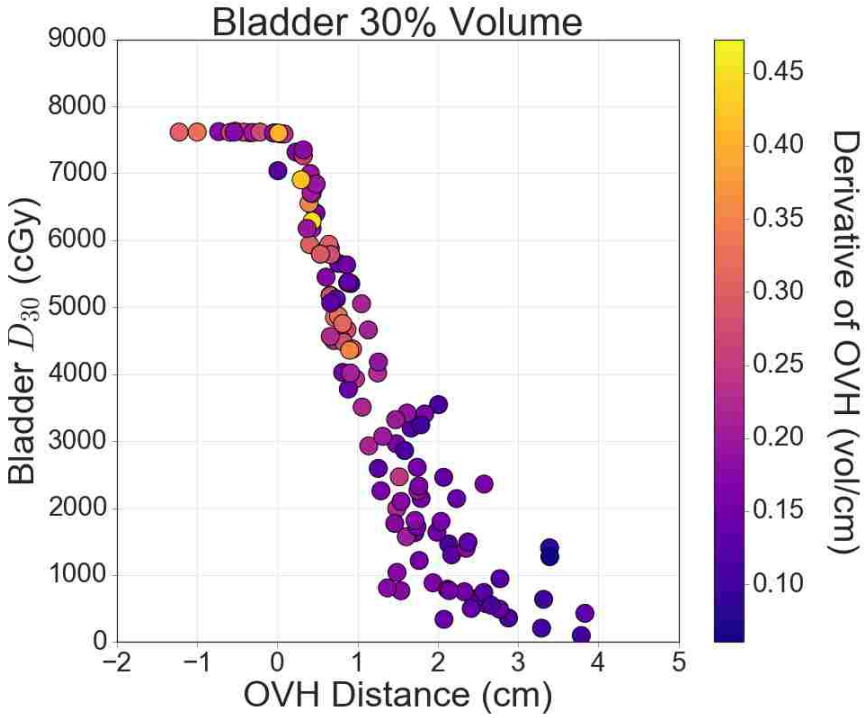

Figure 22: Color bar scatter plot for distance-to-dose relationship for 30% of the bladder, where the color-mapped variable is the derivative of the OVH.

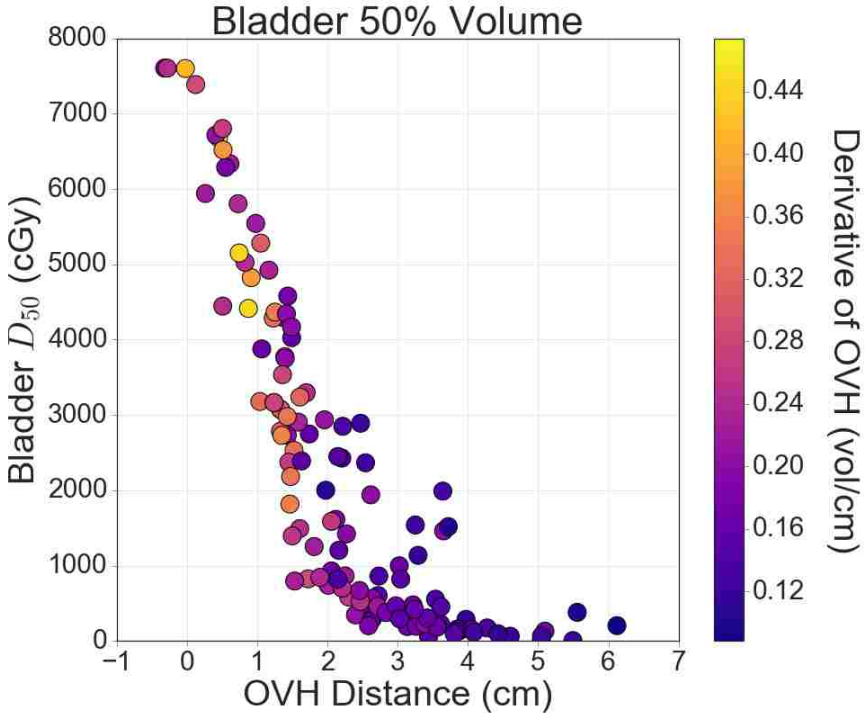

Figure 23: Color bar scatter plot for distance-to-dose relationship for 50% of the bladder, where the color-mapped variable is the derivative of the OVH.

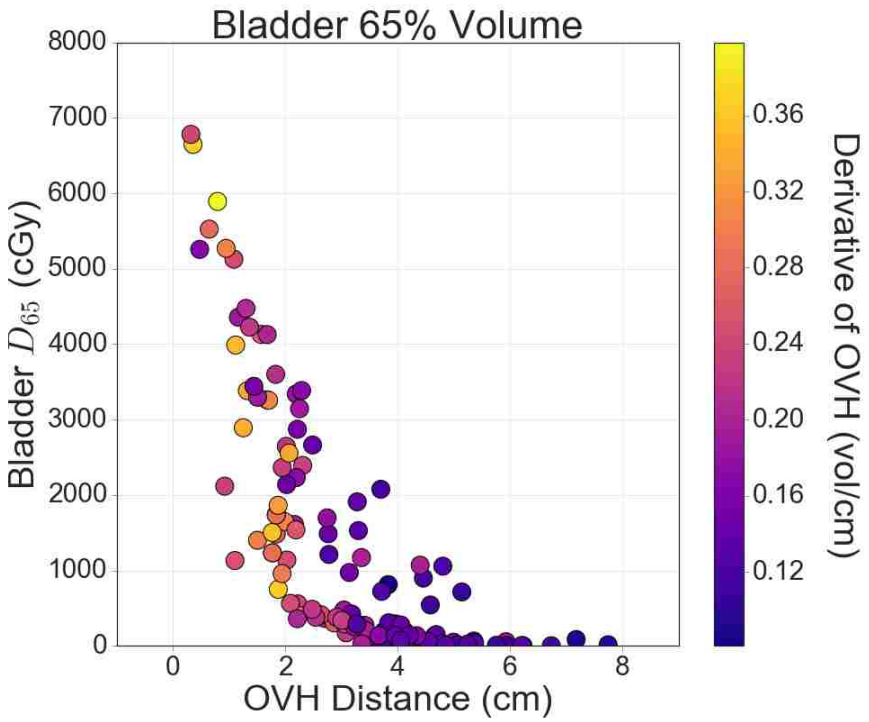

Figure 24: Color bar scatter plot for distance-to-dose relationship for 65% of the bladder, where the color-mapped variable is the derivative of the OVH.

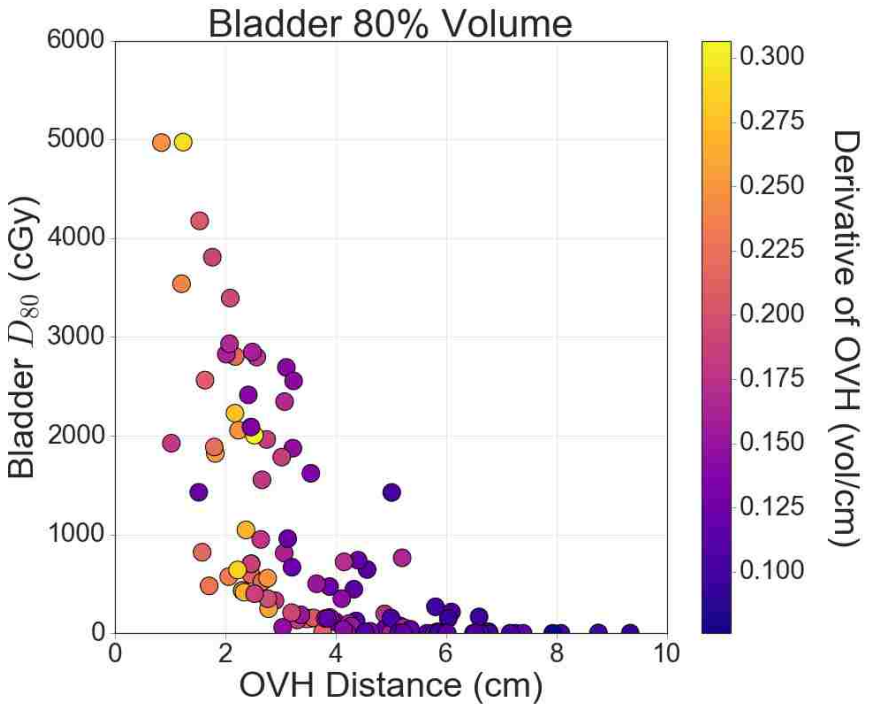

Figure 25: Color bar scatter plot for distance-to-dose relationship for 80% of the bladder, where the color-mapped variable is the derivative of the OVH.

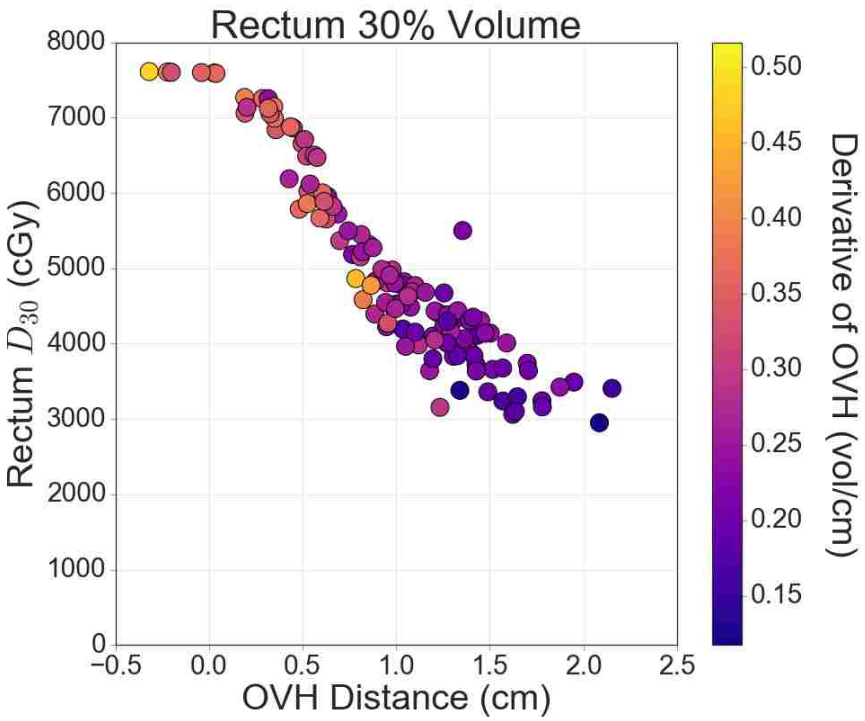

Figure 26: Color bar scatter plot for distance-to-dose relationship for 30% of the rectum, where the color-mapped variable is the derivative of the OVH.

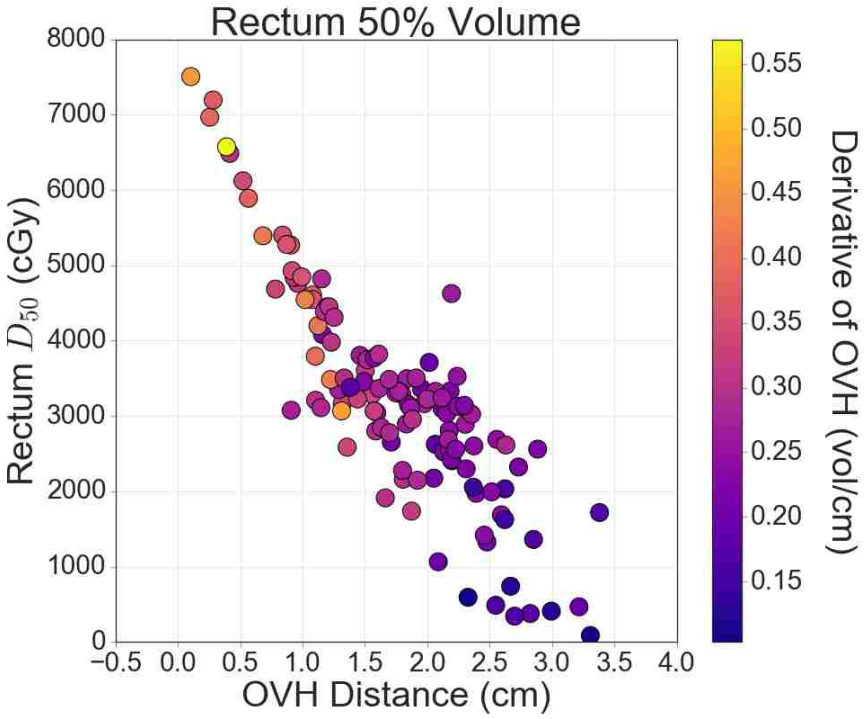

Figure 27: Color bar scatter plot for distance-to-dose relationship for 50% of the rectum, where the color-mapped variable is the derivative of the OVH.

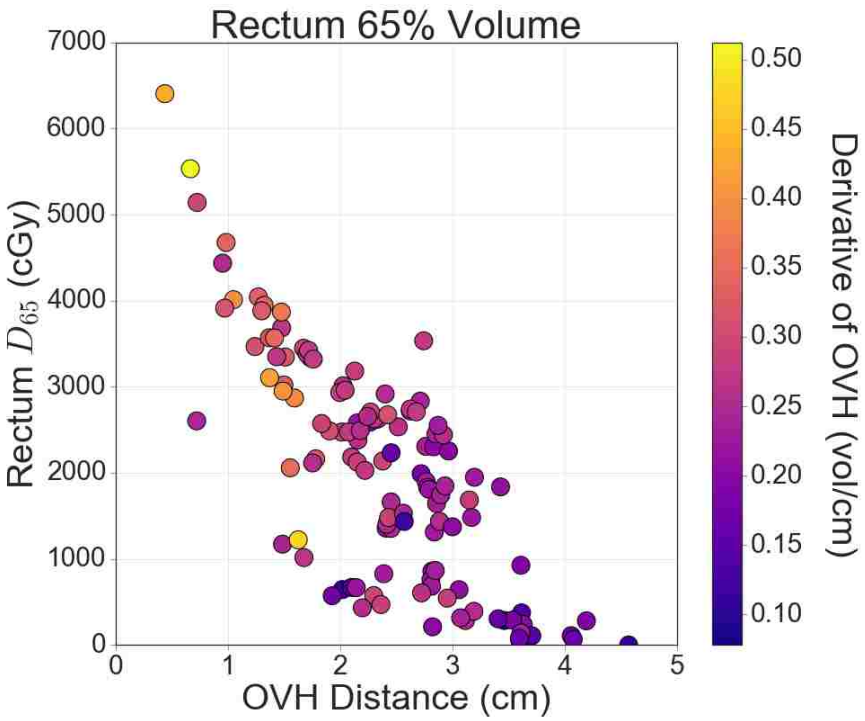

Figure 28: Color bar scatter plot for distance-to-dose relationship for 65% of the rectum, where the color-mapped variable is the derivative of the OVH.

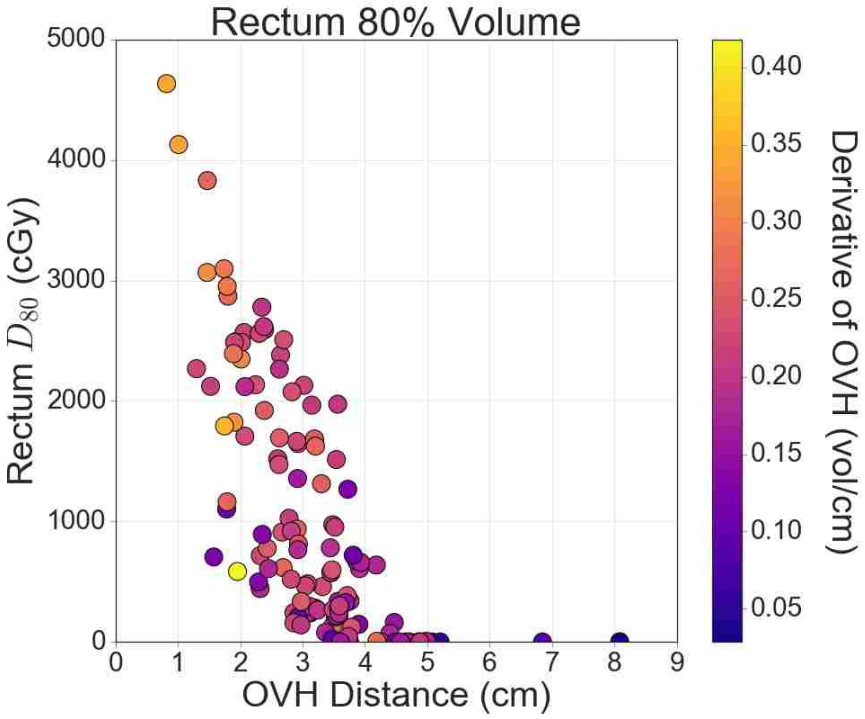

Figure 29: Color bar scatter plot for distance-to-dose relationship for 80% of the rectum, where the color-mapped variable is the derivative of the OVH.

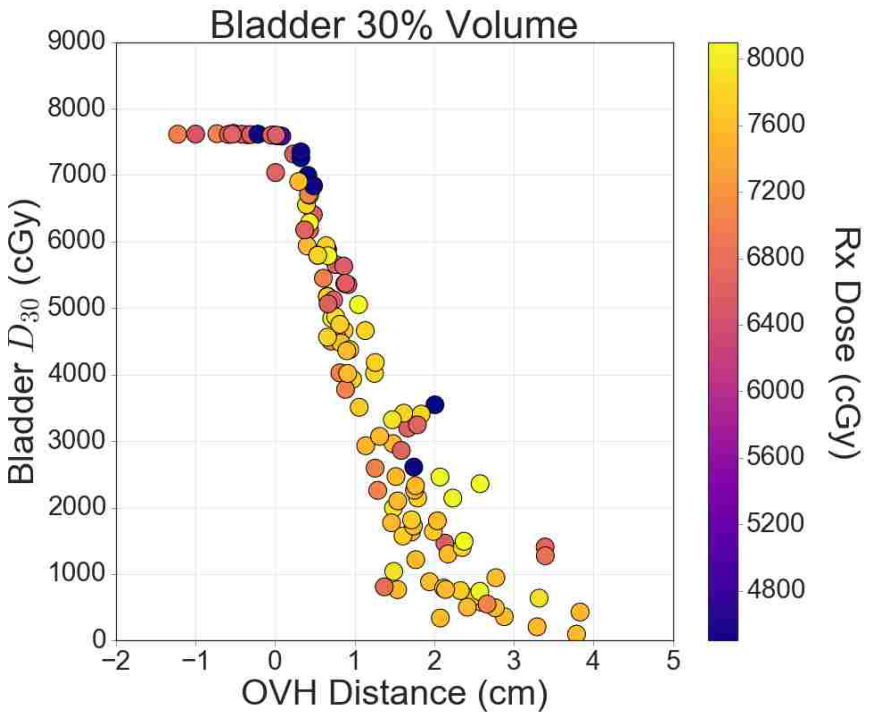

Figure 30: Color bar scatter plot for distance-to-dose relationship for 30% of the bladder, where the color-mapped variable is the prescription dose.

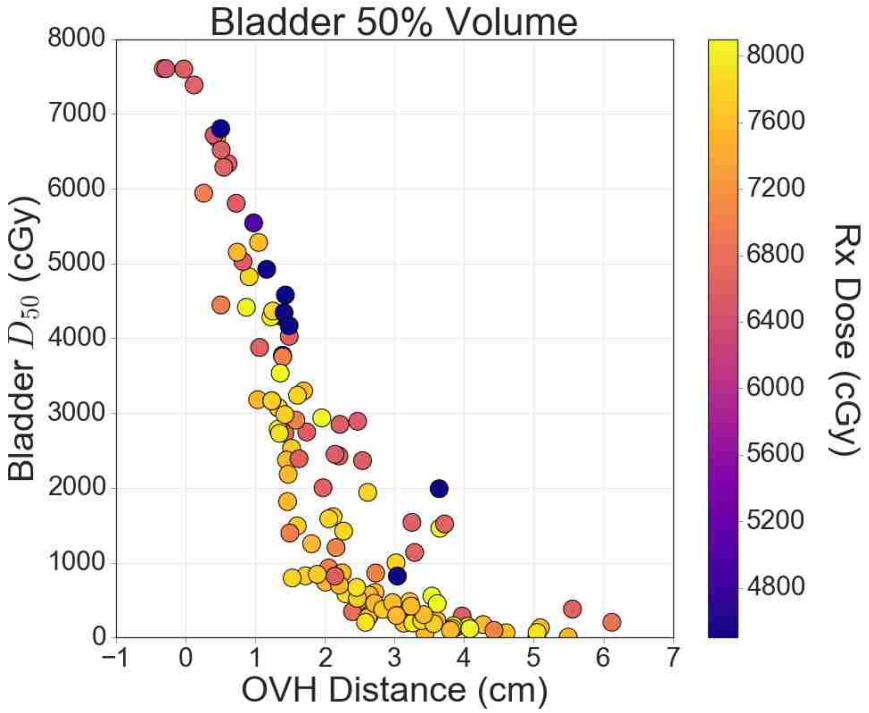

Figure 31: Color bar scatter plot for distance-to-dose relationship for 50% of the bladder, where the color-mapped variable is the prescription dose.

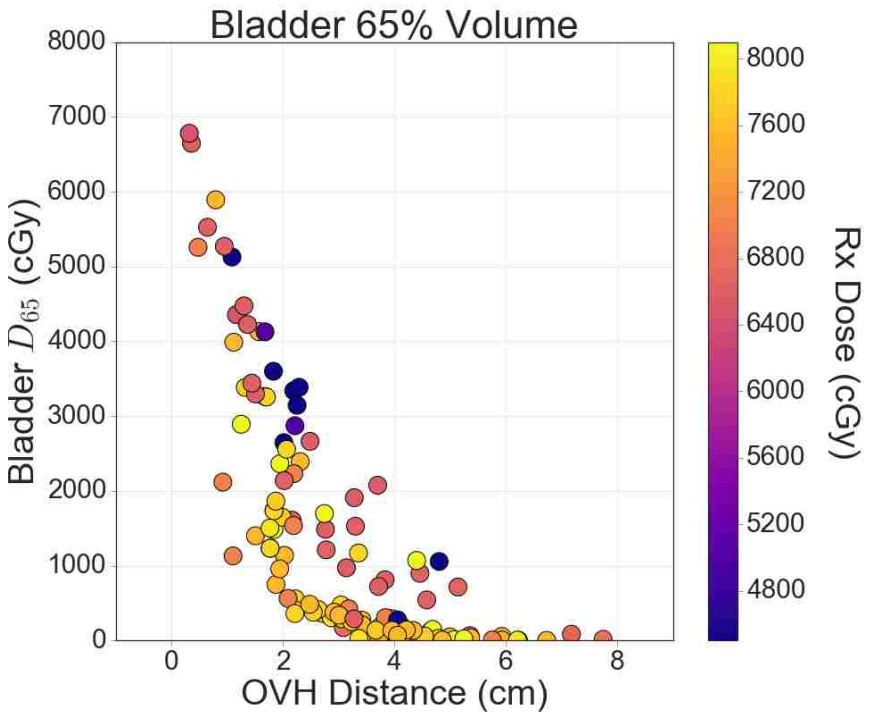

Figure 32: Color bar scatter plot for distance-to-dose relationship for 65% of the bladder, where the color-mapped variable is the prescription dose.

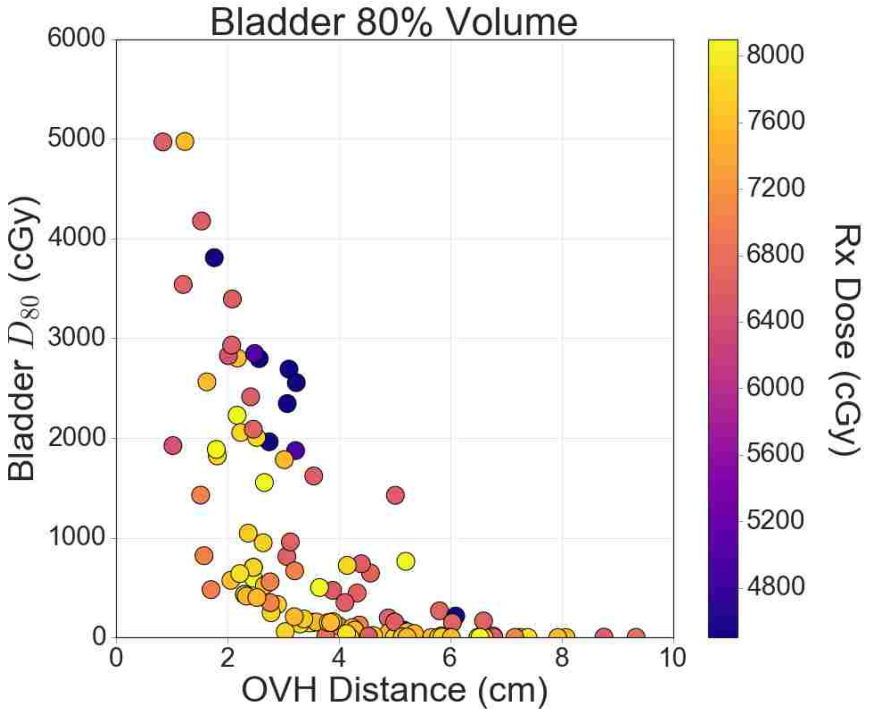

Figure 33: Color bar scatter plot for distance-to-dose relationship for 80% of the bladder, where the color-mapped variable is the prescription dose.

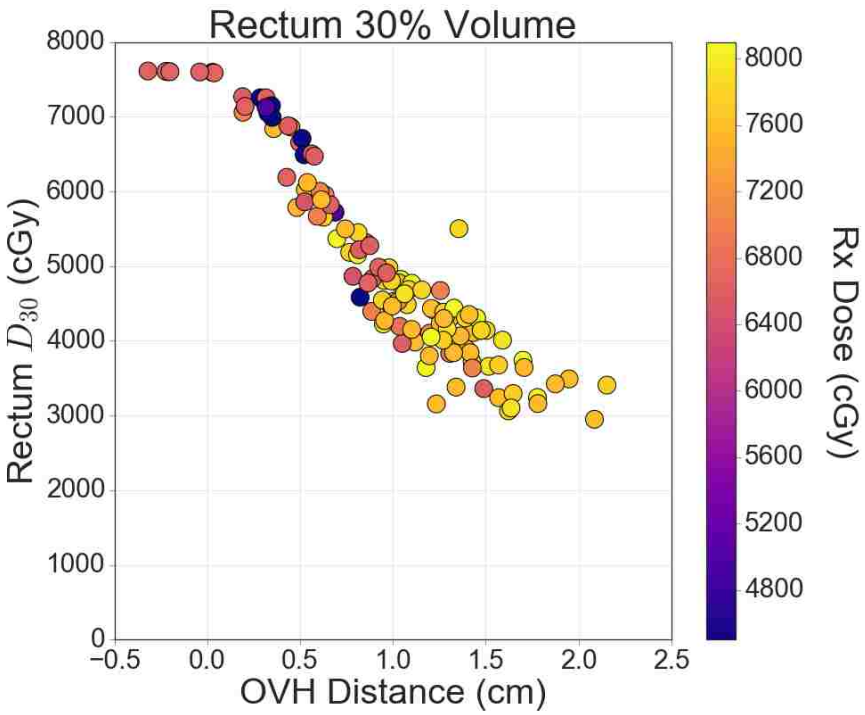

Figure 34: Color bar scatter plot for distance-to-dose relationship for 30% of the rectum, where the color-mapped variable is the prescription dose.

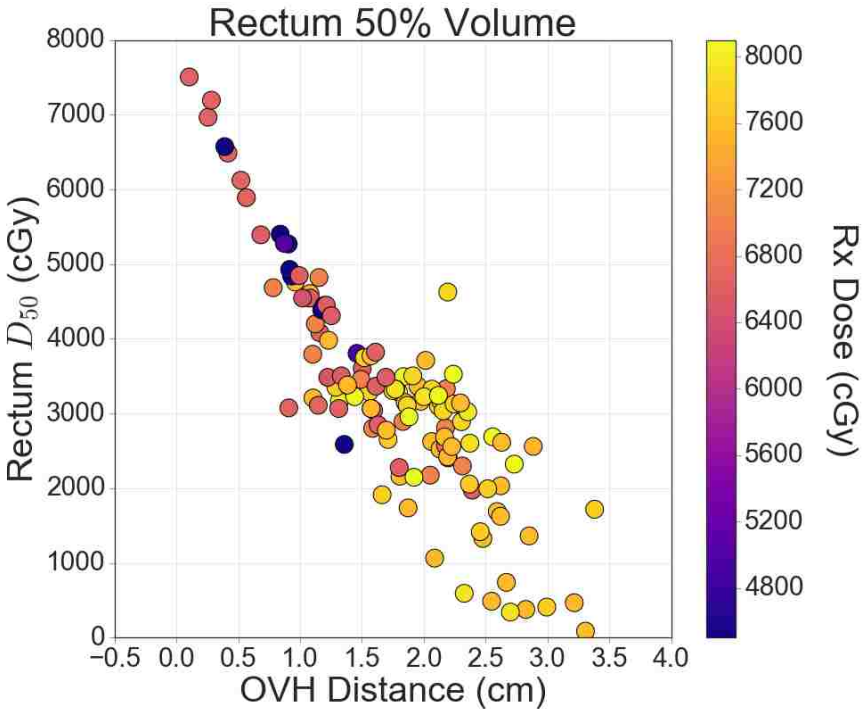

Figure 35: Color bar scatter plot for distance-to-dose relationship for 50% of the rectum, where the color-mapped variable is the prescription dose.

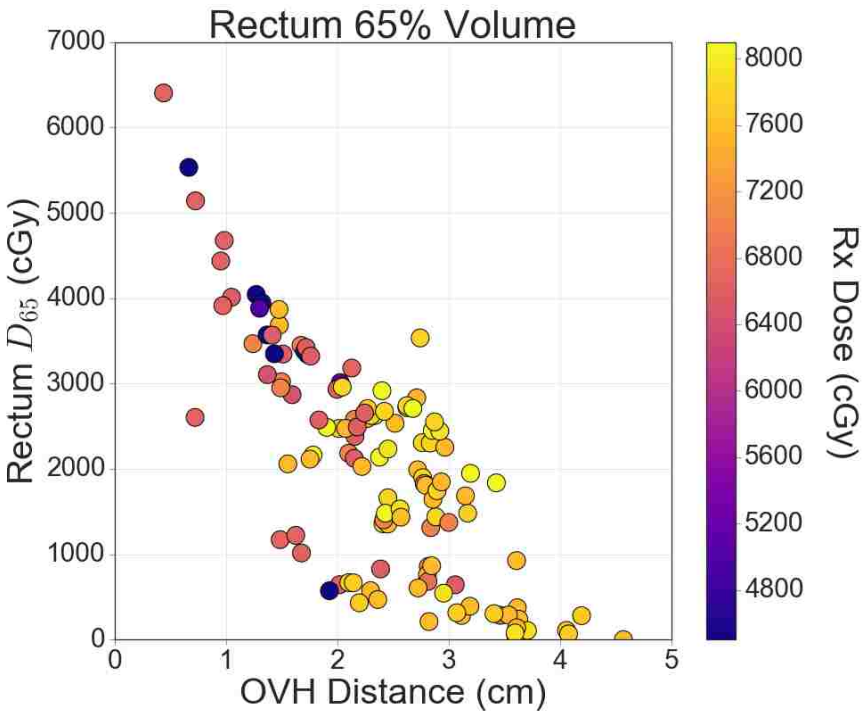

Figure 36: Color bar scatter plot for distance-to-dose relationship for 65% of the rectum, where the color-mapped variable is the prescription dose.

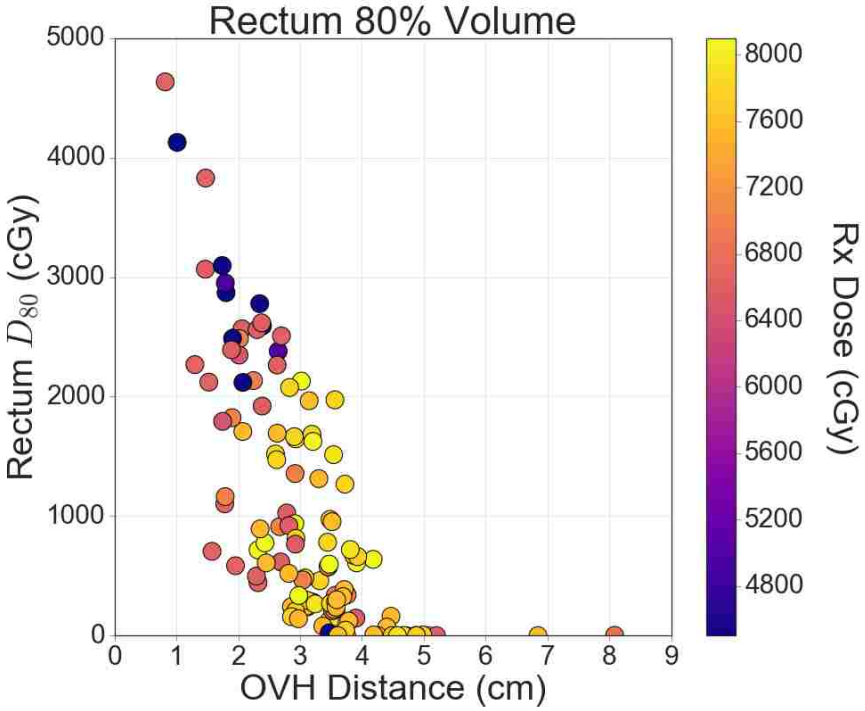

Figure 37: Color bar scatter plot for distance-to-dose relationship for 80% of the rectum, where the color-mapped variable is the prescription dose.

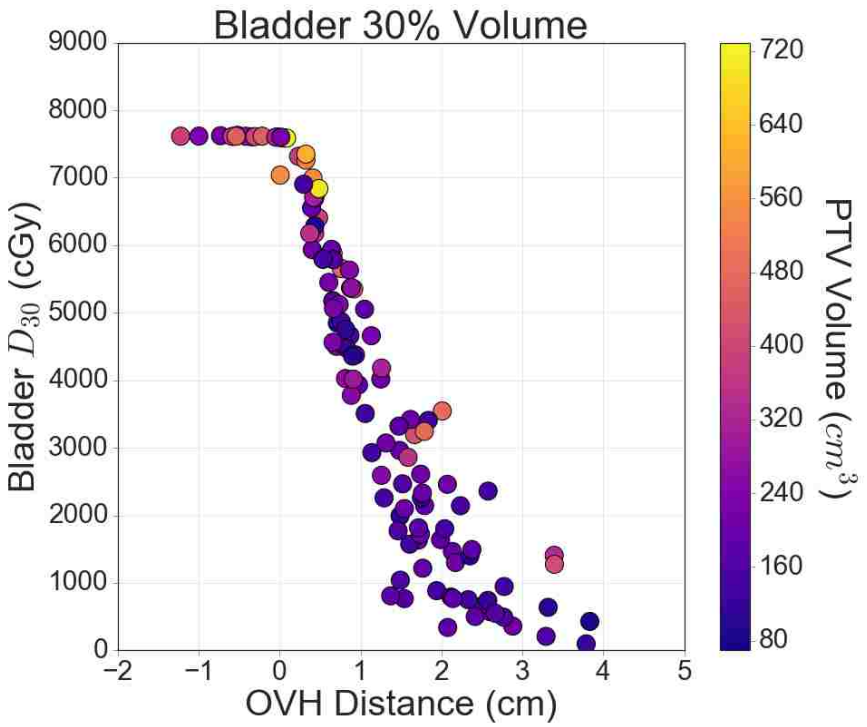

Figure 38: Color bar scatter plot for distance-to-dose relationship for 30% of the bladder, where the color-mapped variable is the PTV volume.

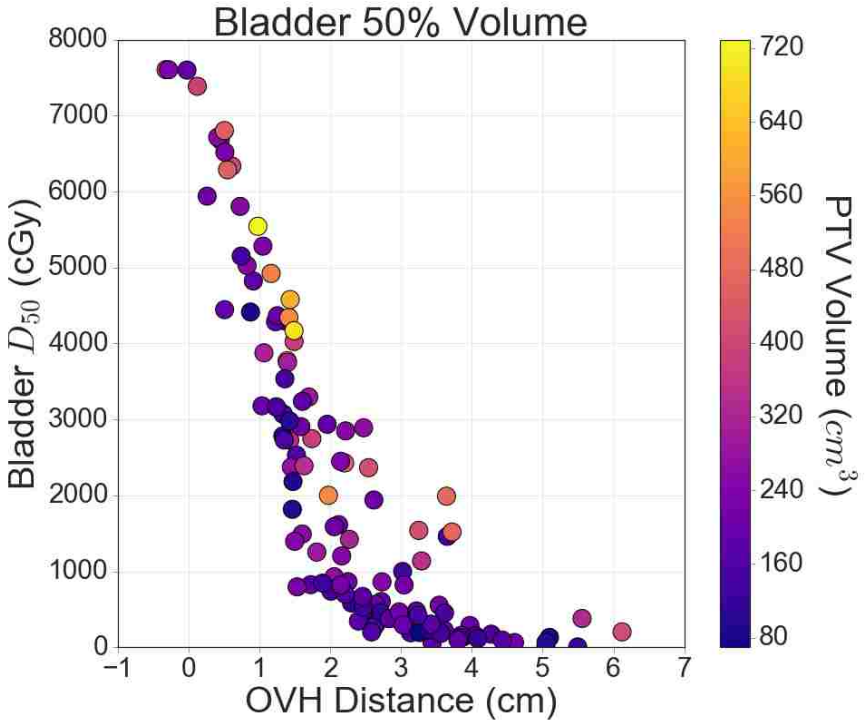

Figure 39: Color bar scatter plot for distance-to-dose relationship for 50% of the bladder, where the color-mapped variable is the PTV volume.

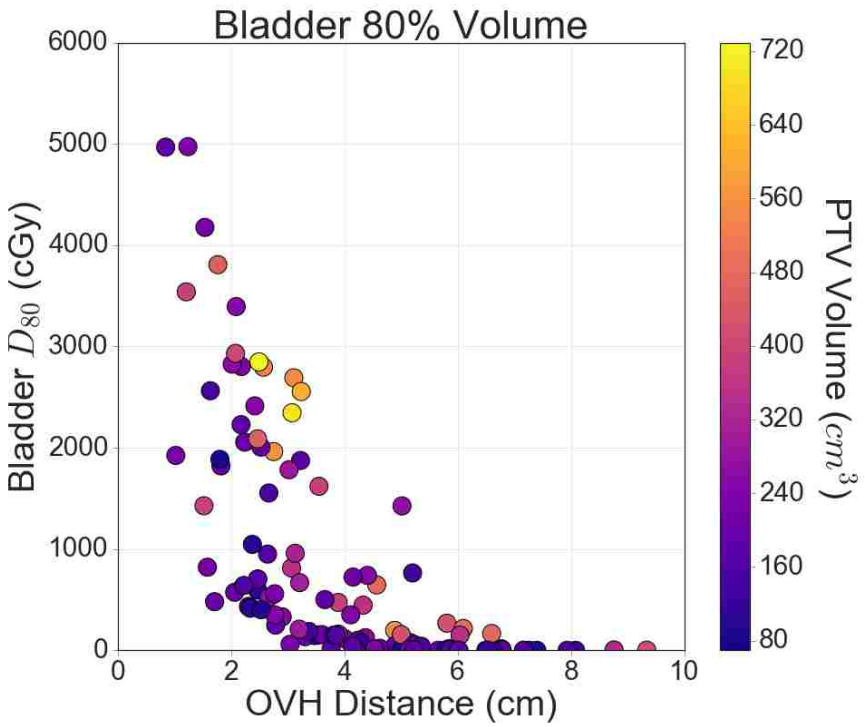

Figure 40: Color bar scatter plot for distance-to-dose relationship for 80% of the bladder, where the color-mapped variable is the PTV volume.

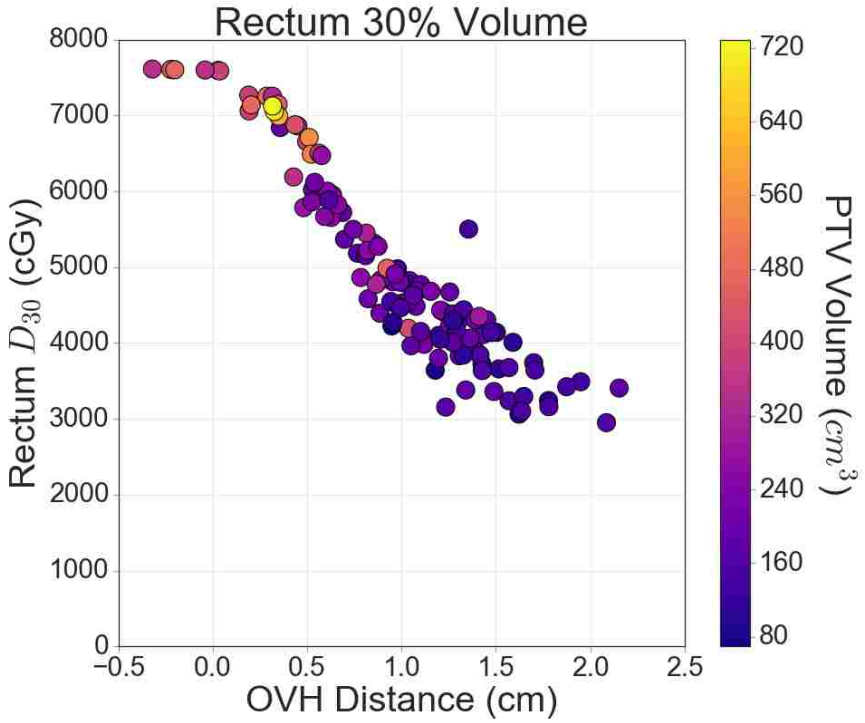

Figure 41: Color bar scatter plot for distance-to-dose relationship for 30% of the rectum, where the color-mapped variable is the PTV volume.

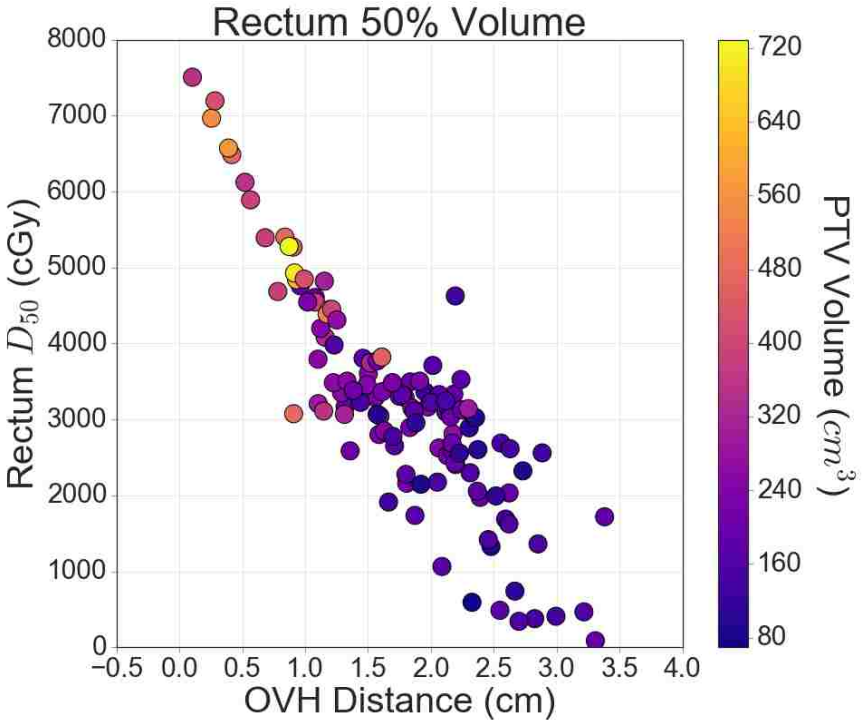

Figure 42: Color bar scatter plot for distance-to-dose relationship for 50% of the rectum, where the color-mapped variable is the PTV volume.

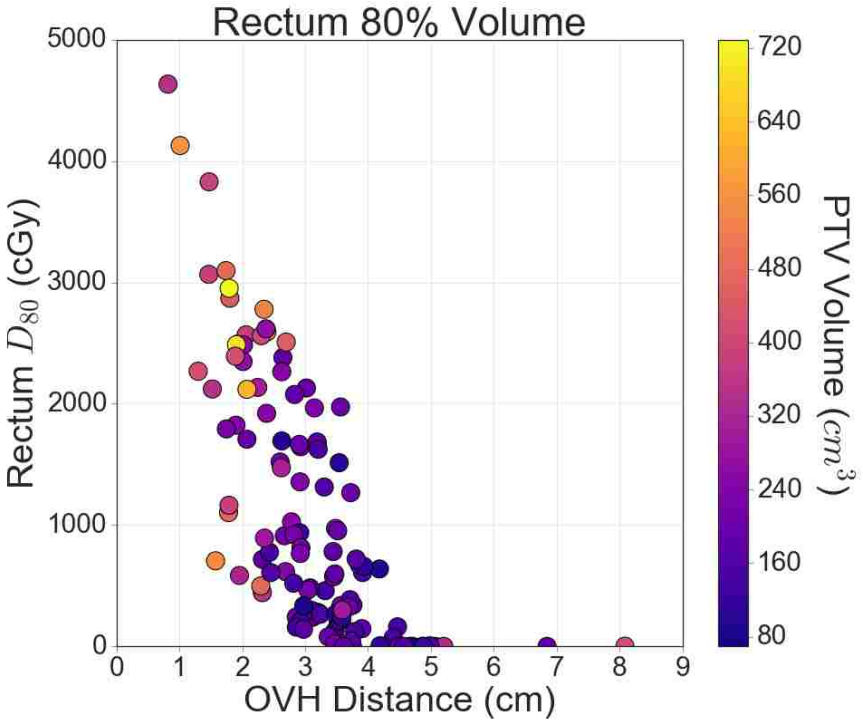

Figure 43: Color bar scatter plot for distance-to-dose relationship for 80% of the rectum, where the color-mapped variable is the PTV volume.

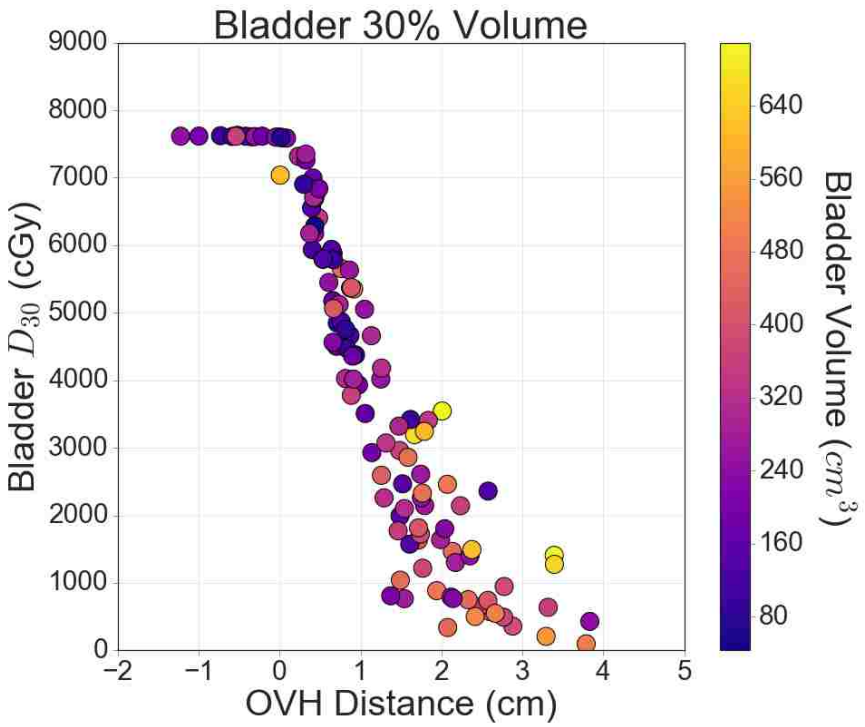

Figure 44: Color bar scatter plot for distance-to-dose relationship for 30% of the bladder, where the color-mapped variable is the bladder volume.

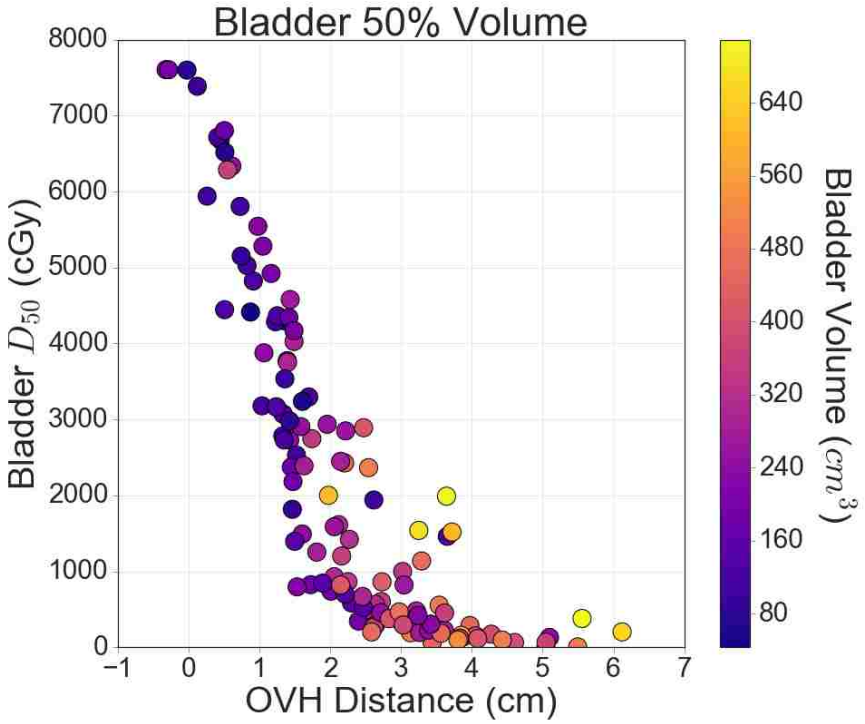

Figure 45: Color bar scatter plot for distance-to-dose relationship for 50% of the bladder, where the color-mapped variable is the bladder volume.

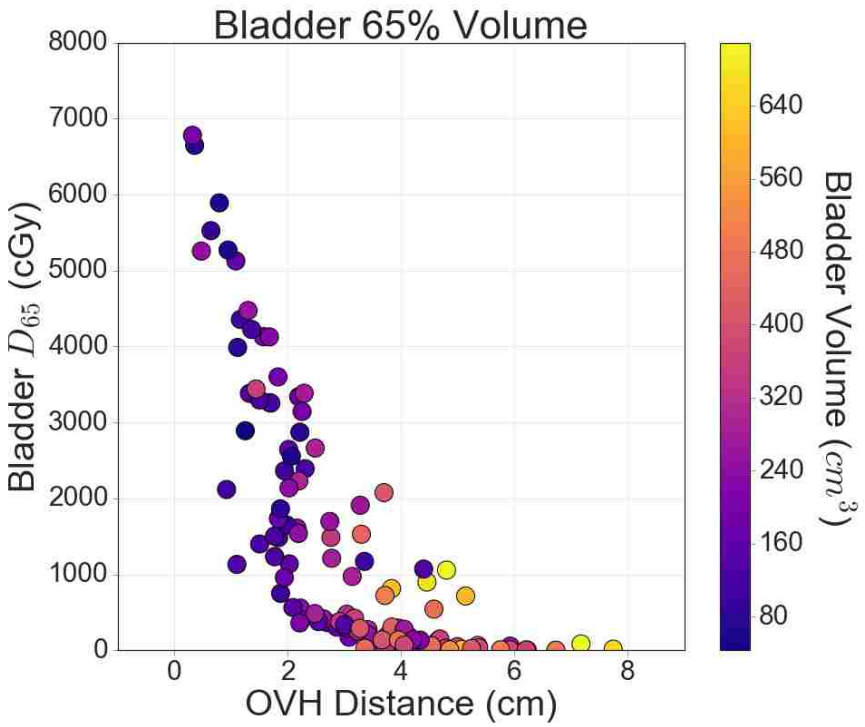

Figure 46: Color bar scatter plot for distance-to-dose relationship for 65% of the bladder, where the color-mapped variable is the bladder volume.

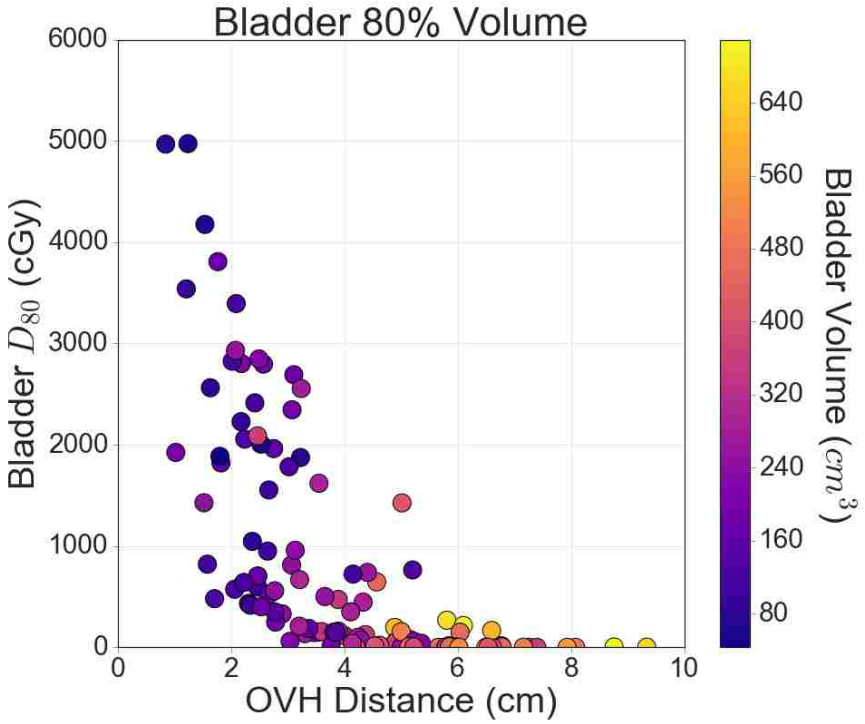

Figure 47: Color bar scatter plot for distance-to-dose relationship for 80% of the bladder, where the color-mapped variable is the bladder volume.

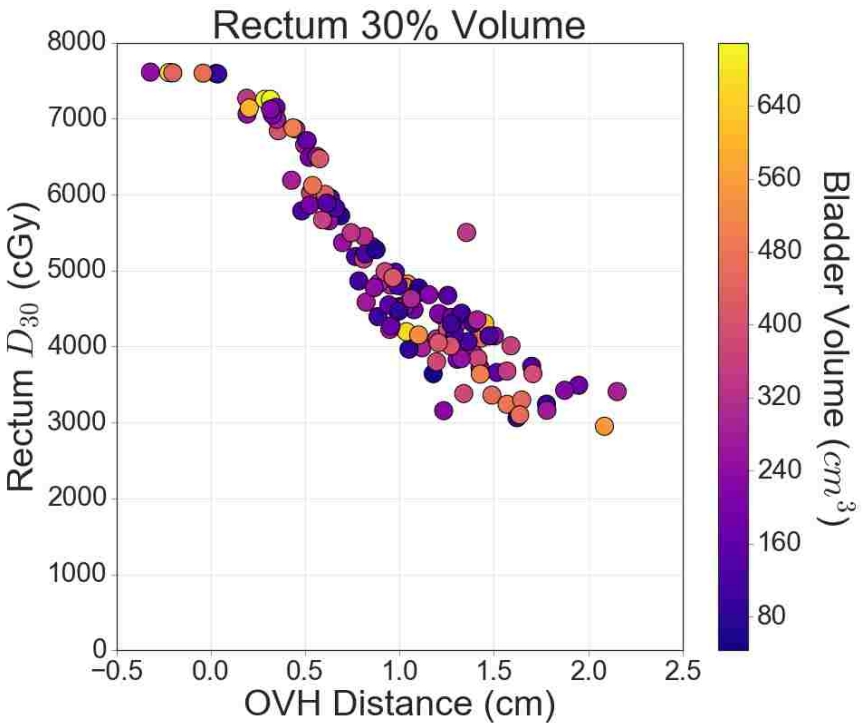

Figure 48: Color bar scatter plot for distance-to-dose relationship for 30% of the rectum, where the color-mapped variable is the bladder volume.

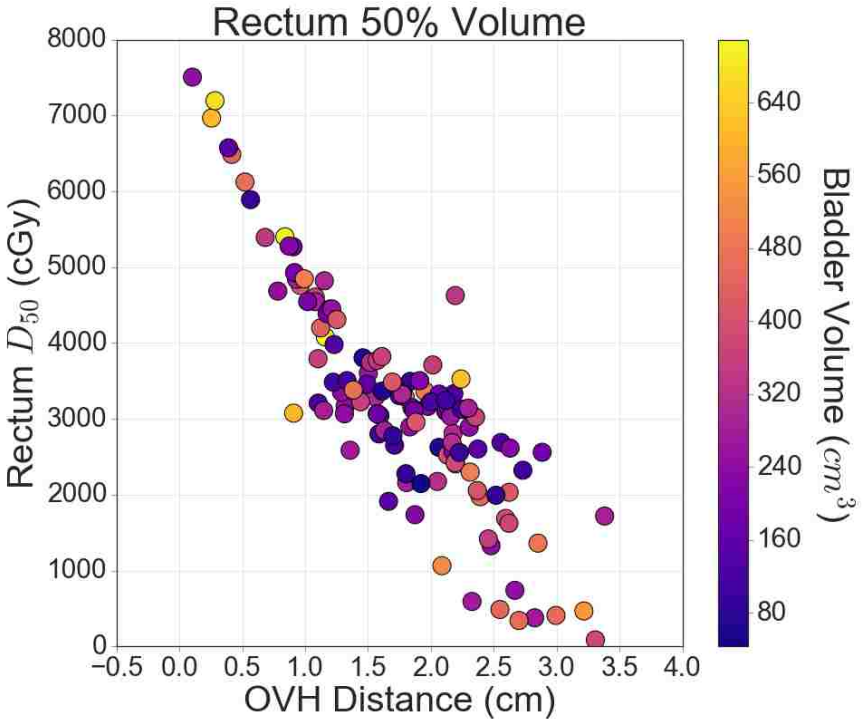

Figure 49: Color bar scatter plot for distance-to-dose relationship for 50% of the rectum, where the color-mapped variable is the bladder volume.

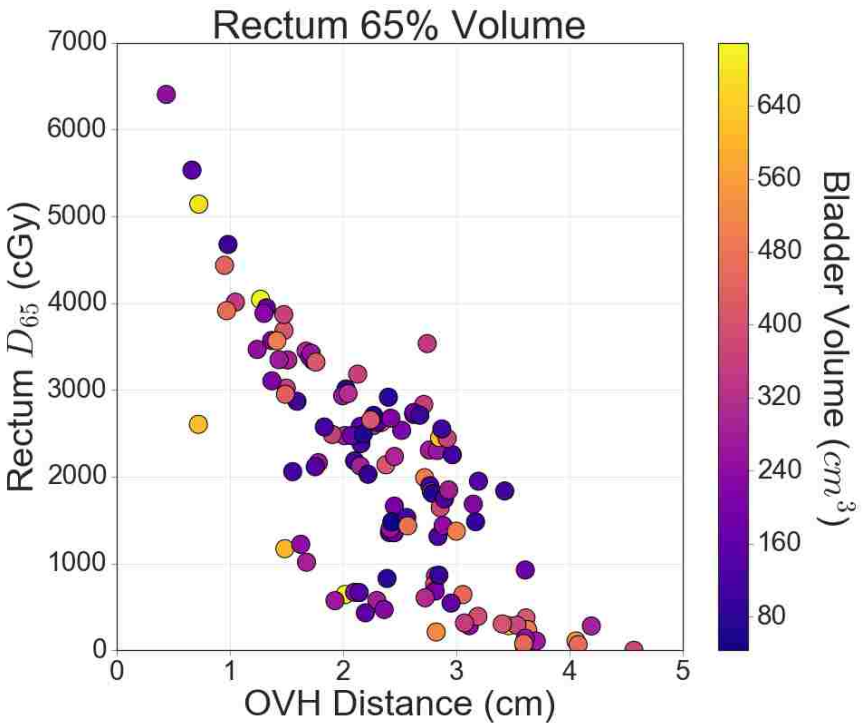

Figure 50: Color bar scatter plot for distance-to-dose relationship for 65% of the rectum, where the color-mapped variable is the bladder volume.

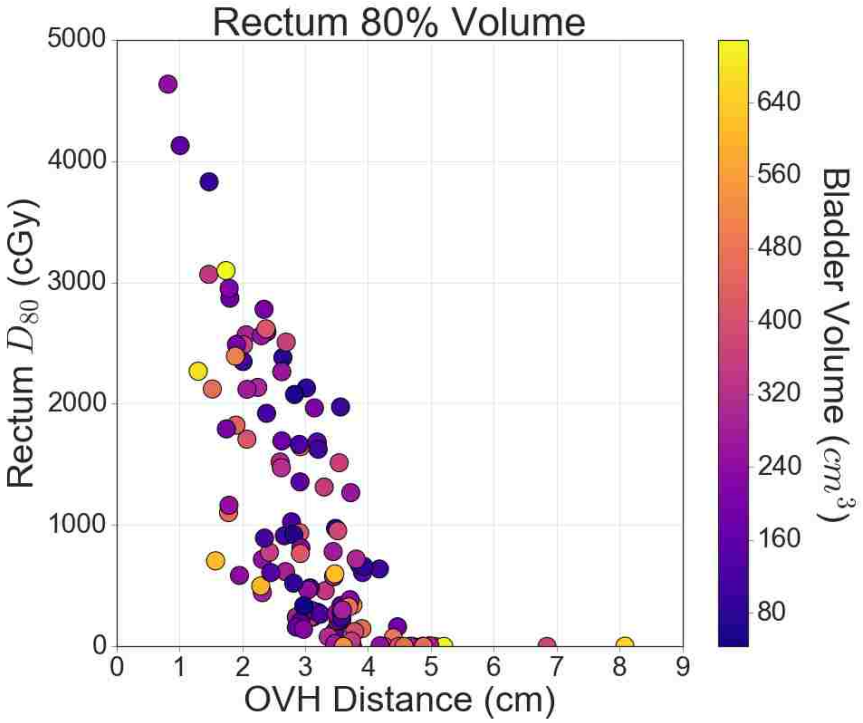

Figure 51: Color bar scatter plot for distance-to-dose relationship for 80% of the rectum, where the color-mapped variable is the bladder volume.

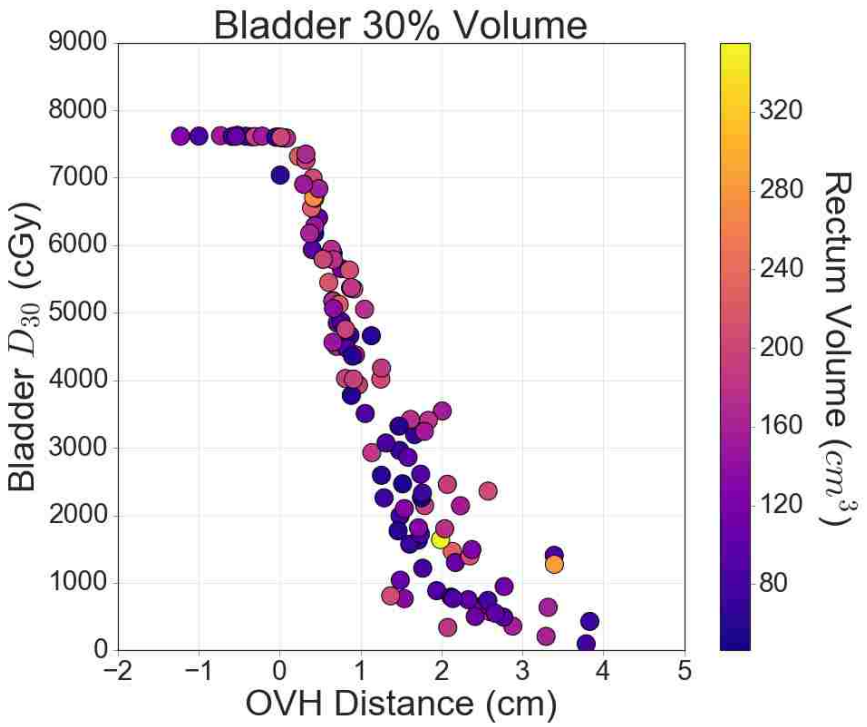

Figure 52: Color bar scatter plot for distance-to-dose relationship for 30% of the bladder, where the color-mapped variable is the rectum volume.

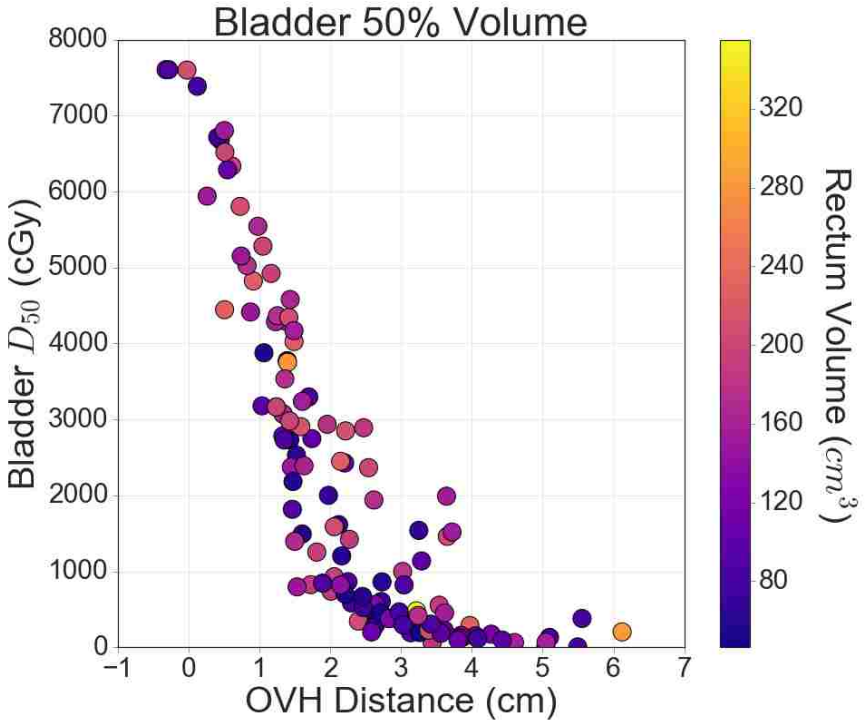

Figure 53: Color bar scatter plot for distance-to-dose relationship for 50% of the bladder, where the color-mapped variable is the rectum volume.

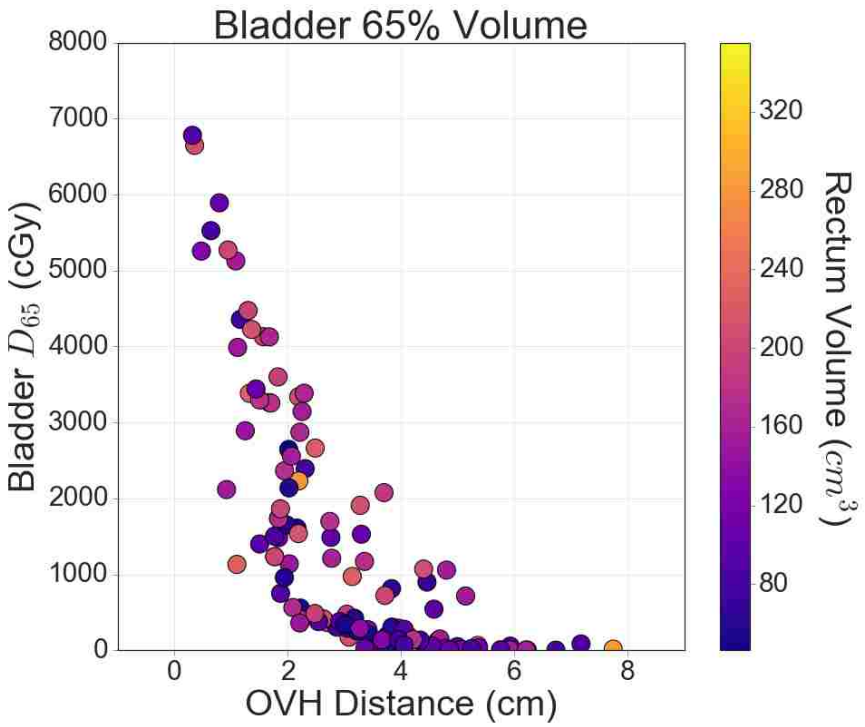

Figure 54: Color bar scatter plot for distance-to-dose relationship for 65% of the bladder, where the color-mapped variable is the rectum volume.

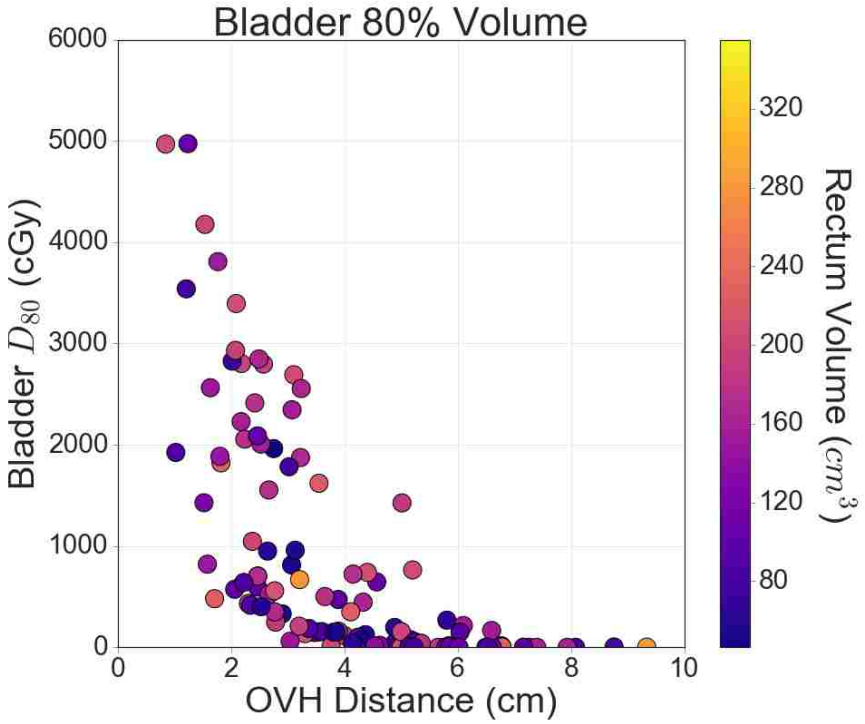

Figure 55: Color bar scatter plot for distance-to-dose relationship for 80% of the bladder, where the color-mapped variable is the rectum volume.

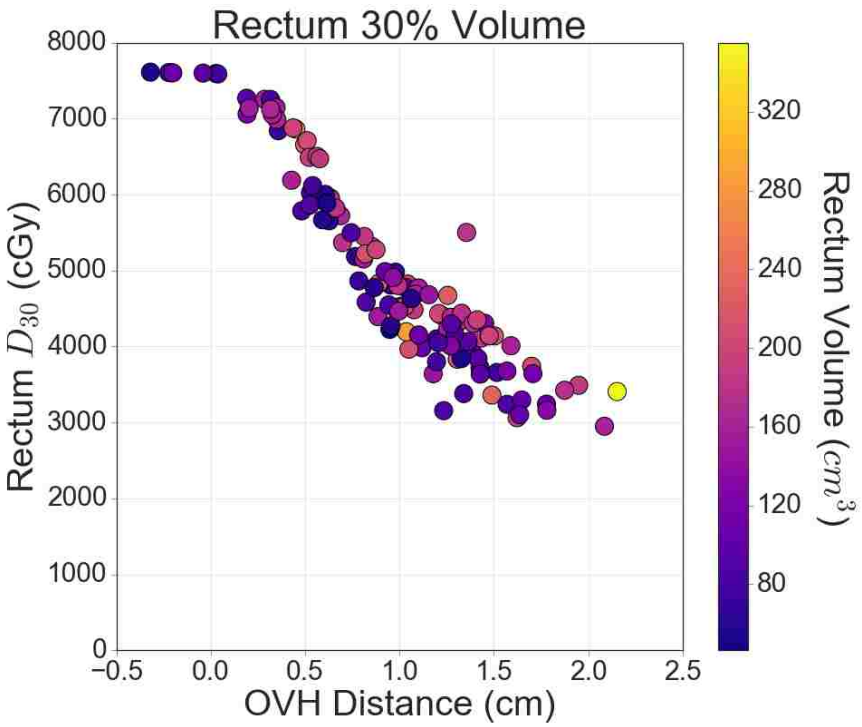

Figure 56: Color bar scatter plot for distance-to-dose relationship for 30% of the rectum, where the color-mapped variable is the rectum volume.

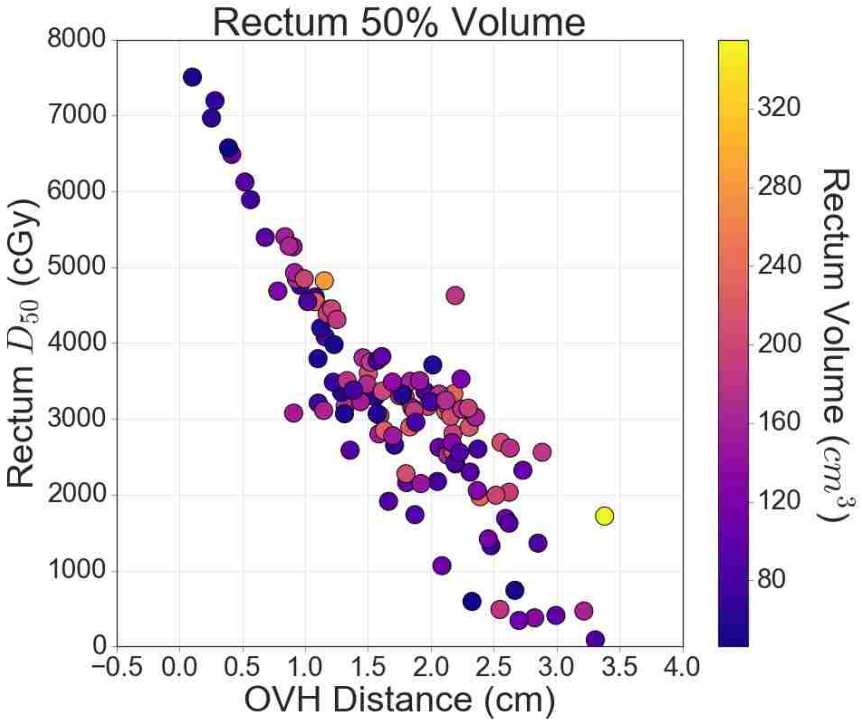

Figure 57: Color bar scatter plot for distance-to-dose relationship for 50% of the rectum, where the color-mapped variable is the rectum volume.

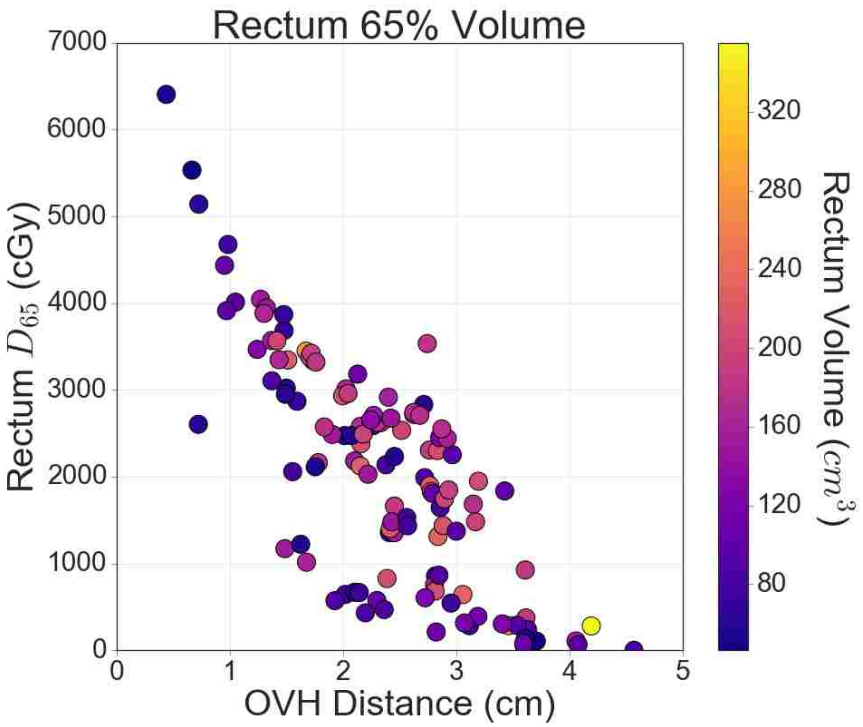

Figure 58: Color bar scatter plot for distance-to-dose relationship for 65% of the rectum, where the color-mapped variable is the rectum volume.

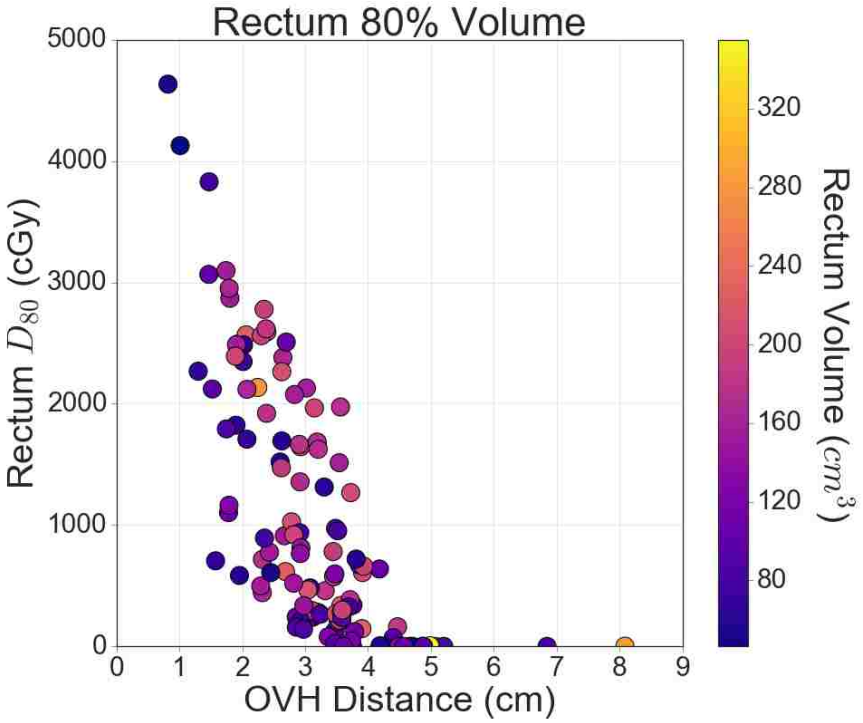

Figure 59: Color bar scatter plot for distance-to-dose relationship for 80% of the rectum, where the color-mapped variable is the rectum volume.

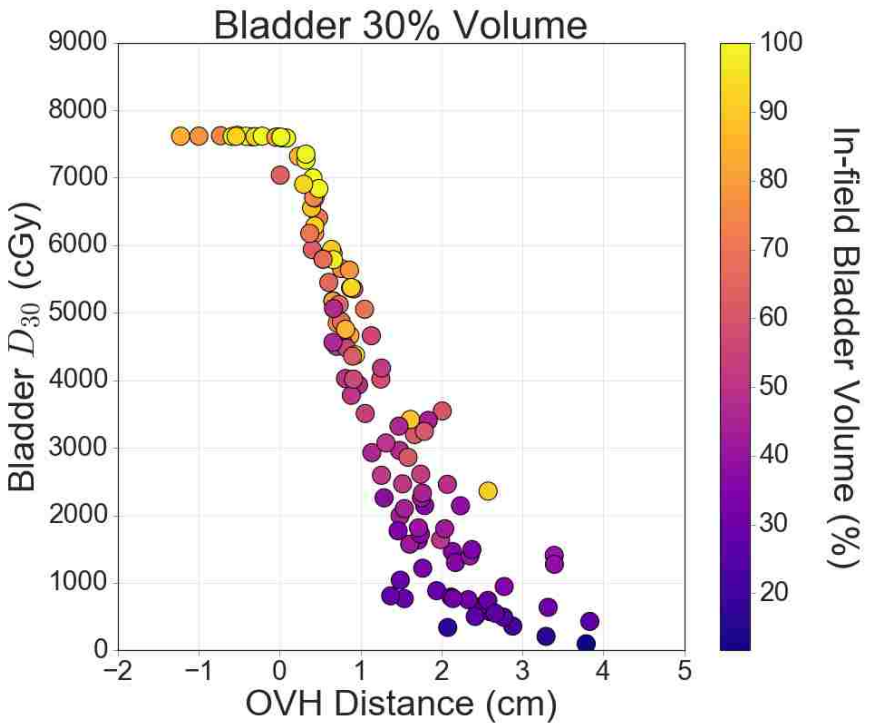

Figure 60: Color bar scatter plot for distance-to-dose relationship for 30% of the bladder, where the color-mapped variable is the in-field OAR volume.

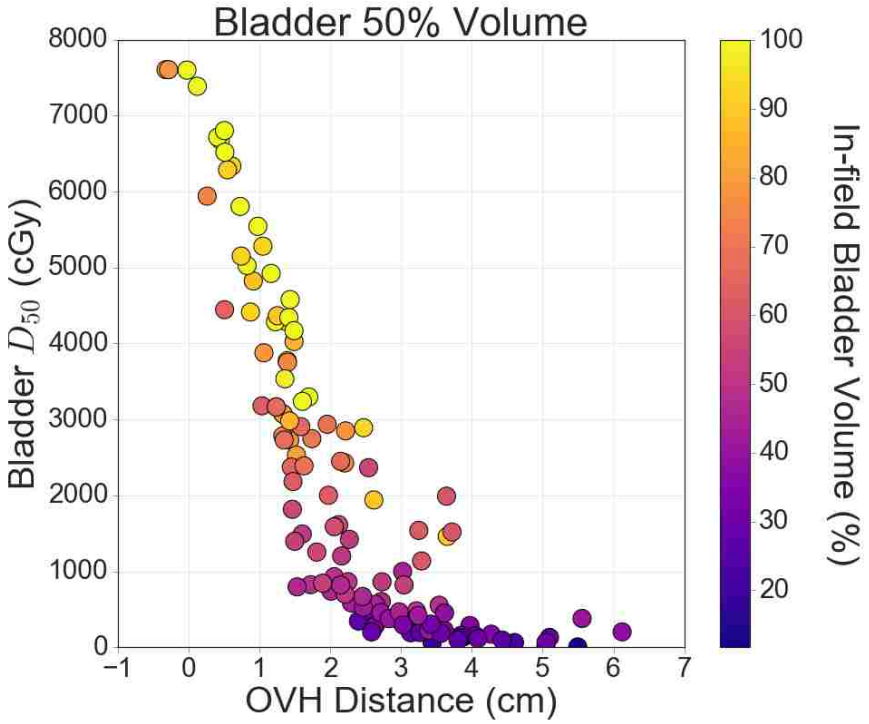

Figure 61: Color bar scatter plot for distance-to-dose relationship for 50% of the bladder, where the color-mapped variable is the in-field OAR volume.

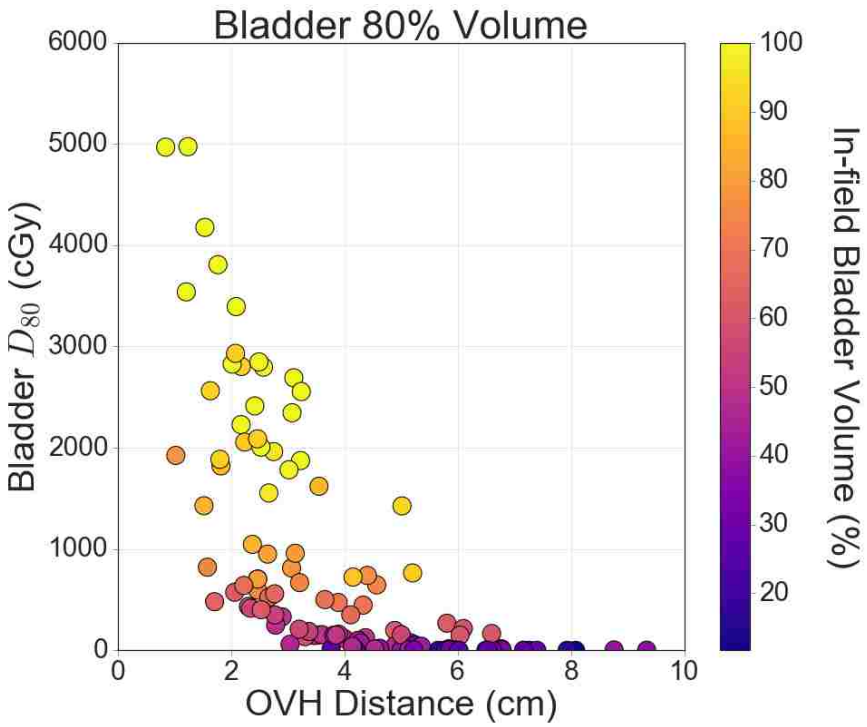

Figure 62: Color bar scatter plot for distance-to-dose relationship for 80% of the bladder, where the color-mapped variable is the in-field OAR volume.

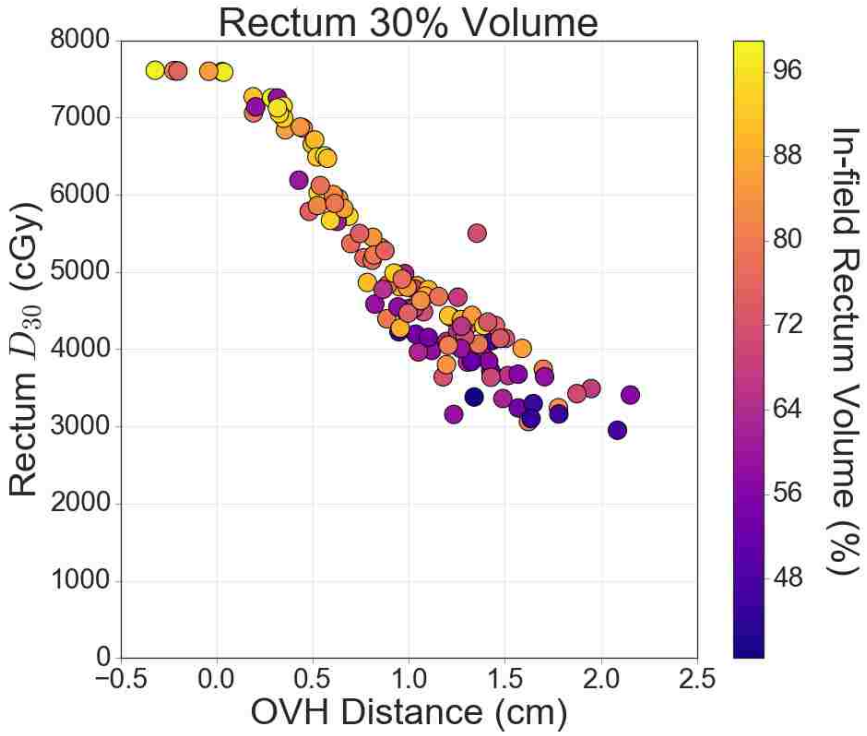

Figure 63: Color bar scatter plot for distance-to-dose relationship for 30% of the rectum, where the color-mapped variable is the in-field OAR volume.

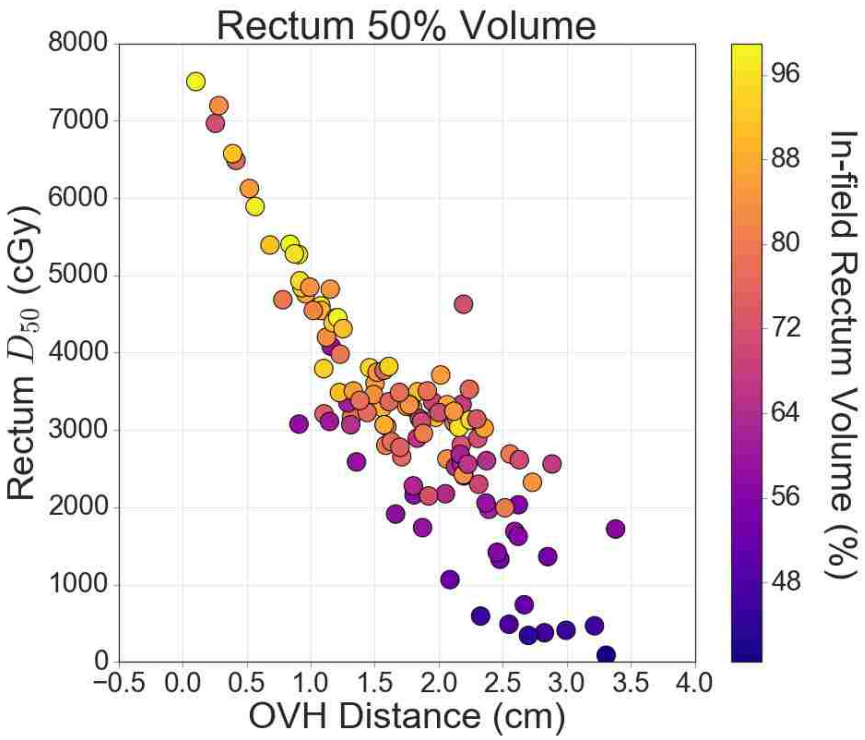

Figure 64: Color bar scatter plot for distance-to-dose relationship for 50% of the rectum, where the color-mapped variable is the in-field OAR volume.

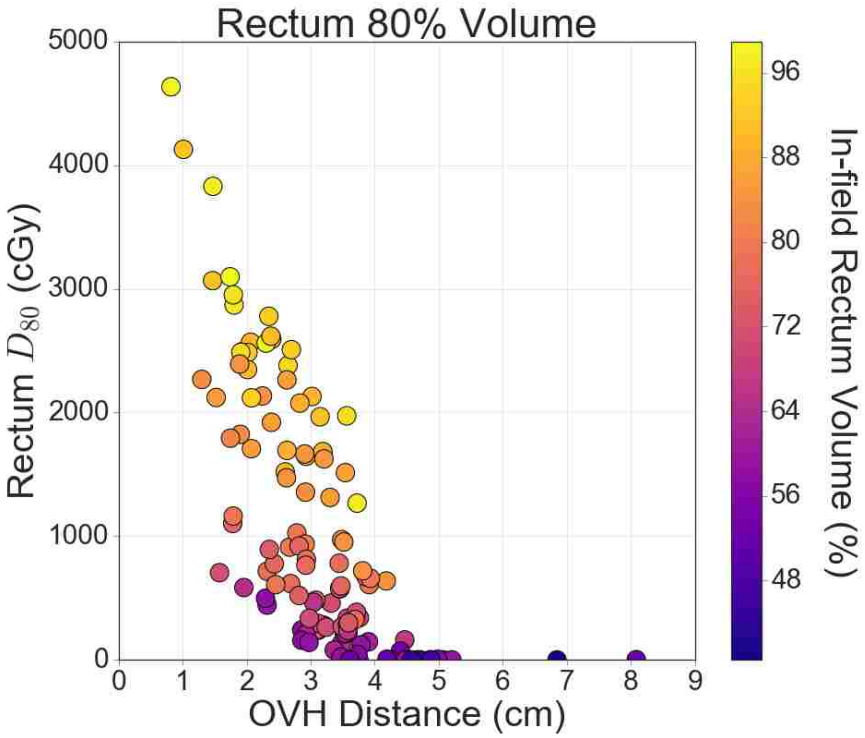

Figure 65: Color bar scatter plot for distance-to-dose relationship for 80% of the rectum, where the color-mapped variable is the in-field OAR volume.

APPENDIX D. NOMINAL VERSUS IN-FIELD OVH DISTANCE-TO-DOSE CORRELATIONS

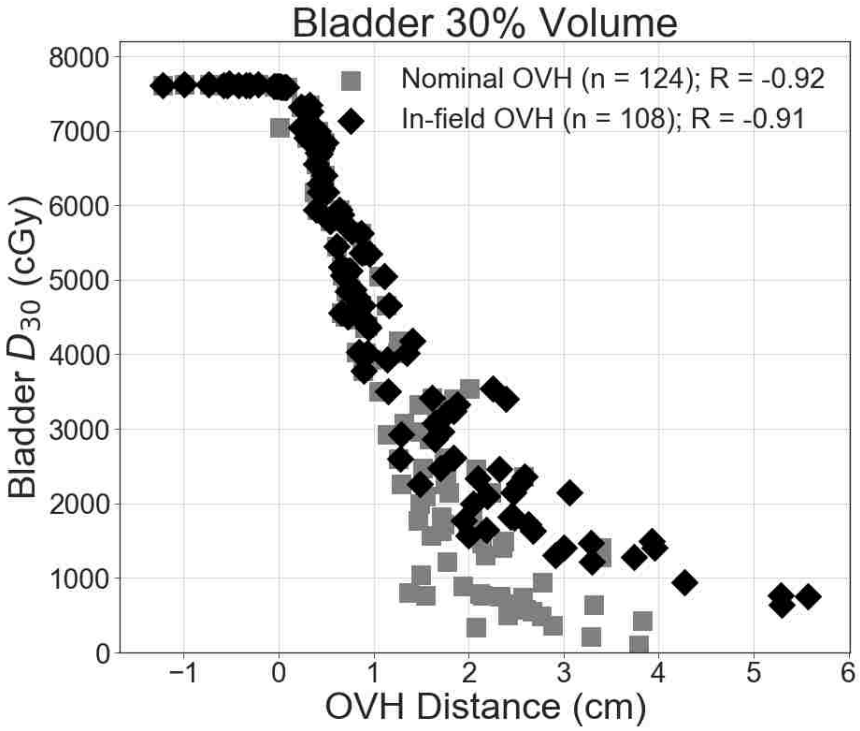

Figure 66: DVH-OVH correlation (R) using nominal OVH data (squares) and in-field OVH data (diamonds) for the 30% dose-volume of the bladder.

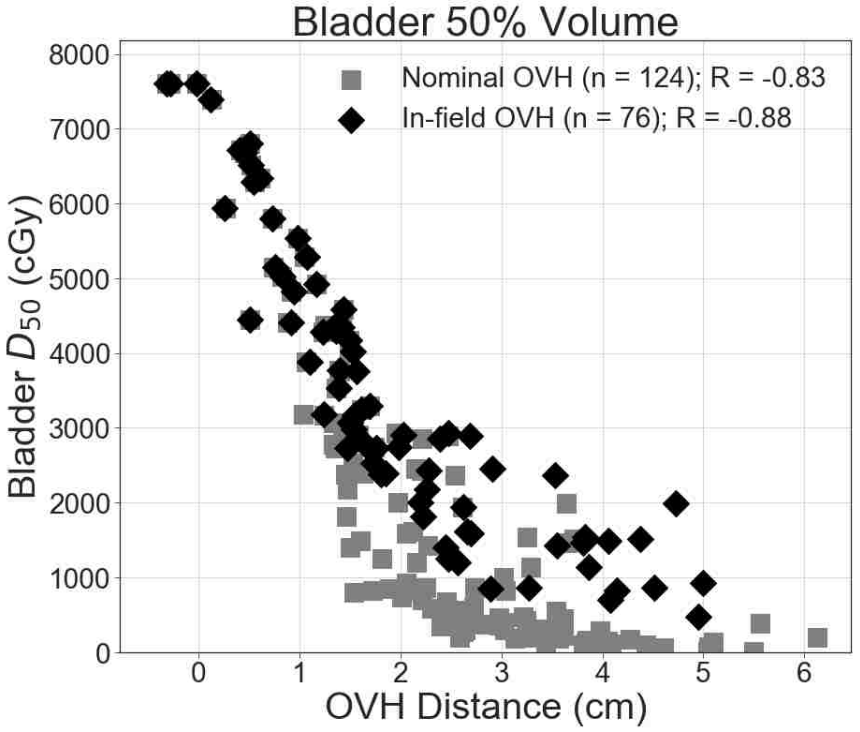

Figure 67: DVH-OVH correlation (R) using nominal OVH data (squares) and in-field OVH data (diamonds) for the 50% dose-volume of the bladder.

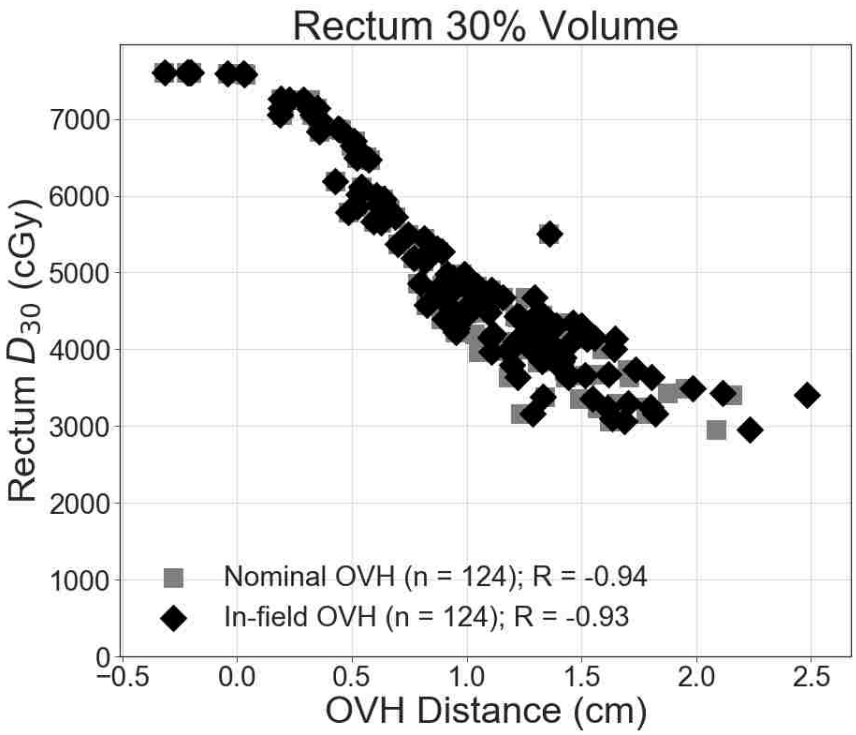

Figure 68: DVH-OVH correlation (R) using nominal OVH data (squares) and in-field OVH data (diamonds) for the 30% dose-volume of the rectum.

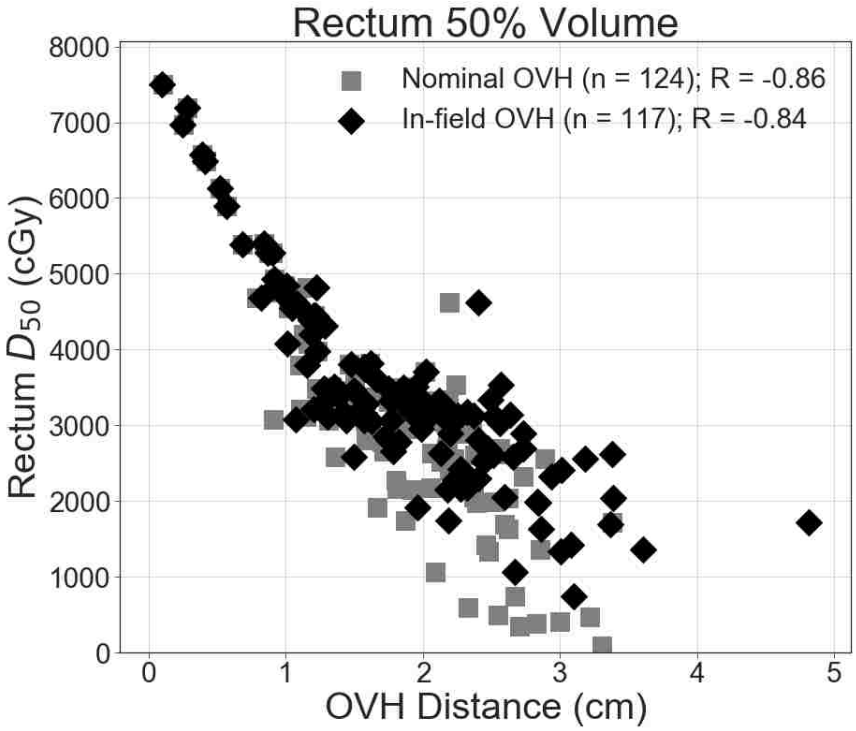

Figure 69: DVH-OVH correlation (R) using nominal OVH data (squares) and in-field OVH data (diamonds) for the 50% dose-volume of the rectum.

APPENDIX E. PLAN DATABASE DOSIMETRIC COMPARISON

Table 15: Statistical results of the dose comparison between the two plan databases for the PTV and secondary OARs. The mean differences between the MCOD and CPD dose metrics were averaged over the 124 database patients.

Dose Metric	Mean MCOD – CPD	Wilcoxon *p*-value
PTV		
D_2 (cGy)	-140.8	< 0.001*
D_{50} (cGy)	-124.6	< 0.001*
D_{98} (cGy)	133.4	< 0.001*
D_{min} (cGy)	650.5	< 0.001*
D_{mean} (cGy)	-101.5	< 0.001*
D_{max} (cGy)	-62.3	< 0.001*
V_{95} (%)	0.56	< 0.001*
V_{98} (%)	1.40	< 0.001*
V_{100} (%)	-6.05	< 0.001*
V_{107} (%)	-0.23	< 0.001*
HI	-0.03	< 0.001*
CI	-0.13	< 0.001*
Left Femoral Head		
D_2 (cGy)	-2506	< 0.001*
D_{max} (cGy)	-2077	< 0.001*
D_{mean} (cGy)	-2189	< 0.001*
Right Femoral Head		
D_2 (cGy)	-2492	< 0.001*
D_{max} (cGy)	-2058	< 0.001*
D_{mean} (cGy)	-2187	< 0.001*
Penile Bulb		
D_{mean} (cGy)	-994	< 0.001*

*Indicates a statistically significant result of $p < 0.05$

Table 16: Statistical results of the dose comparison between the two plan databases for the primary OARs. The mean differences between the MCOD and CPD dose metrics were averaged over the 124 database patients.

Dose Metric	Mean MCOD – CPD (cGy)	Wilcoxon *p*-value Re-plan vs. Clinical
Bladder		
D_{10}	-542	< 0.001*
D_{30}	-879	< 0.001*
D_{50}	-643	< 0.001*
D_{65}	-520	< 0.001*
D_{80}	-473	< 0.001*
D_{mean}	-581	< 0.001*
Rectum		
D_{10}	-137	< 0.001*
D_{30}	-434	< 0.001*
D_{50}	-541	< 0.001*
D_{65}	-578	< 0.001*
D_{80}	-557	< 0.001*
D_{mean}	-435	< 0.001*

*Indicates a statistically significant result of $p < 0.05$

APPENDIX F. PATIENT-BY-PATIENT PREDICTION ACHIEVABILITY PLOTS

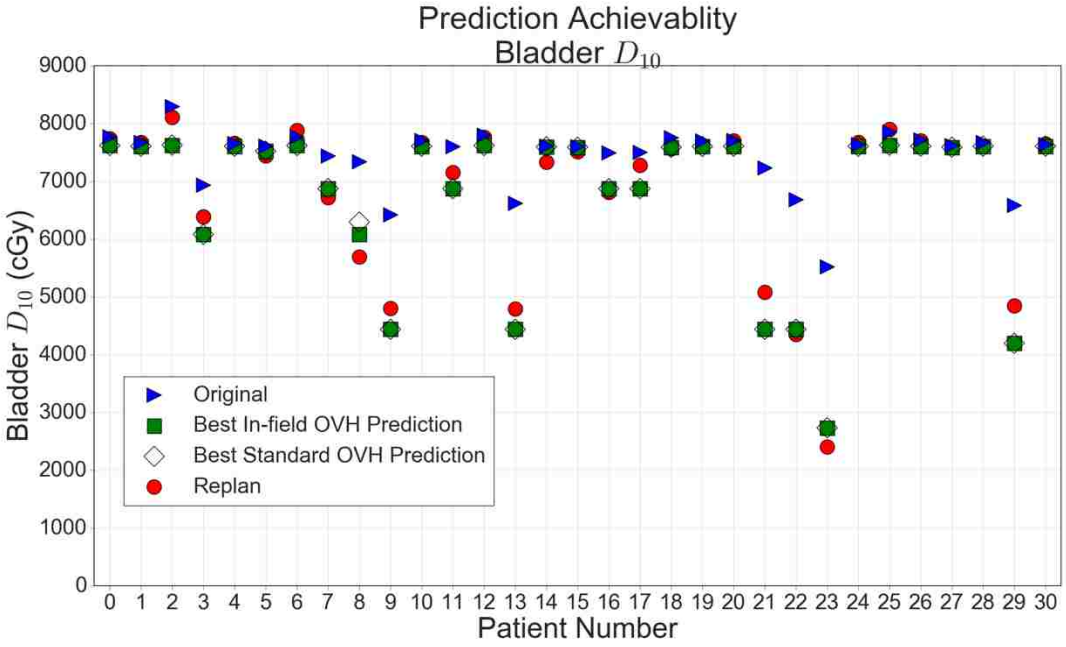

Figure 70: Patient-by-patient data from re-planning study comparing the original, clinical value (triangle), in-field OVH KBP prediction (square), standard OVH KBP prediction (diamond), and re-planned value (circle) for bladder D_{10}.

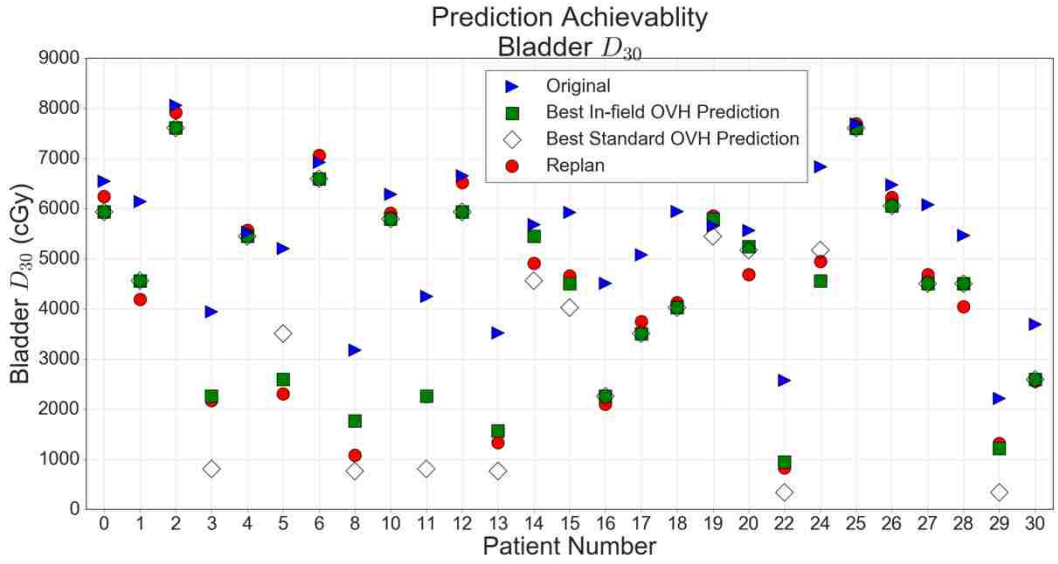

Figure 71: Patient-by-patient data from re-planning study comparing the original, clinical value (triangle), in-field OVH KBP prediction (square), standard OVH KBP prediction (diamond), and re-planned value (circle) for bladder D_{30}.

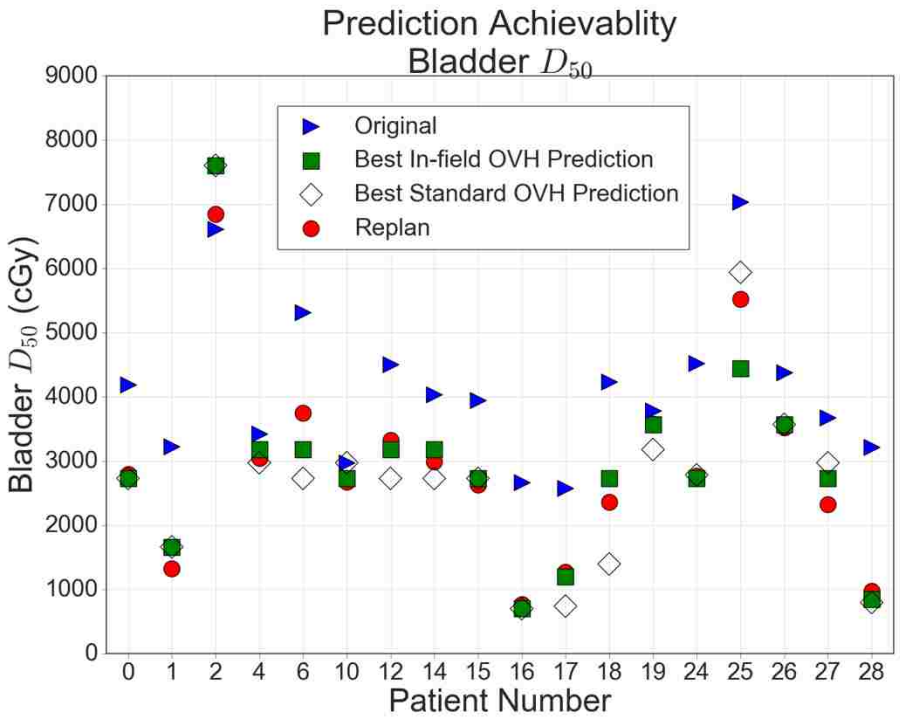

Figure 72: Patient-by-patient data from re-planning study comparing the original, clinical value (triangle), in-field OVH KBP prediction (square), standard OVH KBP prediction (diamond), and re-planned value (circle) for bladder D_{50}.

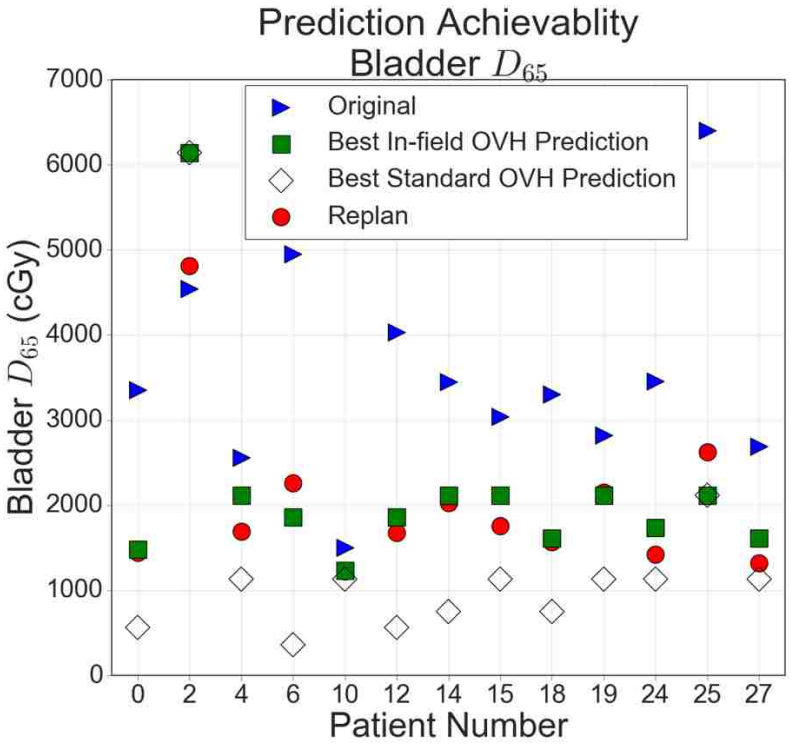

Figure 73: Patient-by-patient data from re-planning study comparing the original, clinical value (triangle), in-field OVH KBP prediction (square), standard OVH KBP prediction (diamond), and re-planned value (circle) for bladder D_{65}.

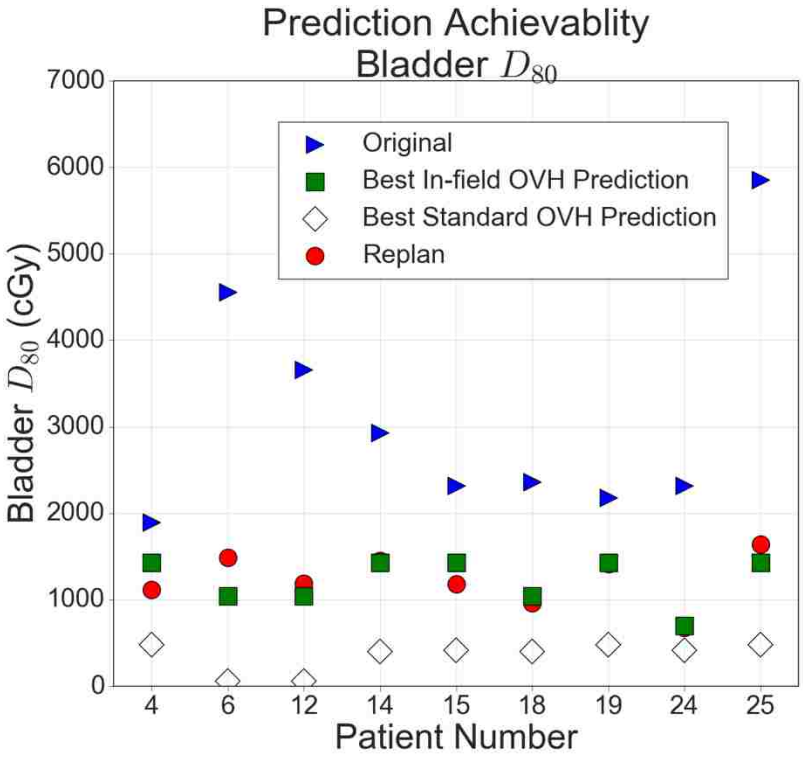

Figure 74: Patient-by-patient data from re-planning study comparing the original, clinical value (triangle), in-field OVH KBP prediction (square), standard OVH KBP prediction (diamond), and re-planned value (circle) for bladder D_{80}.

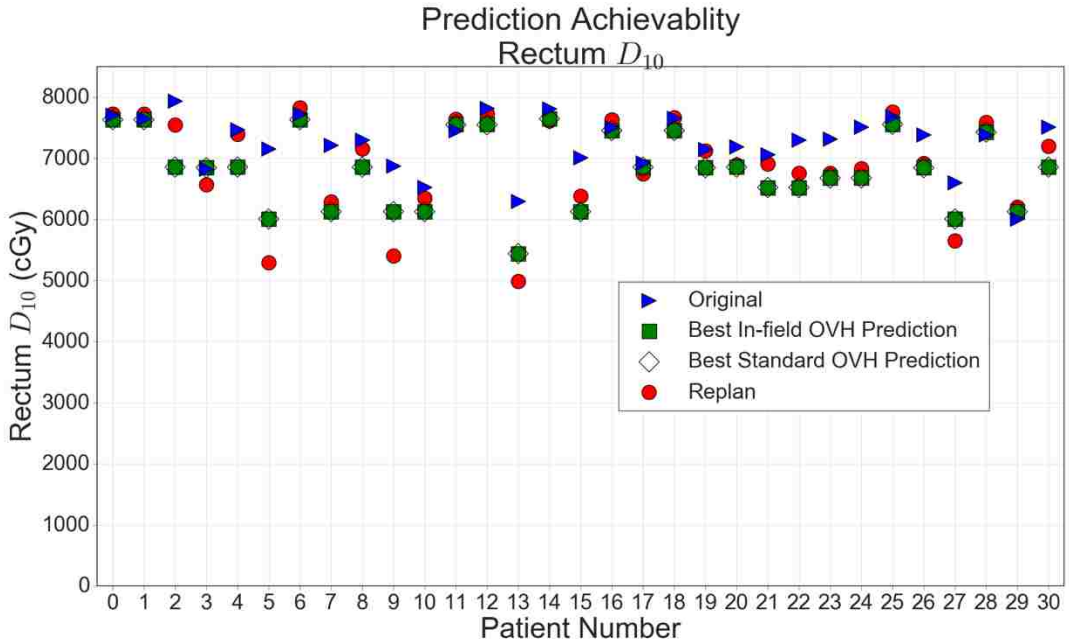

Figure 75: Patient-by-patient data from re-planning study comparing the original, clinical value (triangle), in-field OVH KBP prediction (square), standard OVH KBP prediction (diamond), and re-planned value (circle) for rectum D_{10}.

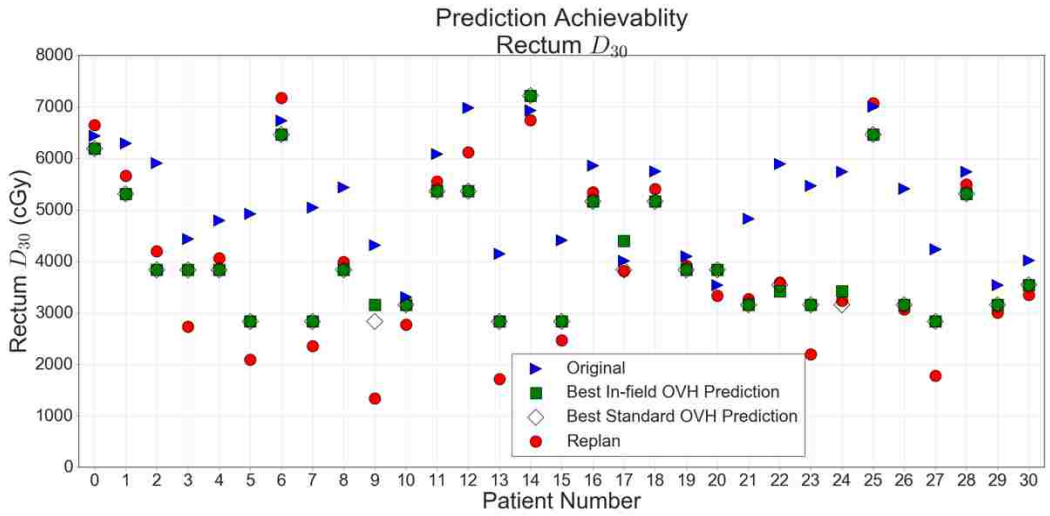

Figure 76: Patient-by-patient data from re-planning study comparing the original, clinical value (triangle), in-field OVH KBP prediction (square), standard OVH KBP prediction (diamond), and re-planned value (circle) for rectum D_{30}.

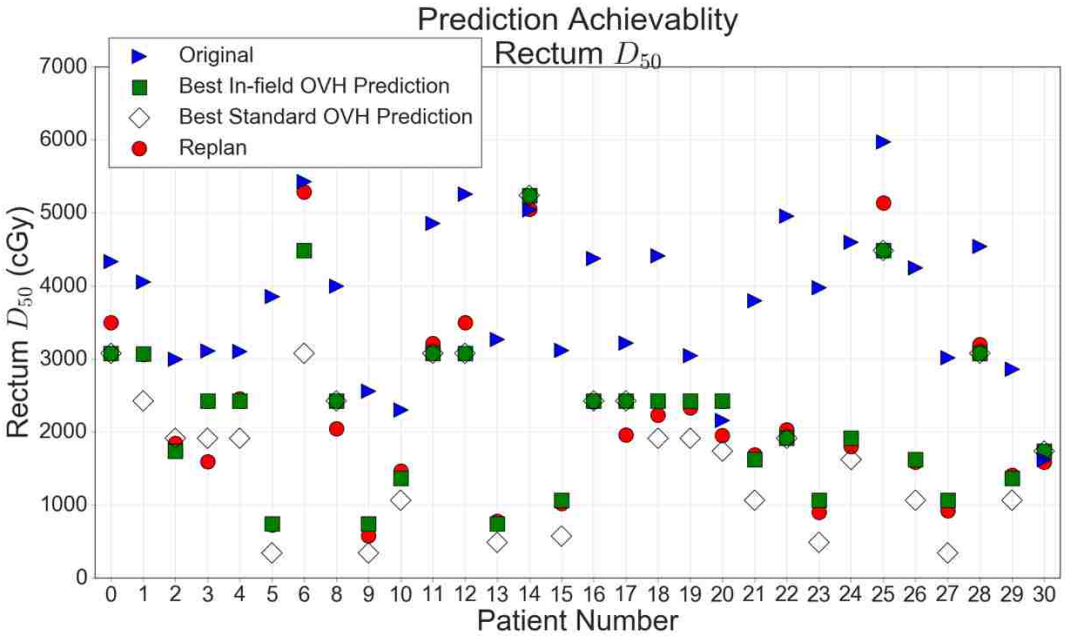

Figure 77: Patient-by-patient data from re-planning study comparing the original, clinical value (triangle), in-field OVH KBP prediction (square), standard OVH KBP prediction (diamond), and re-planned value (circle) for rectum D_{50}.

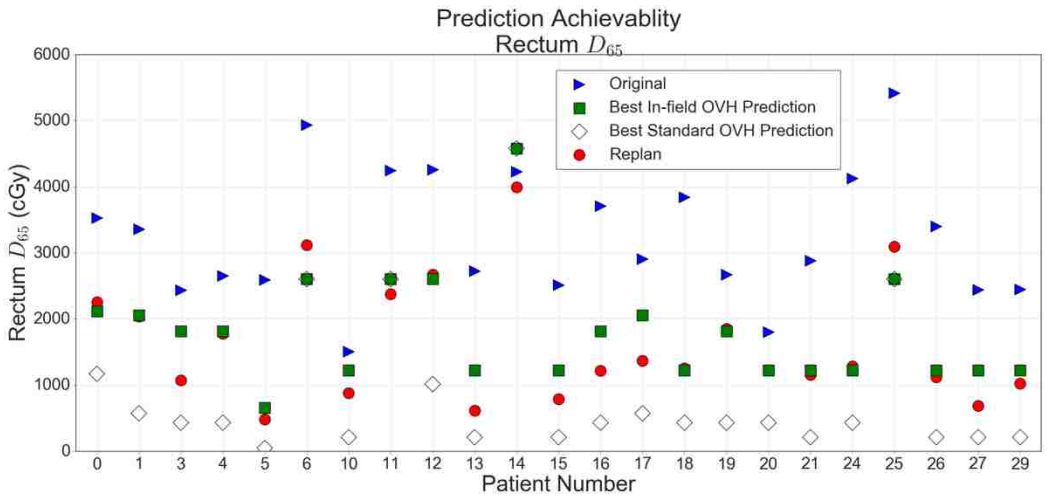

Figure 78: Patient-by-patient data from re-planning study comparing the original, clinical value (triangle), in-field OVH KBP prediction (square), standard OVH KBP prediction (diamond), and re-planned value (circle) for rectum D_{65}.

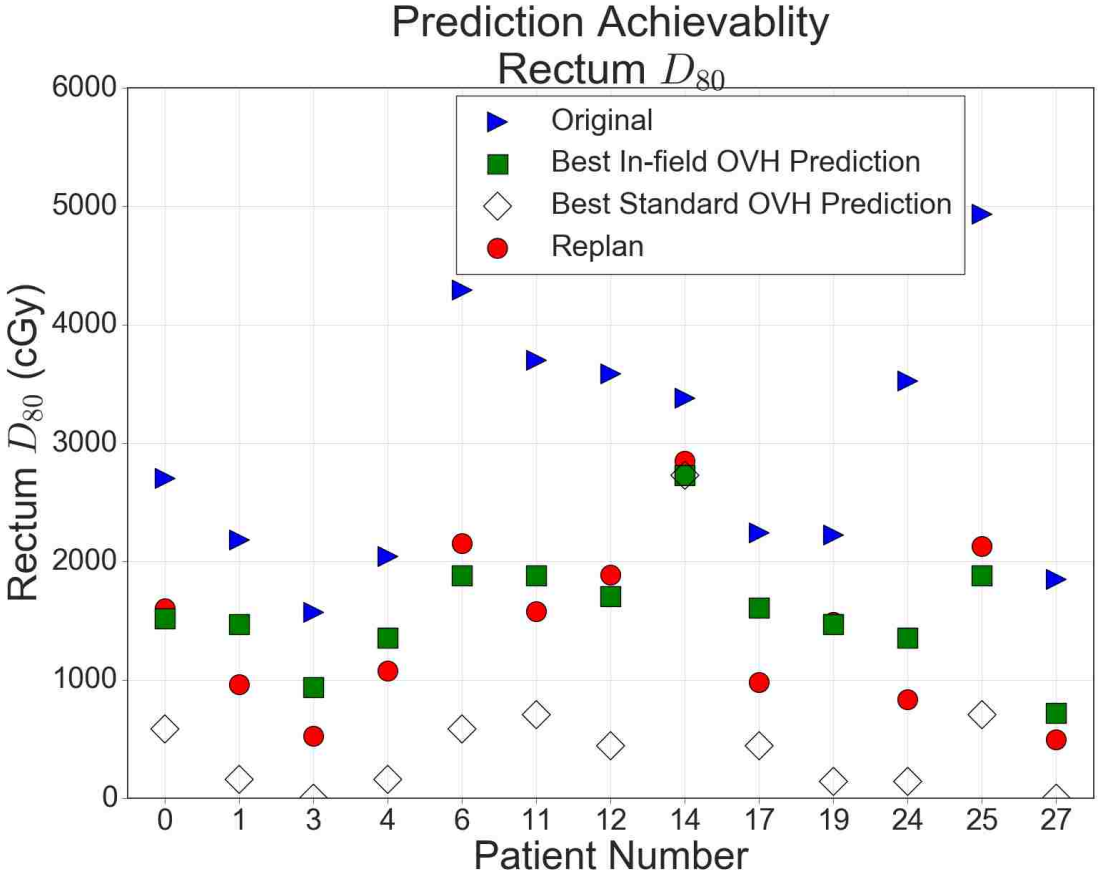

Figure 79: Patient-by-patient data from re-planning study comparing the original, clinical value (triangle), in-field OVH KBP prediction (square), standard OVH KBP prediction (diamond), and re-planned value (circle) for rectum D_{80}.

APPENDIX G. PRELIMINARY ACHIEVABILITY RESULTS FOR NOMINAL VERSUS IN-FIELD OVH PREDICTIONS

Table 17: Statistical results comparing predictions from KBP model using the in-field OVH versus the nominal OVH feature metric.

Dose Metric	Predictions	Mean In-field – Nominal OVH Prediction (cGy)	Wilcoxon p-value: In-field vs. Nominal OVH
Bladder			
D_{10}	31	-6.9	0.32
D_{30}	27	239.0	0.05*
D_{50}	18	97.6	0.25
D_{65}	13	776.1	0.003*
D_{80}	9	865.2	0.007*
Rectum			
D_{10}	31	0.6	0.16
D_{30}	31	33.1	0.14
D_{50}	30	315.4	< 0.001*
D_{65}	23	917.3	< 0.001*
D_{80}	13	1056.2	0.002*

*Indicates a statistically significant result of $p < 0.05$

VITA

Phillip Wall was born in Birmingham, Alabama in 1992, where he was raised before graduating from The Altamont School in 2010. Moving to Davidson, North Carolina, he received a Bachelor of Science degree in Mathematics and Physics from Davidson College in the spring of 2014. Phillip entered the LSU Medical & Health Physics Graduate Program in Baton Rouge, Louisiana in the fall of 2014 as a Master's candidate. He expects to graduate with a Master of Science degree in medical physics in the summer of 2017. After completing the M.S. degree requirements, Phillip will pursue doctoral studies in the LSU Medical & Health Physics Graduate Program.